THE EFFECT OF CURRENT ON WHITE LAYER THICKNESS IN ELECTRICAL DISCHARGE MACHINING PROCESS

2023
MASTER THESIS
MECHANICAL ENGINEERING

Shahad Hatem Hasan HASAN

Thesis Advisors
Assist. Prof. Dr. Bilal ÇOLAK
Prof. Dr. Shukry H. AGHDEAB

THE EFFECT OF CURRENT ON WHITE LAYER THICKNESS IN ELECTRICAL DISCHARGE MACHINING PROCESS

Shahad Hatem Hasan HASAN

Thesis Advisors

Assist. Prof. Dr. Bilal ÇOLAK

Prof. Dr. Shukry H. AGHDEAB

T.C.

Karabuk University

Institute of Graduate Programs

Department of Mechanical Engineering

Prepared as

Master Thesis

KARABUK

Jan 2023

I certify that in my opinion the thesis submitted by Shahad Hatem Hasan titled "THE EFFECT OF CURRENT ON WHITE LAYER THICKNESS IN ELECTRICAL DISCHARGE MACHINING PROCESS" is fully adequate in scope and in quality as a thesis for the degree of Master of Science.

Assist. Prof. Dr. Bilal ÇOLAK .....
Thesis Advisor, Department of Mechanical Engineering

Prof. Dr. Shukry H. AGHDEAB .....
Thesis Advisor, University of Technology, Baghdad

This thesis is accepted by the examining committee with a unanimous vote in the Department of Mechanical Engineering as a Master of Science thesis. Jan 27, 2023

Examining Committee Members (Institutions)	Signature
Chairman : Prof. Dr. Hasan GÖKKAYA (KBU)	.....
Member : Assoc. Prof. Dr. Hüseyin ÇETİN (KTUN)	.....
Member : Assist. Prof. Dr. Bilal ÇOLAK (KBU)	.....
Member : Prof. Dr. Shukry H. AGHDEAB (UOT)	.....

The degree of Master of Science by the thesis submitted is approved by the Administrative Board of the Institute of Graduate Programs, Karabuk University.

Prof. Dr. Müslüm KUZU .....
Director of the Institute of Graduate Programs

"I declare that all the information within this thesis has been gathered and presented in accordance with academic regulations and ethical principles and I have according to the requirements of these regulations and principles cited all those which do not originate in this work as well."

Shahad Hatem HASAN

ABSTRACT

M. Sc. Thesis

THE EFFECT OF CURRENT ON WHITE LAYER THICKNESS IN ELECTRICAL DISCHARGE MACHINING PROCESS

Shahad Hatem Hasan HASAN

Karabük University
Institute of Graduate Programs
The Department of Mechanical Engineering

Thesis Advisors:
Assist. Prof. Dr. Bilal ÇOLAK
Prof. Dr. Shukry H. AGDEAB
Jan 2023, 88 pages

Forecasting the thickness of the white layer is crucial in the current condition because the thickness of the white layer impacts the surface quality of specimens cut using electrical discharge machining (EDM). The onset and progression of white layer formation are of great interest to the industry because of the resulting changes in the mechanical properties of the workpiece surface. To save time and money during tool and process design, the industry requires effective predictive models of white-layer formation. The effect of input parameters (current, pulse on, and pulse off) on white layer thickness when cutting a sample of CK45 DIN 17500 grade material was explored in this study. The selection of EDM machining factors and their impact on the White Layer Thickness (WLT), Material Removal Rate (MRR), Surface Roughness (Ra), and Electrode Wear Ratio (EWR) are the primary topics of the research.

In this study, the mathematical model that was used to forecast the various response quality was built with the software Minitab 17 and used factorial notation. The results of the model were then assessed and compared to the values obtained with Minitab 17. For the testing, the input parameters were taken as current (10, 30, and 50 A), pulse on time (50, 100, and 200 μs), and pulse off time (3, 9, and 18 μs). According to this study, all output parameters increase as Ip increases from 10A to 50A showing that Ip is the most important input parameter affecting the outputs. The IP needs to be decreased to achieve the desired improvements in WLT, Ra, and EWR. On the other hand, IP needs to increase to improve the MRR. For CK45 DIN 17200 grade material, the maximum WLT (335.7469 μm) occurred at the highest current and Ton, while the best WLT (4,17946 μm) occurred at the lowest Ip, Ton, and highest Toff. It was seen that the results obtained in this experimental study were extremely close to the predicted results.

Key Words : Electrical discharge machining, White layer, Current, Material removal rate, Electrode wear ratio, Roughness, factorial analysis.

Science Code: 91438

ÖZET

Yüksek Lisans Tezi

ELEKTRİKSEL DEŞARJLA İŞLEME YÖNTEMİNDE AKIMIN BEYAZ TABAKA KALINLIĞINA ETKİSİ

Shahad Hatem Hasan HASAN

Karabük Üniversitesi
Lisansüstü Eğitim Enstitüsü
Makina Mühendisliği Anabilim Dalı

Tez Danışmanları:
Dr. Öğr. Üyesi Bilal ÇOLAK
Prof. Dr. Shukry H. AGDEAB
Ocak 2023, 88 sayfa

Beyaz tabaka, elektrikli erozyonla (EDM) işlenen numunelerin yüzey kalitesini etkilediğinden kalınlığının tahmini çok önemlidir. Beyaz tabaka oluşumunun başlangıcı ve ilerlemesi, iş parçası yüzeyinin mekanik özelliklerinde meydana gelen değişiklikler nedeniyle endüstri için büyük ilgi görmektedir. Takım ve süreç tasarımı sırasında zamandan ve paradan tasarruf etmek için endüstri, beyaz tabaka oluşumunun etkili tahminine dayalı modellerine ihtiyaç duyar. Bu çalışmada, CK45 DIN 17500 kalitesinde bir malzeme numunesi kesilirken giriş parametrelerinin (akım, darbe açık ve darbe kapalı) beyaz katman kalınlığı üzerindeki etkisi araştırıldı. EDM işleme parametrelerinin seçimi ve bunların Beyaz Tabaka Kalınlığı (WLT), Malzeme Kaldırma Oranı (MRR), Yüzey Pürüzlülüğü (Ra) ve Elektrot Aşınma Oranı (EWR) üzerindeki etkileri araştırmanın öncelikli konularıdır.

Bu çalışmada, çeşitli yanıt kalitelerini tahmin etmek için kullanılan matematiksel model Minitab 17 yazılımı ile oluşturulmuş ve faktöriyel gösterim kullanılmıştır. Modelin sonuçları daha sonra değerlendirildi ve Minitab 17 ile elde edilen değerlerle karşılaştırıldı. Test için giriş parametreleri akım (10, 30 ve 50 A), darbe açık kalma süresi (50, 100 ve 200 µs) ve puls kapanma zamanı (3, 9 ve 18 µs) olarak alınmıştır. Bu çalışmaya göre, IP 10A'den 50A'e yükseldikçe tüm çıkış parametrelerinin artması, IP'nin çıkışları etkileyen en önemli giriş parametresi olduğunu göstermektedir. WLT, Ra ve EWR'de istenen iyileştirmeleri elde etmek için IP'nin düşürülmesi gerekir. Öte yandan, MRR'yi iyileştirmek için IP'nin artması gerekir. CK45 DIN 17200 kalite malzeme için, maksimum WLT (335,7469 µm) en yüksek akım ve TON'da meydana gelirken, en iyi WLT (4,17946 µm) en düşük Ip, TON ve en yüksek TOFF'ta meydana geldi. Bu deneysel çalışmada elde edilen sonuçların tahmin edilen sonuçlara son derece yakın olduğu görülmüştür.

Anahtar Kelimeler : Elektrik erozyon işleme, Beyaz tabaka, Akım, Talaş kaldırma oranı, Elektrot aşınma oranı, Pürüzlülük, faktör analizi.

Bilim Kodu : 91438

ACKNOWLEDGMENT

I would like to thank my God (the most merciful) for giving me knowledge, strength, and the ability to complete my studying and for letting me through all the difficulties.

I would like to give my warmest thanks to my supervisor Dr. Bilal ÇOLAK whose guidance and advice carried me through all the stages of writing my project. and Prof. Dr. Shukry. H. AGHDEAB made this work possible.

Last but not the least, I would also like to give special thanks to my family none of this would be possible without you

CONTENTS

Page

Page

Page

LIST OF FIGURES

Page

Page

LIST OF TABLES

Page

SYMBOLS AND ABBREVITIONS INDEX

SYMBOLS

ρ	: Correlation coefficient
σ	: Standard deviation

ABBREVITIONS

cov	: Covariance
log	: Logarithmic
var	: Variance
Adj MS	: Adjusted Mean Squares ALCA
Adj SS	: Adjusted Sums of Squares
AISI	: American Iron and Steel Institute
ANOVA	: Analysis Of Variance
CAD	: Computer Aided design
CNC	: Computer Numeric Controlled
CK45	: Medium Carbon Steel
DC	: Direct Current.
DF	: Degree of Freedom.
DOE	: Design of Experiments.
EDM	: Electrical Discharge Machining.
EWR	: Electrode Wear Rate
MRR	: Material Removal Rate
USEDM	: Ultrasonic assisted EDM
PMEDM	: Powder-mixed dielectric EDM
PM-USEDM	: Powder mixed dielectric USEDM
HV	: Micro hardness
Cu	: Copper

Gr	: Graphite
Ip	: Peak Current
Ra	: Surface Roughness
RC	: A resistor–capacitor circuit
R-sq	: The determination coefficient
R-sq (adj)	: Adjusted determination coefficient
R-sq (pred)	: Predicted determination coefficient
T.M	: Machining time
T_{off}	: Pulse-off time
T_{on}	: Pulse-on time
V	: Voltage
Wfe	: The final weight of the electrode
Wfw	: The final weight of the workpiece.
Wie	: The initial weight of the electrode.
Wiw	: The initial weight of the workpiece.
W.T	: Working Time
WLT	: White layer thickness
W.P	: Workpiece
ρ	: Density.
SVO	: Servo Feed.
MRR	: Material removal rate
PSBN	: public safety broadband network.
RCI	: rectangular current impulse
(GDOES)	: glow discharge optical emission spectroscopy

PART 1

INTRODUCTION

Electrical discharge machining (EDM), also known as die sinking or flame machining, is a thermal method where materials are removed by the effect of high-power electrical sparks [1].

It is a suitable machining alternative method for producing complex shapes and hard materials that are very strenuous to manufacture by conventional machining methods. EDM process uses electrical energy for cutting materials to the final profile shape and size. In addition, this process doesn't create mechanical pressure between the workpiece and the electrode because there is no direct contact [2].

Also, EDM is used in different fields, such as plastic moldings, die casting, forging dies, automotive, medical components, and aerospace. Tool steel considers very hard to machine using the traditional process because of its quick tool wear rate, limited machining rates, difficulty in creating complex forms, and superior surface finish. Traditional machining techniques usually depend on removing material with tooling stronger than the work material [3]. Figure 1.1. shows some examples of EDM's work.

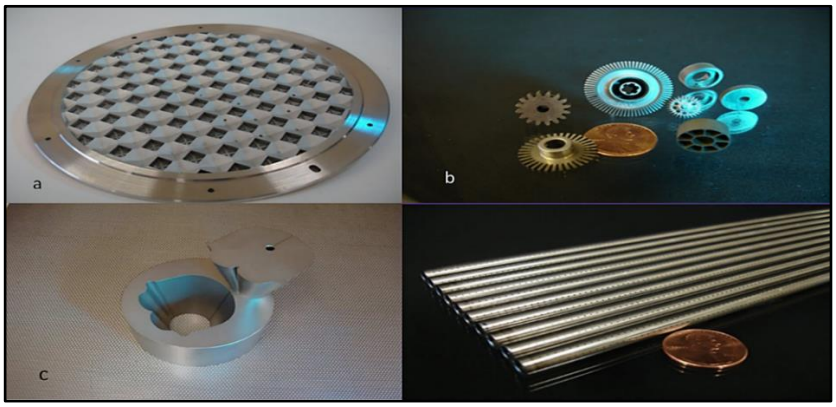

Figure 1.1. Some examples of EDM's work a- Optic Reflector section machined using EDM, b- Aerospace EDM rocket nozzle, and c- Extruded EDM of die components drilling a small hole of a gas tube [4].

1.1. EDM BACKGROUND

The EDM method dates to the 1770s when English scientist Joseph Priestly discovered that the erosive impact of electrical discharges had stripped materials from the electrode surface in his studies. Many developments came after that, but the real development was in the 1960s. EDM machines improved because of the growth of the business, die-sinking machinery became accessible, and high-quality products. Wire-cutting machines were developed between the 1960s and 1970s, which marked the start of employing numerical positional control to make electrode movement more accurate. This enhancement improved the process's precision and helped to advance wire-cutting equipment.

In the mid-1970s, computer numerical control systems were introduced. During the 1980s, the world market for EDM machines began to grow rapidly, and micromachining, servocontrol, and robots were introduced. Finally, during the 1990s, new methods for controlling the EDM process were developed. By changing the method for verification and analysis through experiments, neural networks and fuzzy control were used to predict the materials removal rate (MRR), electrodes wear rate (EWR), and surface roughness (Ra). EDM has been a popular method for cutting conductive materials with high accuracy, tighter dimensional tolerances, and complex profiles in any hardness. However, due to poor materials removal rates and short tool life, EDM has a comparatively slow process compared to traditional machining techniques [5]. The primary components in electric discharge:

- Electric power supply.
- Dielectric medium.
- Workpiece and tool.
- Servo control unit.

The workpiece and tool are connected to a DC power supply with a current density of 1000 A/cm2 and a power density of approximately 500 MW/cm2 (Fig. 1.2.). The gap, also called the spark gap, is the distance between two electrodes from 0.005 mm to 0.5 mm, and the pressure of the dielectric fluid is 2 Kgf/cm2 or less [6].

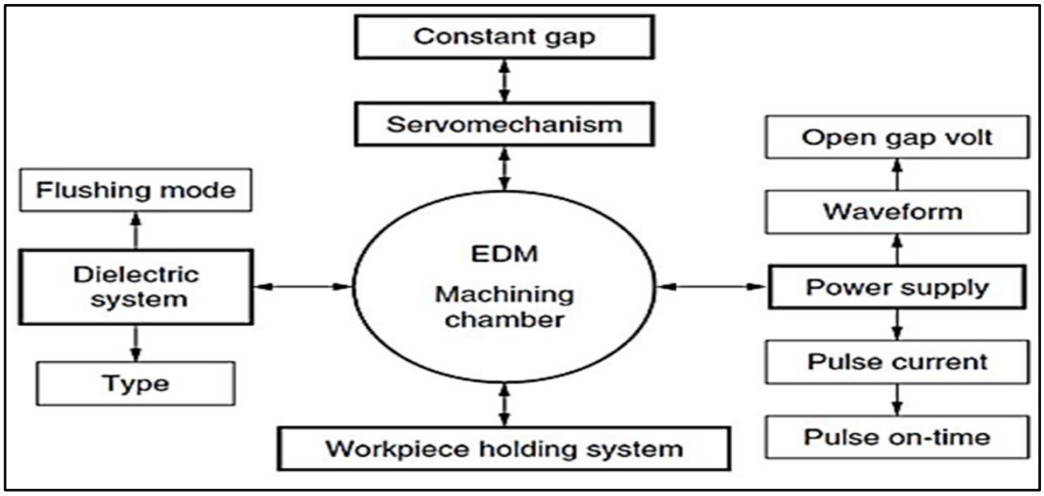

Figure 1.2. The EDM system's parts [6].

1.2. THE EDM PROCESS

Electrical spark machining removes materials by a series of electrical discharges between the tool electrode and the workpiece, immersed in a dielectric liquid. The electrode generally is an anode, and the workpiece (w.p) is a cathode [7]. The cathode and anode are two poles connected by direct circle pulse generation. Unlike other manufacturing processes, the electrode does not create a physical connection with the workpiece for material removal in EDM. Because if the electrode contacts the workpiece, the sparking stops, and no material will remove [8].

An electrode tool is shaped with the desired profile for cutting on a workpiece. A gap isolates the workpiece and tool electrode to create a pulsated spark during a dielectric fluid flowing through ionization [9]. Commonly, the measures of spark radius are tiny, between 100 μm and 200 μm, and even so, the spark energy density is highly proper. The electrode's material melts and vaporizes in a limited area [10]. EDM is a method for removing metals with dimensional accuracy control of any hard and soft metal, as shown in Figure 1.3.

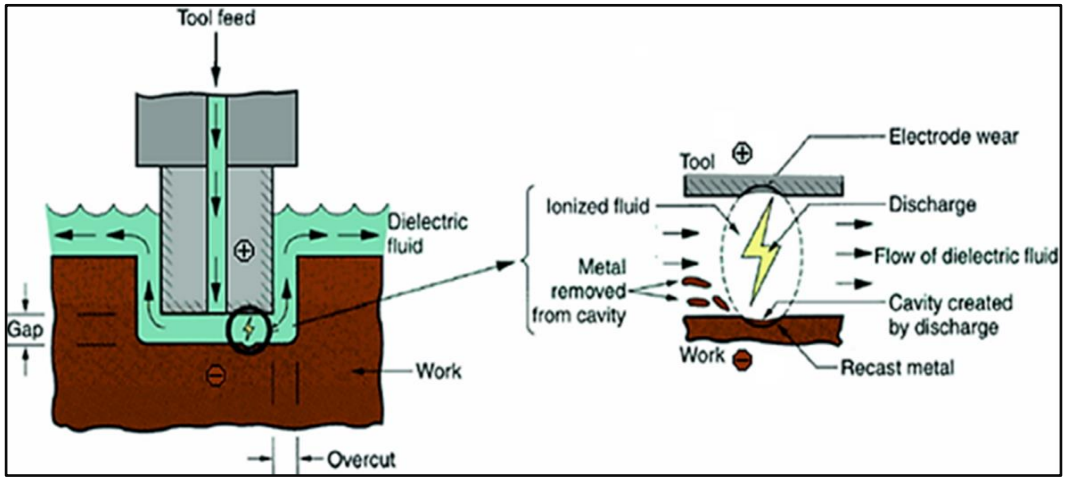

Figure 1.3. The fundamentals of electrical discharge machining include (a) the general setup, (b) a closer look at the gap, which demonstrates the discharge, and the removal of material (MR) [10].

A mechanism of EDM generally depends on converting electrical energy to thermal energy through sporadic electrical discharge, which occurs between a dielectric liquid-immersed workpiece and the electrode tool. The heat energy generates a plasma channel between the w.p and the tool. A pulses voltage range between 20-120 volts with a frequency of nearly 5 kHz that's applied between the w.p and the electrode is isolated by a tiny gap, usually between 0.01 – 0.5 mm [11], as shown in Figure 1.4.

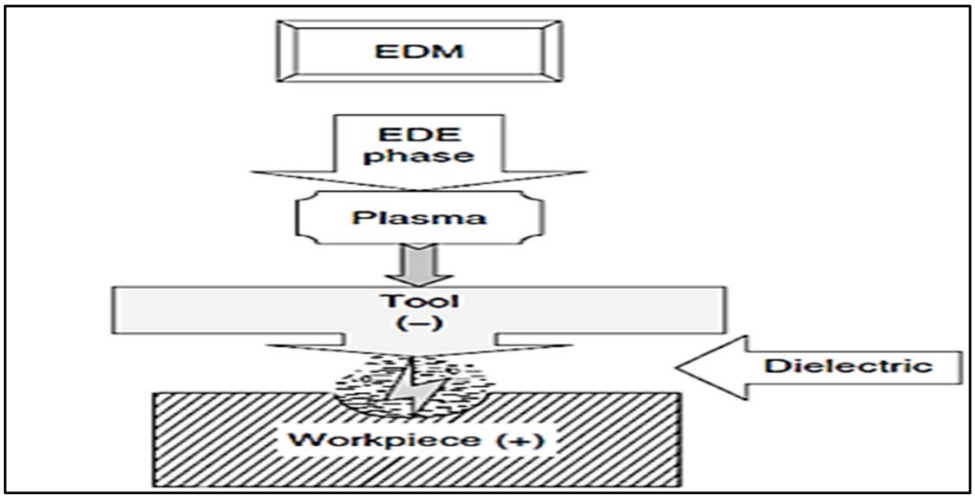

Figure 1.4. The mechanism of EDM [11].

The parameters are the peak current, pulse on, and pulse off, as illustrated in Figure 1.5. The resistance-capacitance generator pulses off voltage to remove the deposits during machining as shown in Figure 1.5 and Figure 1.6.

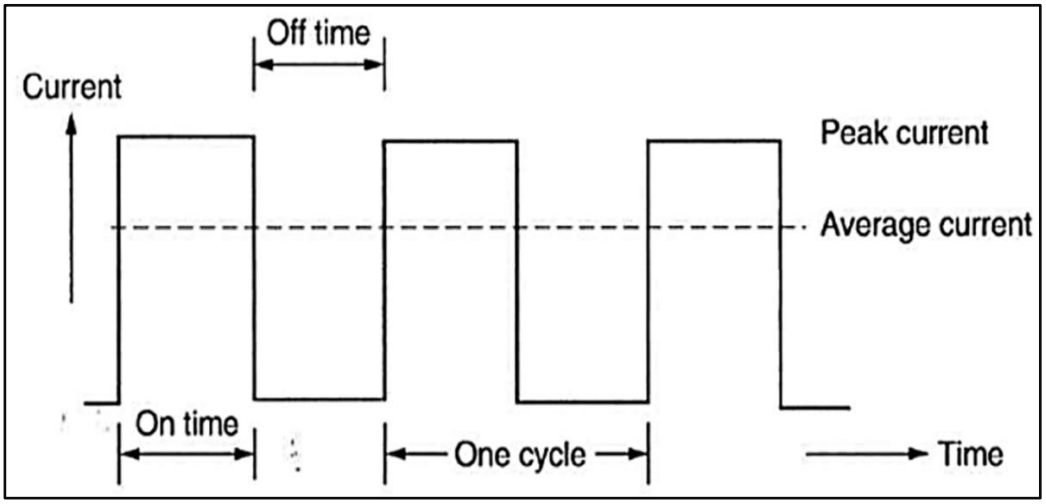

Figure 1.5. An example of the pulse current series for controlling the pulse generator [11].

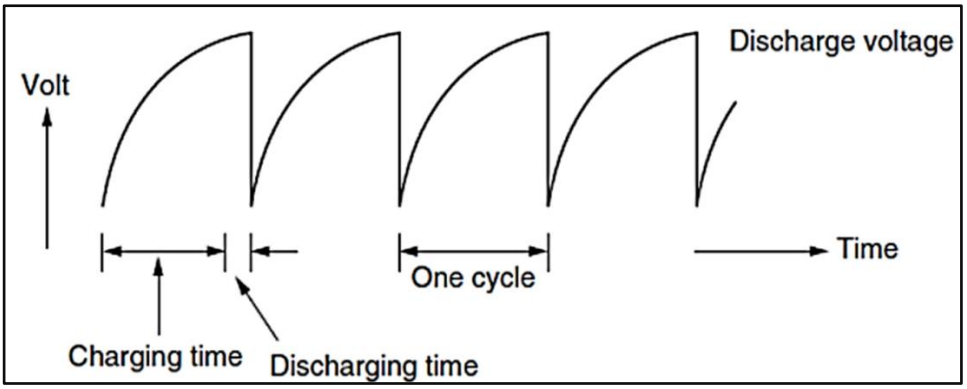

Figure 1.6. Calculating the voltage difference over time utilization of an RC generator [11].

1.3. ADVANTAGES AND DISADVANTAGES OF EDM

Advantages;

- EDM can be used to machine material that conducts electricity.
- It can produce complex and unique shapes.
- Easily automated.
- It is possible to achieve high accuracy and an amazing surface finish.
- All hard materials can be cut.
- Can complete all holes or curves with one pass.
- Repeatability

- It can create solid die preventing sectionalizing and grinding
- There is no tool force on the machine, the electrode, or the workpiece [12,13].

Disadvantages:

- The workpiece must be electrically conductive.
- The rate of material removal is slower.
- Inaccuracies can be caused by electrode wear.
- Cavities may be slightly tapered.
- May we need to use several tools because of electrode wear.
- EDM machine is expensive.
- Surface layer is relatively shallow and highly strained.
- The dielectric vapor might be dangerous [12,13].

1.4. APPLICATION OF EDM

The EDM method makes many tools, fixture components, and dies. The procedure can be used on many materials, from strong die steel alloys to soft copper, from big parts such as forging dies to sensitive workpieces like copper parts for vacuum tubes. EDM is finding a lot of usage in the industry for machining difficult-to-machine materials, including hard carbides, refractory metals, and heat-treated steels. It can also be used to cut workpieces that are too delicate to sustain the cutting force required by traditional machining [14], as shown in Figure 1.7.

There are many applications of the EDM method:

- EDM is most commonly used to manufacture molds in the tooling, die, and mold-making sectors. However, the aerospace, automotive, and electronic industries are seeing a growing need for EDM to produce prototypes and manufacturing parts.
- In addition, it can be used to mill particularly difficult metals, such as alloys, tool steels, and tungsten carbides, because of their extreme hardness.

- It is useful for curved hole drilling [15].
- For cold and hot forging, re-machining and repairing damaged dies is required.
- Making forging dies, such as forging dies for connecting rods.
- Dies for sintering.
- Tools for calibrating.

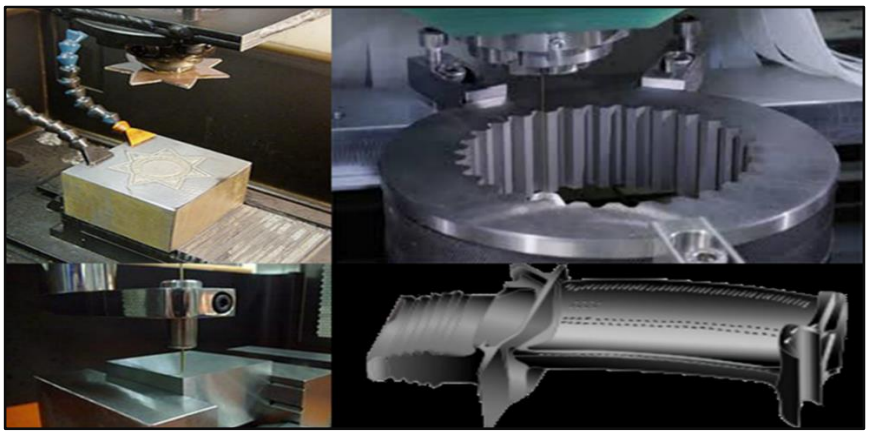

Figure 1.7. Applications of EDM [15].

1.5. TYPES OF THE EDM PROCESS

1.5.1. Sinking EDM

Two machining systems are used in the sinking-type EDM process. A regulated electrical spark is repeated till the electrode's shape is duplicated over the workpiece in the first system. And at the second system, the electrodes move in three-dimensional (3D) space to create a complicated 3D shape on the work surface. The temperature of the machining zone rises sharply throughout the sink EDM process (from 8000 to 12,000 °C). The machining variables are controlled and monitored by an EDM machine's unit control system, which also displays the process execution sequence. Various electrode (anode) materials are employed in the sinking EDM process. These are determined by the materials used in the workpiece, such as copper and copper-doped metals with graphite, etc. The electrode is frequently re-shaped during finishing procedures due to electrode wear. Because of its beneficial influence on the surface roughness and electrode wear rate, this method often employs a hydrocarbon dielectric fluid (EWR) [16], as shown in Figure 1.8.

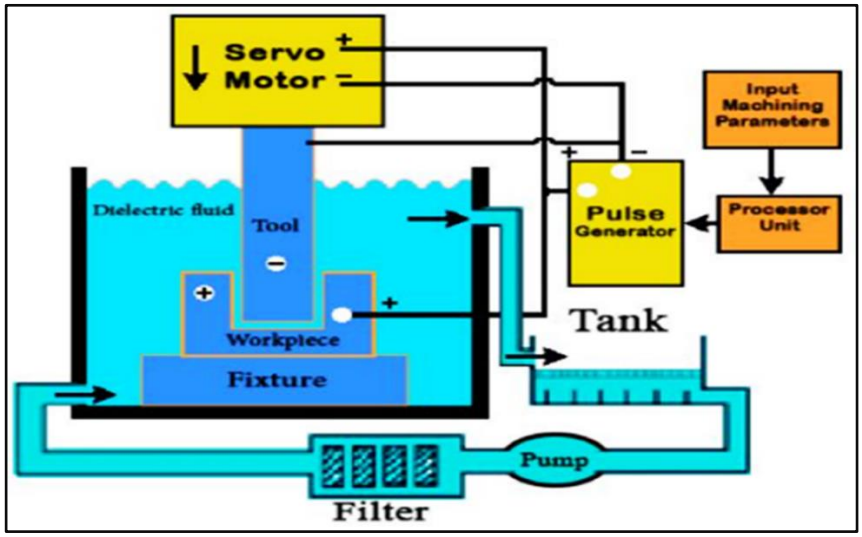

Figure 1.8. Die-sinking EDM [16].

1.5.2. Wire-cut EDM

EDM is performed using wire. Machining, also known as Spark EDM, is a type of electric thermal manufacturing technology that uses heat generated by electrical sparks to cut through metal. Machining uses deionized water, which is used to transport electricity, and a thin single-strand metal wire (typically brass). While feeding a thin single-strand brass wire through the workpiece, the tank containing the dielectric fluid, typically deionized water, is submerged. When working with exceptionally hard metals, the wire-cut EDM technique is a common way of cutting plates up to 300mm thick and creating punches, die sets and other equipment. Wire-cutting EDM is widely utilized for the removal of materials that have very few residual stresses because of the minimal cutting force needs that it has. Because of the low residual stresses, the mechanical properties of a material are expected to remain the same even if the energy or power per pulse is relatively low. On the other hand, material that has not been stress-relieved can deform while machining if stresses have not been alleviated. With wire electrical discharge machining (EDM), it is possible to produce intricate and accurate parts from conductive materials that are difficult to machine [17], as shown in Figure 1.9.

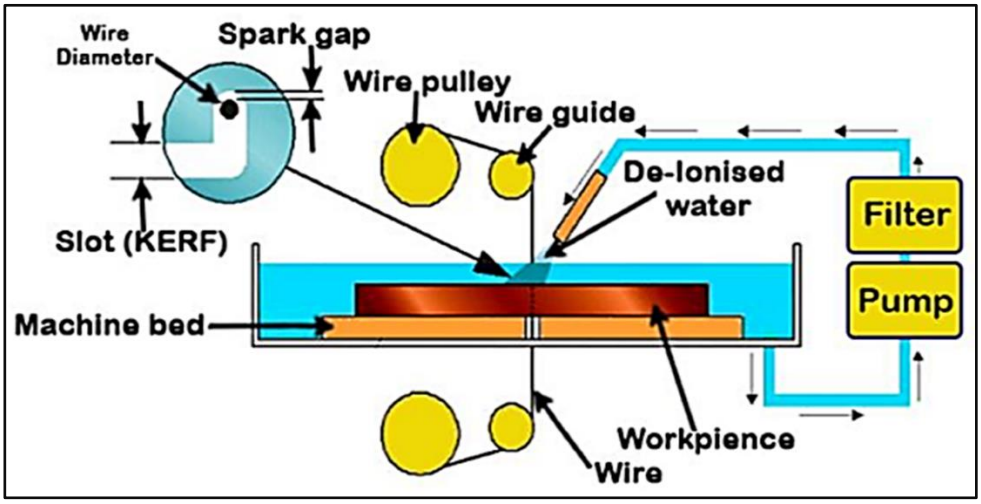

Figure 1.9. Wire EDM machining [17].

1.5.3. Micro EDM

It is the method of removal of materials by evaporation and melting during electric discharge. Micro EDM surface is damaged because of the effect thermally, which leads to a white layer and heat-affected zone, and the surface layer consists of residual stresses and micro-cracks. Also, the material removed from the two electrodes (workpiece and electrode tool) and the final surface have high roughness [18], as shown in Figure 1.10.

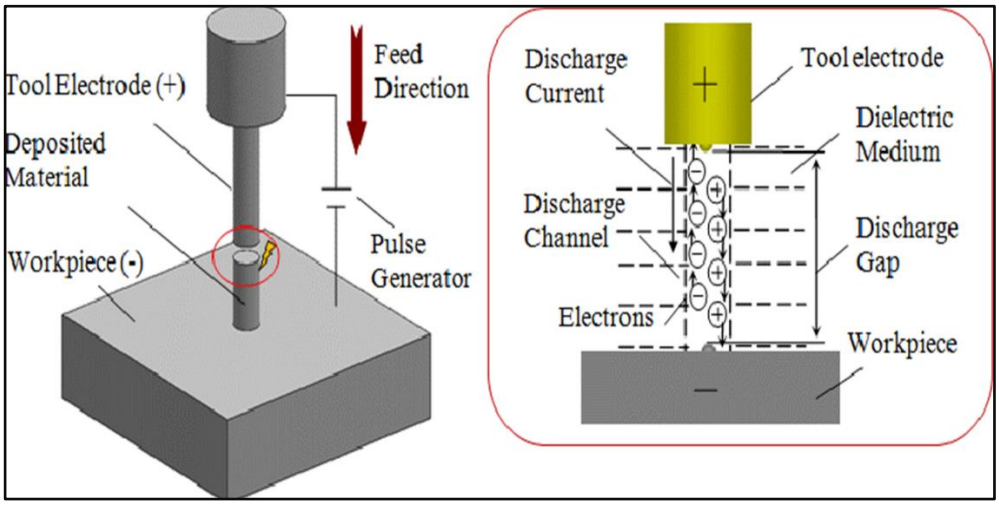

Figure 1.10. MICRO EDM process [18].

1.5.4. Powder-Mixed EDM

Powder-mixed EDM (PMEDM) is the fine-grained conductive powder added to the dielectric fluid in the EDM process to promote ionization and reduce the frequency rate of sparks between the electrode (tool) and workpiece. PMEDM generally depends on parameters such as powder materials, particle concentration, and particle size, as shown in Figure 1.11.

In this method, the appropriate materials of powder compose is mix up in the tank of dielectric fluid for the best circulation of the dielectric by mixing with the system that includes graphite (5%), silicon carbide (0.3%), chromium (0.9%), aluminum (20%), copper, etc. The addition of this powder alters the process mechanism significantly from that of traditional EDM.

The spark gap is improved by the other particle that ranges in size from 1 to 25 micrometers, and the applied voltage ranges from 80 to 320 volts [19].

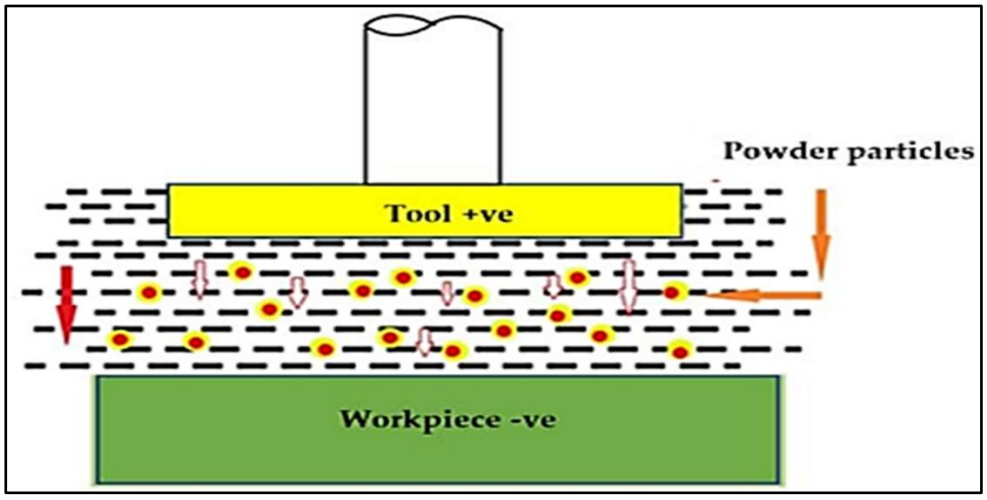

Figure 1.11. Powder-mixed EDM [19]

1.5.5. Dry EDM

Dry EDM is an environmentally responsible alternative to using air or gas as a dielectric medium in the EDM process to make oil-based EDM more environmentally friendly. Compressed air, argon, oxygen, nitrogen, helium, and other gases can be a

dielectric medium in dry EDM. Dry-EDM can achieve a higher materials removal rate, best surface roughness, low electrode wear, and fewer heat-affected zone for surface workpieces than the type of EDM in the fluid dielectric. In addition, high-pressure gas is fed into the tool electrode, removing molten material from the operating gap and cooling the electrode and workpiece. Moreover, dielectric gas is once used only [20], as shown in Figure 1.12.

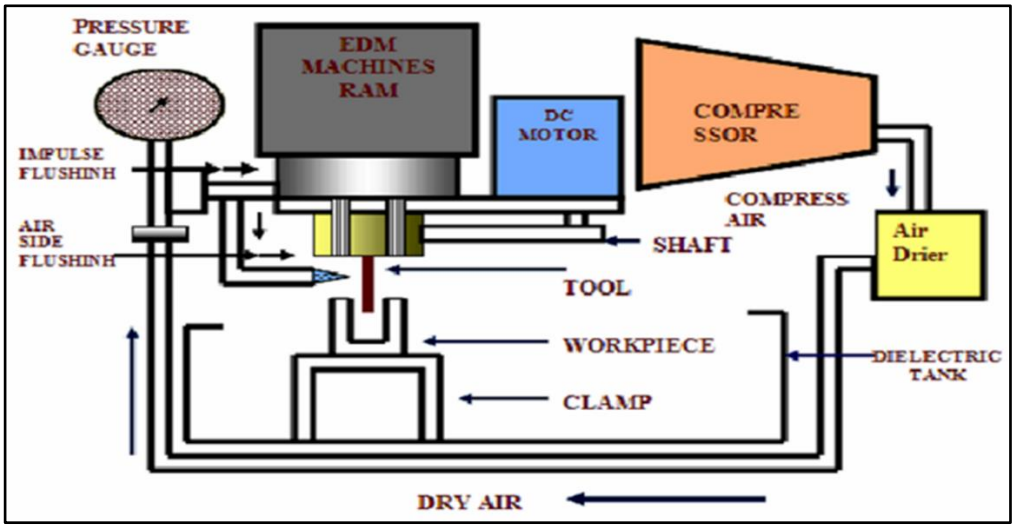

Figure 1.12. Dry – EDM [20].

1.5.6. Electrical Discharge Texturing (EDT)

Electrical discharge texturing (EDT) is an adaptation of formerly established electrical discharge machining (EDM) to the steel industry to meet the demands for roll surfaces. EDM is an eroding and removing process of the material from the surface by the quick action of electric sparks, commonly used to produce dies. In EDT, this process is achieved by applying consecutive spark discharges between a rotating roll and electrodes moving in the radial direction, which are separated by a small gap in hydrocarbon-based dielectric liquid Figure 1.13. In both processes, each spark melts and even evaporates a small amount of material due to the high local temperatures. Then, all is evaporated, and the fraction of the melted material is removed from the surface due to the flushing action of the dielectric liquid. The result is a small crater on the surface with a rapidly re-solidified layer. Successive discharges at high frequencies produce many randomly placed overlapping craters. The shape and the

depth of the craters, which determine the surface roughness of the rolls, depend mainly on the operational parameters such as discharge current, discharge duration, and polarity used [21].

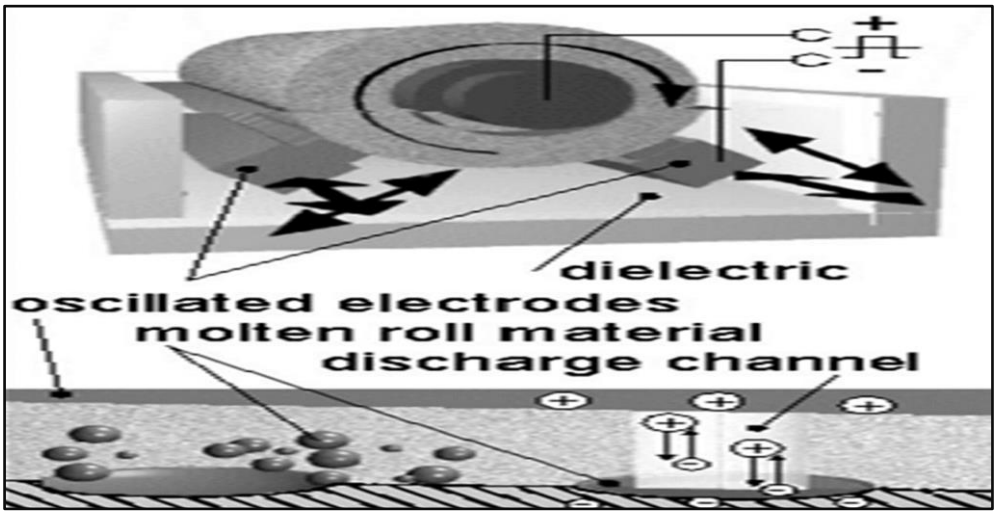

Figure 1.13. EDT process [22].

The molten metal solidifying at an extremely high rate after the discharge process forms the outermost recast layer observed on the cross-section, known as the white layer (WL), due to its resistance to conventional metallographic reagents. It is reported that WL is heavily alloyed with the pyrolysis products of cracked dielectric and by graphite or copper electrodes. Below this layer is a heat-affected zone (HAZ) where the emerged heat is not enough to cause melting but is sufficiently high to induce microstructural transformations. HAZ is composed of structurally different layers, such as the untempered martensite (UTM) layer and the over-tempered martensite (OTM) layer. The more intense pulse energy gives the thicker WL and heat-affected layers on the cross-section.

EDT deteriorates the mechanical properties of the skin pass mill work roll through softening of WL and OTM layer. The softening, particularly in the WL, would negatively affect the service life and the performance of work rolls. Consequently, chromium plating of EDT work rolls has been a common method, providing four times longer service life with an additional advantage of a higher Pc value for a skin pass mill work roll [23].

1.6. SURFACE LAYERS AFTER EDM

According to the research, when manufacturing tool steel, three different layers can be seen in the surface layers: white layer, heat zone, and tempered. The EDM's work has changed the recast layer's characteristics and metallurgical structure. A white layer on top of the liquid crystallizes when it is cooled at a high rate. The energy and length of the pulse determine the thickness of this bottom melted zone. A chemically affected layer lies underneath the top layer, with changes in average chemical properties and potential phase changes. Removed melting and a small amount of electrode materials produce spheres and splash the workpiece's surface, resulting in a scattered EDM surface layer. The impacts of this layer may induce early failure of the participant in some applications if it is too thick or is not decreased or eliminated by polishing [24], as shown in Figure 1.14.

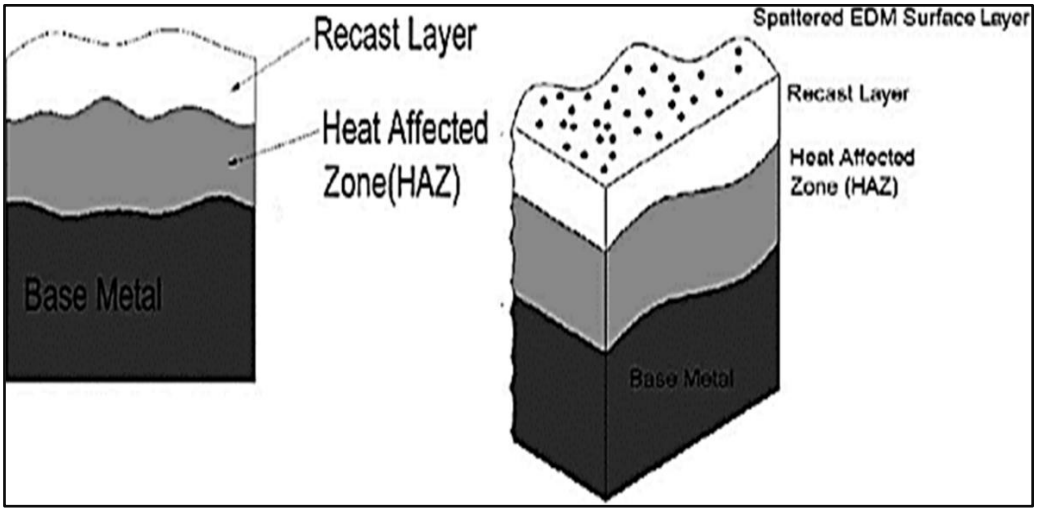

Figure 1.14. Surface layers after the EDM process [25].

1.7. PROBLEM OF RESEARCH

White layer thickness plays a critical role in the electrical discharge machining methods that directly affect the surface's accuracy and roughness.

1.8. THE AIM OF THIS THESIS

- Is to reduce the thickness of the harmful white layer as a result of cutting by an electric spark.
- Searching for suitable current values for the electric spark-cutting process.
- Improving the performance of the product surface as much as possible.
- Reduce the surface roughness value of the product.

1.9. THESIS LAYOUTS

This thesis includes five chapters, as follows:

- Chapter One: The introduction and principle of the electrical discharge machining (EDM) process.
- Chapter Two: Review of the literature
- Chapter Three: The experimental work.
- Chapter four: The experiment results and discussion.
- Chapter five: The main conclusions of the thesis and recommendations for future work

PART 2

LITERATURE REVIEW

2.1. LITERATURE RELATED TO THE WHITE LAYER THICKNESS IN (EDM) PROCESS

Dinesh Kumar et al. (2022) [26], studied the prediction of the white layer thickness of AISI A2 steel, and a response-surface methodology-based comprehensive mathematical model was created. Also, the impacts of various process factors on the WLT were shown. The best combination of process variables was determined, and the minimum value of WLT was attained by combining low pulse-on time and current with high-value pulse-off time.

Li Li et al. (2021) [27], studied the effects of tools specifications, including (ceramic tools and PSBN tools) on the (WLT) generated by cutting harding steel with various thermal conductivity and wear with various cutting speeds. The author found that the tools' thermal conductivities, wear rates, and cutting speed had an important impact on the WLT, cutting temperature, and cutting force. In addition, the WLT increased initially, then reduced with rising flank temperature. The maximum temperature range at the maximum WLT was the final temperature for austenite transformation, according to the finding.

M. Neslusan et al. (2020) [28], studied the surface integrity of hard steel 100Cr6 by analyzing the function of electrode tool wear and the thermo-mechanical loads due to forming surface and how it gives rise to the white layer thickness. The total force was divided into components related to chip separation Fγ and component Fα, primarily related to flank wear land. The results showed that quick self-cooling in hard turning affected surface integrity when the heating rates were very high. In addition, the hard-turning machine can form a white layer. The insert rake geometry, which contributes

to the cutting force component of F associated with chip separation, was also substantially influenced by tool wear. As a result, chip formation was determined by the tool wear rate.

T. Muthuramalingam et al. (2019) [29], predicted white layer thickness using ANFIS on machining treated silicon steel. Three parameters were used for training because of their importance in determining the (WLT), such as circuit voltage, duty factor, and peak current. The reliability of prediction was determined when comparing the predicted results from the model testing with the real-time measured values. According to the results of the experiments, the created adaptive network-based fuzzy inference system can accurately estimate the average of (WLT) with a 96.8% accuracy. Electrical process parameters have also been found to play a significant role in determining average WLT.

Saad M.Ali and Ahmed N.Al-khazraji (2021) [30], studied the EDM process, final heat generated on WLT, and fatigue of die steel type AISI D2, finite elements from ANSYS 15.0 were used to set up the transient thermal and multiphysics analyses domain loading models. The electrode tool materials were graphite and copper. Two load stages, six sub-periods, four heating, two cooling cycles, six temperature values, and four thermal or convective models were used to simulate the entrance setting time research. Workpiece and kerosene dielectric, electrode heat flux fractions, discharge channel averages, discharge spark averages, heat generation averages, and more are all factors that need to be considered (WLT). When utilizing graphite tool electrodes for the EDM process, the minimum WLT values were 8.32 meters, in contrast to the copper tool electrodes, which produced higher WLT values. A forty percent increase above the previous situation. While utilizing graphite tool electrodes, the diameters of the discharge spark craters were evaluated and found to be at their smallest possible values. This was determined through the use of micrographics and microstructures.

Shukry H. Aghdeab and Haneen L Aldulaimy (2018) [31], studied the influence of various fluid dielectrics on MRR, WL, and SR in EDM machining. Different fluids, such as transformer oil, gas oil, and vegetable oil, were used to get the higher values of MRR with the lowest roughness of the surface and the minimum values of WLT of

the 316L stainless steel (workpiece), and the electrode was copper. The results showed the direct effect of current and pulse on time by causing higher MRR, SR, and the WLT was thicker. It also showed that the vegetable kind causes high MRR, less SR, and the best oil used in EDM. The dielectric viscosity was an important feature that influenced WLT. At lower viscosity, a thinner white layer is produced.

Arfaoui, S. et al. (2017) [32], studied the relationship between the cutting parameters and the thickness of the white layer, while 2D orthogonal cutting with hardened AISI52100 steel was developed to look at the effect of the cutting parameter (CPP) on the thickness of the white layer (WL). The tools' flank wear, geometry, materials characteristics, and cutting condition were all numerical simulations. The numerical findings showed that thick WLs were unavoidable except for low workpiece hardness, where relatively thin WLs are observed. The results also showed that the WL thickness was affected by all of the CPPs used.

Maher, I.(2017) [33], discussed the effects of many factors on the quality of the surface by reducing the WLT. The result discovered that WLT increased when the pulse on-time was increasing and decreased when the pulse off-time was growing. In addition, the thickness of (WLT) was depended on the properties of wire electrodes, such as mechanical, electrical, physical, and geometrical.

F. Klocke et al. (2016) [34], studied the composition and structure of (WLT) in the WEDM process and showed that the top surface of the workpiece is stretched the greatest in components in bending load. As a result, the mechanical performance of the element is highly dependent on the features of this layer. The results achieved the compositions of a white layer were examined first. The recast layer contains copper and zinc from the wire electrode and molybdenum from the molten parent material's carbides. Chromium and vanadium were not assigned to a specific layer and were mixed up with the white layer. In the second step, TEM analyses were used to identify the metallurgical state of the recast layer. The amorphous microstructure dominates the white layer. Crystalline structures extend into amorphous regions at the material's border. In the third step, the next phase involved determining the local hardness of the white coating and the area beneath it. The recast layer's toughness had been greatly

improved. Compared to the original material, the white layer's hardness roughly doubles, and the effects of the workpiece edge's geometry could be eliminated.

Ahmed Al-Khazraji et al. (2016) [35], studies impacting the powder mixing (EDM) variables using graphite and copper electrodes and the SiC powder on the (WLT) and found that the lowest value of WLT is 5.0 μm and 5.57 μm was reached at a high degree of current and low degree of current together with a low pulse. It meant there was an improvement in WLT by 134% & 110% compared to using the graphite and copper electrodes and kerosene dielectric lonely.

I. Maher et al. (2016) [36], studied the comparison and discussion of measured values of WLT using a neuro-fuzzy inference system (ANFIS) to predict the (WLT) in (WEDM) utilizing CuZn-covered wire electrode. The conclusion was that the minimum rate of WLT when the current and TON were low, and WLT reached high levels when TOFF was high.

U. Shrinivas Balraj et al. (2014) [37], studied the thickness of the white layer and the density of the surface crack of RENE80-Nickel super alloy during EDM. In addition, the direct effect of parameters studied, such as current, pulse on-time, pulse off-time, and the speed of rotation of electrodes on the surface safety specifications, such as (WLT) and (SCD), using the Taguchi method. The results showed the responses were influenced directly by current and pulse-on, where the IP and Ton increased due to an increase in WLT, but the rise of current and TON was according to the reduce in the surface crack density.

R. Matin et al. (2013) [38], studied the effects of electrodes tools geometry in EDM on the surface integrity components of DIN 1.2379 tool steel. The components are WLT, microhardness, density crack, and HAZ. The results were that the depth of the heat zone and WLT on the geometry of the square electrode was maximum, and the highest rate of crack density was with a triangular electrode. At the same time, the microhardness results indicated an increase in the degree of hardness in the layers closest to the surface and then a decrease in it.

Ulas Caydas and Ahmet Hascalik (2007) [39], studied the analysis and modeling of electrode wear and (WLT) during responsibility surface methodology using the sinking EDM method. The results showed that the IP was the critical factor affecting EW and WLT. On the second hand, whereas there were no effects on the (EW and WLT) either by pulse off-time.

W.J. Tomlinson et al.(1991) [40], studied the white layer's nature formed of EN.24 steel, whereby centerless grinding. The impact of the workpiece's speed rate and the grinding-wheel stipulation on the white layer thickness found the thickness of WLT increased when the level of infeed increased, decreased when the speed of work increased and expanded when the grinding wheels corrosion.

2.2. LITERATURE RELATED TO DIE-SINKING AND THE PARAMETERS IN (EDM) PROCESS

Shukry H. Aghdeab et al. (2021) [41], studied the effect of I_P, T_{ON}, and T_{OFF} on MRR and SR for workpiece tool steel AISI L2 and the electrode is pure copper during EDM machining. A Full factorial technique was Applied to design machine parameters and identify the best process parameters for an electric spark. The results demonstrated the perfect surface roughness of AISI L2 created at a minimum degree of current, TON, and TOFF, so low current and pulse on time were used to achieve good surface roughness. In addition, the maximum MRR was created at a high current and pulse on time. As shown in Fig. (2.1)

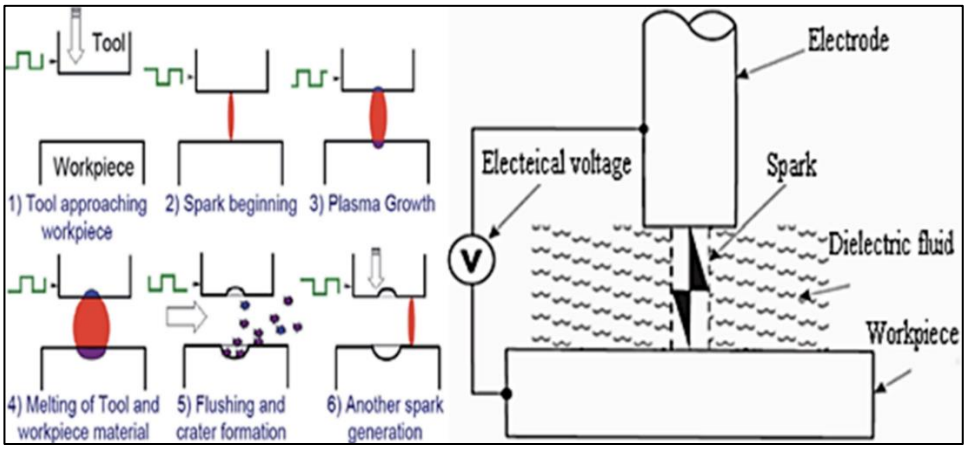

Figure 2.1. Spark beginning in EDM process and EDM Process Mechanism.

Esmaeil Jafari et al. (2020) [42], investigated the impact of EDM parameters such as current, voltage, pulse off, and pulse on of the machined surface microstructure. The procedure creates thermal stresses, which cause extensive micro-cracks to appear on the top surface of the spark EDM-treated object. The impact of EDM settings on surface roughness and the strength of microcracks has been quantified using test findings and regression analysis. The results revealed that the current pulse-on is the direct parameter affecting the accuracy of the final surface generated by the spark of the EDM process. The link between micro-cracks intensity and the characteristic diameter of the sparks erosion layer in the spark EDM method was investigated for various pulse-on parameters. The association established for the early stage of the pulse on the parameter is comparable to that found for the voltage, current, and off-time parameters. An increase in the on-time parameter reduced micro-crack strength due to heat transfer caused by the longer pulse length on the parameter. The excellent heat treatment response of CK45 tool steel resulted in a relatively homogeneous dispersion of micro-cracks on the machined surface. The bidirectional performance of the pulse on the parameter is projected to be resolved by using a dielectric liquid with much-improved heat transferability.

Shukry H.Aghdeab et al.(2020) [43], studied the best parameters in EDM through high-speed steel AISI M2. The material of the workpiece and electrode used copper and brass, respectively. Current (10, 24, and 42A), pulse on time (100, 150, and 200μm), and pulse off time (4, 12, and 25 μm) are parameters that affected MRR and EWR. The results revealed that the copper electrode provided a higher MRR and a lower EWR value, and the pulse current was the most important component that influenced the process response of EWR and MRR.

Shukry H. Aghdeab and Anwer Q. Abdulnabi (2022) [44], investigated the influence of changed voltage degrees on EWR using EDM machining and stainless steel materials AISI 444. The parameters used in this research were voltage, current, TON, and TOFF. The results found that the EWR increased with voltage, current, and TON, but the EWR reduced when increasing TOFF. EWR reached 0.270633 mm3/min at Toff 3μs and the greatest voltage 240 V, current 50A, and Ton 400μs.

EWR was 0.093507 mm3/min at Toff 12 μs, voltage 140 V, current 12 A, and Ton 400 μs.

ShukryH. Aghdeaba et al. (2021) [45], analyzed the influence of gab space on the surface roughness and how reducing the roughness using copper electrode about AISI M6. The values of input parameters used current (10, 25, and 50A), gab distance (0.015, 0.12, and 0.24mm), and Ton (100, 200, and 300μs). Experiments found that increased gab space (SG) decreased surface roughness (RA).

Rogério F. Santos et al.(2016) [46], analyzed nitriding-AISI 4140-steel with electric discharges generated by sink EDM equipment. The machining process used a copper electrode tool and a dielectric fluid made of deionized urea and water. Laser profilometry, glow discharge optical emission spectroscopy (GDOES), x-ray diffraction (XRD), scanning electron microscopy (SEM), and optical microscopy were some of the techniques used. The proposed mechanism for the nitriding process was ion implantation, and the layer under investigation was demonstrated to have toughened. However, when the hardness declined under the surface, it reduced the amount of nitrogen injected.

Harpreet Singh and Amandeep Singh (2012) [47], investigated the influence of TON and TOFF on the operation of die steel type AISI D3 and used brass and copper electrode in the EDM, also using the kerosene oil as a dielectric. The results showed that the MRR increased when the pulse-off increased. In addition, in the brass electrode, the MRR increased with increasing of Toff, and in the copper electrode, it decreased.

G.P. Rodriguez et al. (2009) [48], studied the experimental surface alloying of chromium martensitic tool steel elements (AISI H13, ~55HRC) in die-sinking EDM used powder metallurgy electrodes as a technique of improving specimen wear resistance without having to resort to a subsequent coating procedure. When utilizing WC/Co electrodes, optical and SEM studies revealed an ~ 8-meter recast cemented layer. The author showed that compared to those achieved using typical copper and graphite electrodes, the white coatings of machined steel surfaces were larger and more

uniform. The modified/alloyed surfaces had fewer micro-cracks and interface imperfections. When non-conventional electrodes were used, surface degradation was shown to be significantly decreased. Martensite and substoichiometric compositions, such as Co6W6C, W3C, and WC1-x, made up most of the changed EDM surface layers. This was caused by powder material being transferred from the electrode to the surface of the workpiece during the machining process.

Abedpour S et al. (2008) [49], studied the effects of EDM's characteristic parameters on the surface's microstructure in alloy steel ck45. A thorough experimental program was carried out to investigate the impact of types of EDM parameters on the machined surface quality. The relationship between EDM parameters was quantified using regress analysis and test results. As a result of this study's prediction of the effect of EDM parameters on surface quality, it will be possible to make informed decisions about how to set parameters to their optimal values and create the best die surface quality in a reasonable amount of time and money.

Y Y Tsai and C. T.Lu, (2007) [50], studied the effect of current on EDM machining and used different current features, such as initial current, current increasing slope, and impulse patterns. The workpiece used tungsten carbide. Rectangular current impulse (RCI) produced a high value in MRR and high RWR; because of the low beginning current and long rising time, the energy density was low, resulting in a low MRR and wear ratio. However, a low initial current and a long time for the current to rise causes a larger discharge arc. When used (trapezoidal current impulse) TCI with small beginning current due to reducing RWR and the MRR became low. The results found a small energy density when applying a small beginning current and low MRR and WR.

Masanori Kunieda (2005) [51], investigated the measure of the work reaction force created in EDM using the split Hokinson method. The proper form of a wave of the reaction force was acquired using this method, which was not influenced by the measuring system's intrinsic frequency. The response force was studied with the dielectric and discharge point, and it found When compared to one pulse discharge in liquid, the reaction force caused by a single pulse discharge in the air is negligibly

small. When a one-pulse discharge happened at an off-centered position, the reaction force acting was minimum, and the bubble's oscillation period was shorter. Also, when two pulse discharges occurred in quick succession at the same location, the second discharge did not affect the reaction force. When two pulse discharges happen at different points in quick succession, the reaction force was a combination of the separate reaction forces created by each discharge. However, the second discharge's reaction force was less.

Yongshun Zhao et al, (2003) [52], explained the development of a modeling process for the EDM die-sinking process with a linear motor. The advantages of incorporating a linear motor into an EDM die-sinker were discussed. The current model was used to determine the minimum gap distance required for sparks to form and to assess the potential of spark creation between the electrode and workpiece surfaces. The crater created by the single spark was also computed. The topology of the final machined surface was projected. The total surface roughness simulated as a function of current and discharge duration. The experiment was carried out to investigate the impacts of machining conditions and to test the accuracy of the established geometric model.

Masanori Kunieda and Masakazu Kiyohara(1998) [53], used a new simulation approach to simulate workpiece geometry degraded by the die-sinking EDM for a faithful copy of the real events occurring in the gap. The algorithm was a simple procedure cycle, which included determining the following discharge location with the lowest dielectric breakdown strength, removing the anode and cathode, supplying the tool electrode, and spreading the debris particle. The simulation considered several relevant aspects, including tool electrodes wear, gap width allocation, tool electrode curvature, and inclination, all of which interact in a complicated way.

The innovation of the research:

According to the literature, as mentioned above study, whereas more experimental research investigated input parameters, the type of metal, and the voltage value for the electrical discharge machining process, fewer numerical publications investigated those factors. Many articles investigate the white layer thickness in whole types of

metals. Still, no one has looked into the effects of white layer thickness in CK45 DIN 17200 in electrical discharge machining because it is challenging to investigate the WLT for the workpiece experimentally. The numerical analysis can be useful in this case. The current uses three steps: pulse on time, pulse off time, and pulse on time. The effect of current and pulse time on WLT will be examined in this research.

This thesis examines the machining of medium carbon steel CK45 DIN17200 with the EDM method and suitable input parameters (Ip, Ton, and Toff). This study aims to reduce the thickness of the white area caused by the thermal effect of the electric spark during the cutting process by using different current and pulse duration values, and also to calculate the amount of material removed, electrode wear, and surface roughness of the cut product. The procedure (full factorial design) and the mathematical model that was used to predict the various response quality were built with the software Minitab 17 and used factorial notation. The model's results were then assessed and compared to the values obtained through experimentation in Minitab 17.

PART 3

EXPERIMENTAL WORK

3.1. INTRODUCTION

In this section, the practical experimentation and selection of EDM machining parameters are the primary topic. In the EDM process, the input parameters are current (IP), pulse on-time (TON), and pulse off-time (TOFF). The effect of input parameters on white layer thickness (WLT), material removal rate (MRR), surface roughness (Ra), and electrode wear ratio (EWR) have been assessed. This part also contains the characteristic of the CHMER machine, dielectric liquid, electrode, and workpiece. Figure 3.1. shows the experimental procedure.

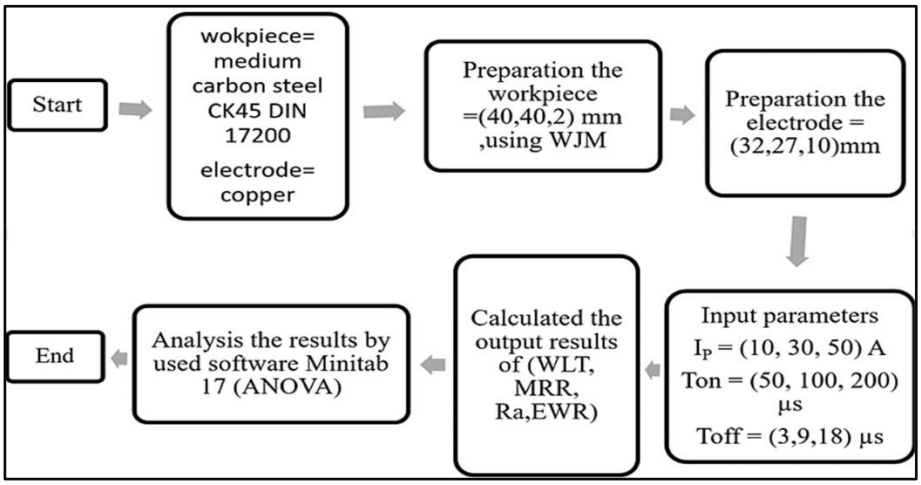

Figure 3.1. Experimental plan chart.

3.2. EDM MACHINE

The experiments were carried out on a CHMER brand CM 323C model EDM machine in the training and workshop center of the Baghdad University of Technology. Figure 3.2. and 3.3. shows the machine and electrode holder of the machine, respectively.

This machine was designed by a Computer Aided Design (CAD) technique to ensure that it performs without deformation. The electrode's polarity was set to positive, while the workpiece was set to negative. Other features of the machine, which consist of many components such as a dielectric liquid tank, a pumping system, a table for placing the workpiece, a filtration system, and a tool holder to hold the electrode on the workpiece, are given in Table 3.1. Specifications of the power source by which the machine was powered in this experiment are listed in Table 3.2.

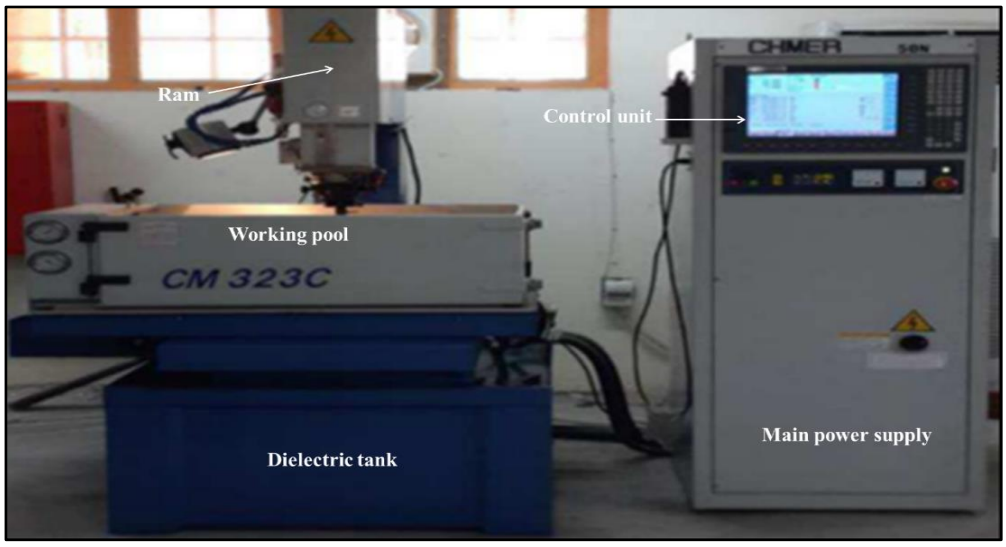

Figure 3.2. CHMER EDM machine at the UOT's training and workshop center.

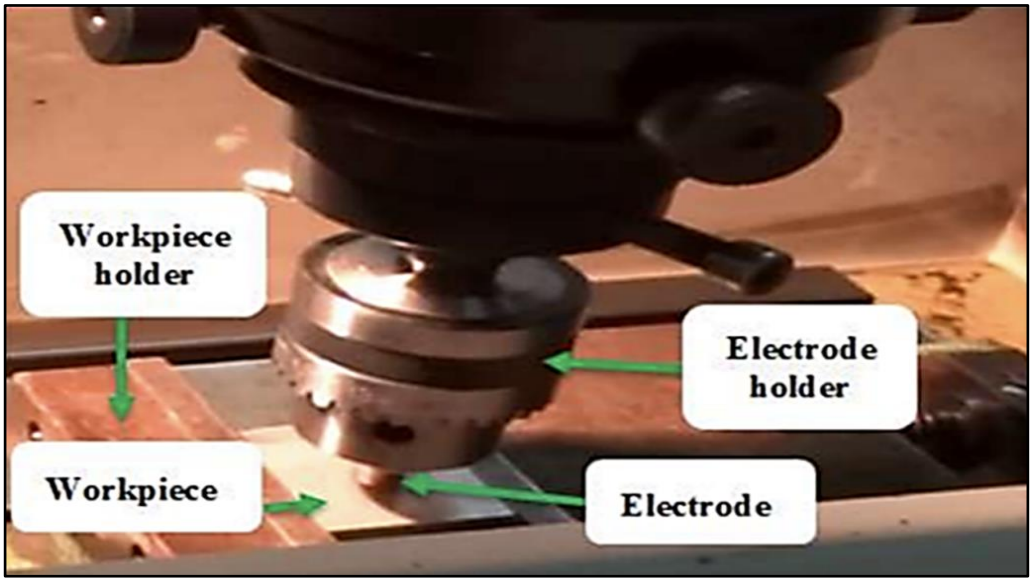

Figure 3.3. Workpiece, electrode, and its holder.

Table 3.1. CHMER EDM machine specs [54]

Table size (W×D)	**500×350 mm**
Work tank size (W×D×H)	820×500×300 mm
Table travel (X, Y)	300×200 mm
Ram travel (Z)	300 mm
Maximum electrode weight	60 kg

Table 3.2. The power supply specifications [54].

Model	**50N**	**Unit**
Maximum machining current	50	A
Maximum power input	5	kVA
Electrode Wear rate	0.2	%
Best surface roughness (Ra)	0.25	μm
Outside dimensions	620×850×1860	μm
Weight	180/396	kg/lb

3.3. THE FLUID OF THE DIELECTRIC

The dielectric fluid impacts various characteristics of the EDM process, including productivity in terms of WLT, MRR, and EWR, cost, and the Ra of the produced component. To name a few obligatory considerations, we must consider health, safety, and the surrounding environment. In this experiment, dielectrics such as transformer oil are used to cut medium carbon steel. Table 3.3. lists the physical parameters of transformer oil.

Table 3.3. Transformer oil's physical properties.

Density (g/cm^3) at 15 °C	**Viscosity at 23°C**	**Boiling point °C**	**specific heat (KJ=kg.K)**	**Flashpoint °C**
0.850	28.01	280	1.63	140

3.4. THE WORKPIECE MATERIAL

When choosing materials for this research, it is critical to consider great hardness. As a result, CK45 DIN17200 was used. It is a medium carbon steel and also a general engineering structural steel. It has good machinability and high tensile properties. CK45 steel normally supplies steel plates, round, flat, square, and hexagonal bars, moreover pipes. It usually provides the hot rolled black surface, cold drawn bright surface, large size forging is better. Delivery hardness 18-25HRc. Ck45 DIN17200 usage is very wide in industry products. Such as axles, nuts, bolts, crankshafts, gears, bearings, guide bars, wheel forging, etc. According to American: ASTM A29/A29M AISI 1045, the specifications of medium carbon steel metal material is (40x40x2) mm for the workpiece. The shape of the workpiece is depicted in Figure 3.4. And Table 3.4. presents the chemical structure of CK45 DIN 17200. The analysis of the sample's chemical composition, mechanical qualities, and physical features was analyzed according to international standards as specified in Tables 3.4., 3.5., and 3.6.

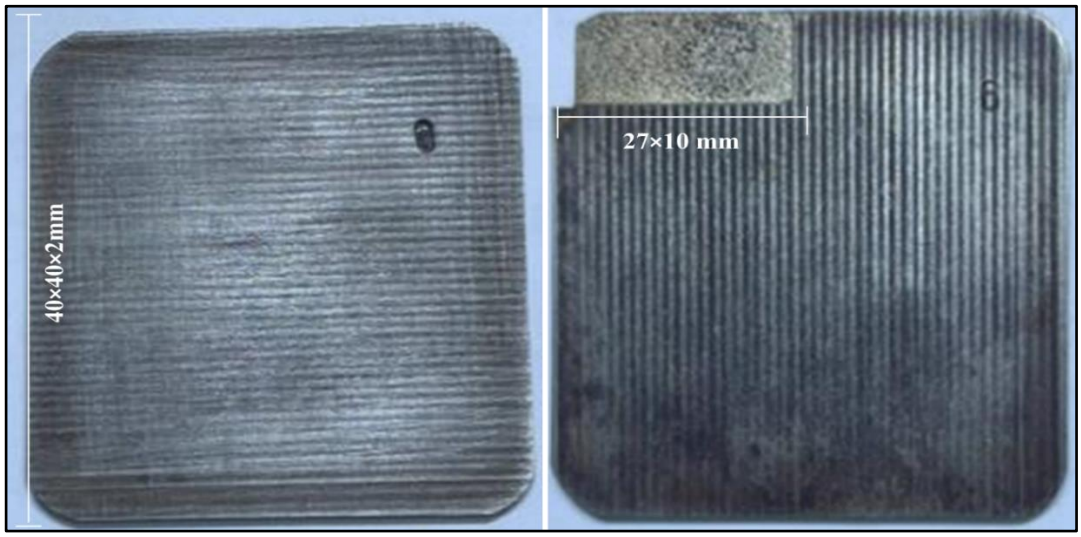

Figure 3.4. The workpiece before and after cutting by EDM machine.

Table 3.4. Chemical composition of the workpiece.

Sample	weight
C	0.41
Si	0.305
Mn	0.677
P	0.018
S	0.0592
Cr	0.139
Mo	0.0307
Ni	0.0771
Al	0.049
Cu	0.199
Co	0.0141
W	0.018
Fe	bal

Table 3.5. The mechanical properties of the workpiece.

Mechanical properties	values
Tensile Strength (MPa)	585
Poisson s ratio	0.29
Yield strength (MPa)	450
Hardness, HRB	79.5
Modulus of Elasticity(GPa)	200
Shear Modulus (GPa)	80

Table 3.6. Physical properties of the electrode.

Physical properties	description
Thermal conductivity at 20°C (w/m.k)	25
Thermal expansion coefficient (10.E-6(1/°C))	11.2
Melting point (°C)	1450
Density (Kg/cm³)	7.85
Specific heat (j/kg.k)	460

3.5. THE ELECTRODE TOOL MATERIAL

Brass, copper, and copper alloys, graphite, molybdenum, silver, and tungsten are all used in EDM electrodes. High corrosion resistance, superior material conductivity, and a high melting point are the most significant factors when choosing EDM electrodes,

as they increase the tool's life. Copper and copper alloys are more resistant to EDM wear than other metals. The size of the copper electrode is (32x 27x 10) mm as shown in Figure 3.5. the chemical composition, physical, and mechanical properties of this electrode are shown in Tables 3.7, 3.8, and 3.9, respectively. These tests were performed at Baghdad's Iraqi Standard and Quality Control Agency.

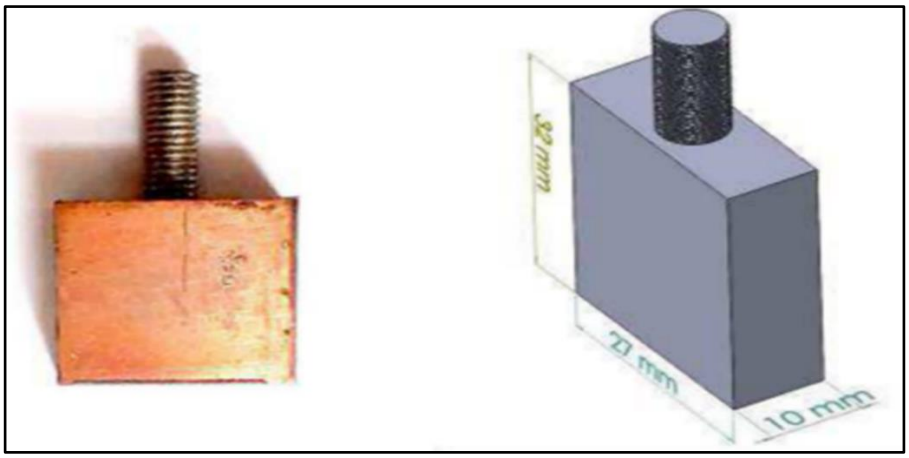

Figure 3.5. Before cutting the electrode, pure copper.

Table 3.7. Chemical composition of the copper electrode.

Sample	Al	S	Sn	P	Fe	Mn	Cr	Sb	Cu
Weight%	0.0023	0.0006	0.0018	0.0008	0.024	<0.0004	0.0071	0.0082	99.9

Table 3.8. Properties of the physical electrode.

Properties of the Physical	
Electrical Conductivity (10.E-6 S/m)	58.55
Thermal Conductivity at 20℃ (W/m.k)	391
Electrical Resistivity at 20℃ (10. E-8Ω.m)	1.7
Thermal expansion Coefficient (10. E-6(1/℃))	17.3
Melting Point (℃)	1083
Density (g/cm³)	8.94

Table 3.9. The electrode's mechanical properties.

Mechanical characteristics	
Tensile Strength (MPa)	620
Elongation	7
Yield Strength (MPa)	579
Hardness (HRB)	62

3.6. PARAMETERS OF THE MACHINING

Depending on a parameter available at the EDM CHMER computer, the parameters involved in this experiment are displayed in Figure 3.5.

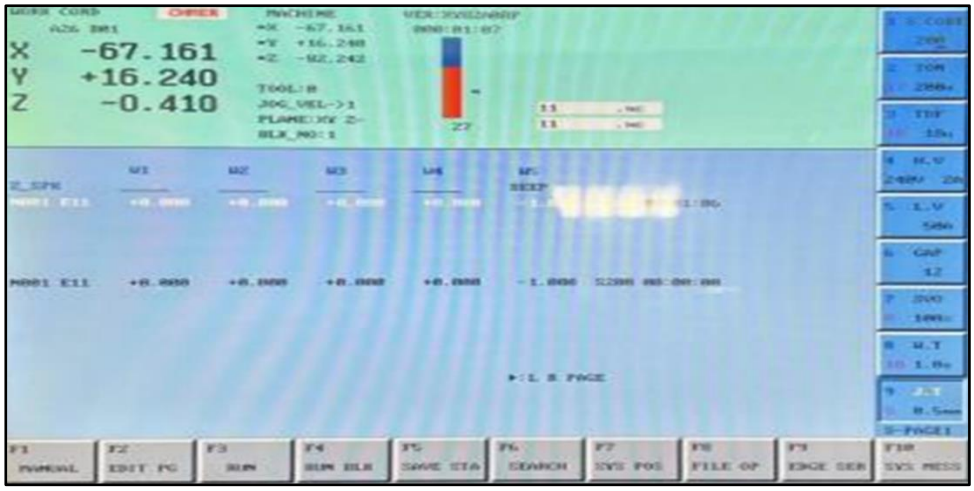

Figure 3.6. CHMER machine EDM monitor.

The EDM machine's settings

The S code number for a function can be located in a list titled "S codes" (0-9). Because the S code (200) is the most suitable response to take in this situation, it has been chosen.

- T_{on} is used to adjust tone, and the step range for tone adjustment is from 1 to 24. Three different values of (Ton) are chosen: 50, 100, and 200 (μs). The pulse-on-time code with the shortest duration is 1, whereas the pulse-on code with the longest duration is (24).

- The pulse-off setting contains a range of steps from 1 to 24 that can be used to set the pulse time off (T_{off}). (Toff) has the values of 3, 9, and 18 milliseconds assigned to them.
- It is choosing an option from the list that drops down from the top (240 V). HV, which stands for "high voltage," refers to operating in high voltage mode. Increasing operational stability and speed is feasible but doing so will extend the cavity and cause the electrodes to wear out faster.
- The discharge rate can be changed using a setting determined by the "current" factor. The numbers: 10, 30, and 50 have been selected at this time (Ampere).
- Knowing about the gap voltage is necessary to calculate the gap discharge voltage. The value determines the distance, so a smaller value means a shorter length. The gap might range from one (1) to (16). Generally, (50 V) and (100 V) are acceptable values. The gap value was selected as the number (12 V), equivalent to (0.3125 mm).
- Adjusting the feed rate of an axis via servo feed can improve discharge stability (SVO). There are a total of sixteen (16) steps to complete. An option is chosen from the list that drops down from the top (100%).
- The WT parameter is used to set the operating time interval, which can be selected from 0.1 to 10 seconds and adjusted in (40) step increments. one second has been decided upon in this study.
- It is used to set the jumping time (JT) length and the distance that they must hop in the opposite direction. The jump's height equals the distance separating the first and second steps (120). The value (0.2 mm) has been decided.

3.7. EXPERIMENT METHODOLOGY

The experiments were carried out on a CHMER brand die-sinking EDM machine. The EDM procedure is carried out on an anode constructed of carbon steel CK45 DIN 17200. A copper cathode tool is used as an electrode, and transformer oil is also utilized. The procedure is as follows:

- Selection of the workpiece and testing on a hardness device in the Lab and Engineering inspection (SIER).as shown in Figure 3.6. and 3.7.

Figure 3.7. AMETEM testing hardness measurement device model (CM 323C).

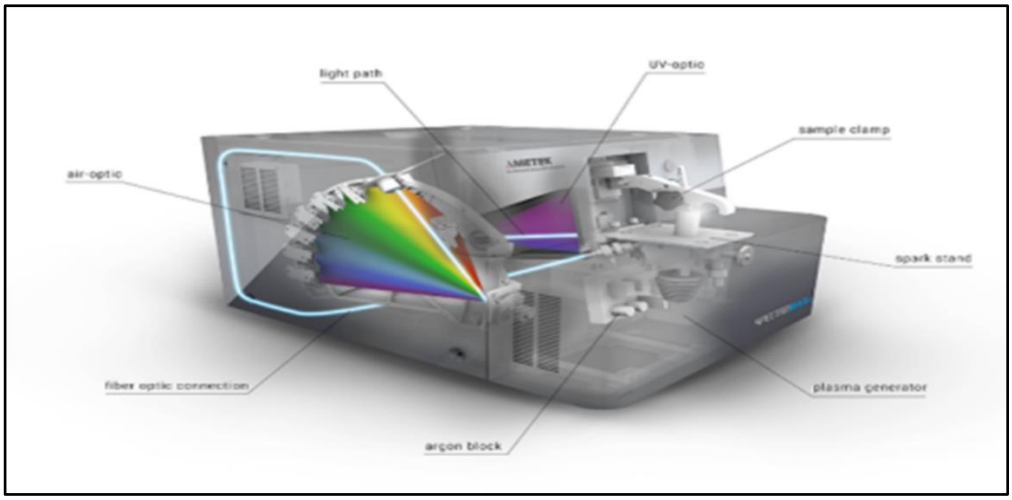

Figure 3.8. Schematics of AMETEM.

- The workpiece is prepared and fabricated as follows. The workpiece sheet has dimensions of 40 millimeters on each side and a thickness of 300 mm. Utilization of wire EDM machining to cut the sheet into small pieces (40 x 40 x 2 mm). as shown in Figure 3.9.

Figure 3.9. Wire EDM machine.

- The copper plate that will serve as an electrode measures (32 x 27 x 10) millimeters and has these dimensions. Before beginning each experiment, a very fine emery sheet is used to polish the end of the electrode.
- Removing contaminants from the workpiece and the electrode in advance of their potential to create a barrier.
- Use the digital balance to determine the weight of both the workpiece and the electrode before and after cutting.
- An indicator gauge was used to secure the electrode in the tool holder that also functions as its cathode terminal. This was done so that the electrode could be balanced.
- The anode was terminated by placing the sample in the workpiece holder and fixing it.
- It is necessary to connect the transformer oil to a pump that recycles fluid to a depth that completely submerges the tool and the workpiece before using the oil.
- Able to determine the machining parameters for each experiment using the machine's window and control panel.
- Consequently, the specimens are all cut to their final dimensions using EDM, which is 39.5 by 40.2 millimeters (0.5 mm).
- After each experiment's conclusion, the dielectric components were eliminated from the sample and the electrode. The subjects' weights were recorded for each trial to calculate the (MRR) and (EWR).

- The machine's window and digital balance are used to capture and record the data.

3.8. PARAMETER MEASUREMENTS

3.8.1. Calculation of Material Removal Rate (MRR) and Electrode Wear Ratio (EWR)

An electronic weighing balance was used to measure the workpiece's weight and electrode before and after cutting, as shown in Figure 3.10. It is a high-precision electrical device with an accuracy of (0.001) g. The weighing apparatus seen in the figure has a range of measurement that extends from 0.1 mg to 210 g. The electrode wear ratio is significant in determining the product's final form and dimensional accuracy. The electrode wear ratio is calculated by dividing the difference in electrode weight before and after machining by the weight electrode before machining. As shown in Figure 3.2.

$$\text{MRR}= \frac{Wiw-Wfw}{t \times \rho} \quad (3.1)$$

$$\text{EWR}= \frac{Wie-Wfe}{t \times \rho} \quad (3.2)$$

Where:

MRR = Material Removal Rate (g/min).
Wiw= Initial weight of the workpiece (g).
Wfw= Final weight of the workpiece (g).
EWR= Electrode Wear Rate (g/min).
Wie= Initial weight of the electrode (g).
Wfe=Final weight of the electrode (g)
ρ= Density (g/cm³)
t = Machining time (min.).

Figure 3.10. The digital balancing device (Denver Instrument).

3.8.2. Calculation of Surface Roughness (Ra)

Three locations on the machined surface were measured for surface roughness (Ra). The average of these three measurements was used to calculate the final surface roughness value, measured in micromillimeters. A Maher Federal Company Pocket Surf PS1 profile meter was used to determine the Ra. The Ra is determined by using the probe to scan the surface and comparing the peaks and troughs it discovers to known values. The probe movement during the trace is digitally shown, as illustrated in Figure 3.11.

Figure 3.11. Surface roughness measurement equipment.

3.8.3. Calculation of the WLT

A series of steps of metal preparation and testing facilities in the Engineering production Department at the University of Technology to manufacture samples that would show the microscopic characteristics of the samples. These steps included:

- **Cutting**

From the same side that was cut in the EDM machine using a wire EDM, all specimens were cut into small pieces with the required dimensions (2 mm x 10 mm) and uniform thickness (2 mm), as illustrated in Figure 3.12.

Figure 3.12. Cutting using wire EDM.

- **Mounting**

After cutting the specimens into small pieces, the mounting procedure begins. The tests must be fitted using a minced self-curing dental consonant base acrylic resin and a fluid mixed quickly and poured into the sample, as demonstrated in Figure 3.13. The mixture is placed on the sample for minutes until it becomes firm and dry.

Figure 3.13. The sample after mounting.

- **Grinding**

Emery paper (sic) with varying degrees of smoothness was used for the grinding process, carried out by a disk-rotary tool with water, commencing at 220, 320, 500, 800, and 1000, respectively as well as finishing at 1200, correspondingly. Figure 3.14. shows a grinding machine (DAP-5 model) that operates at a voltage of 220 V and a current of 3 A.

Figure 3.14. The grinding machine.

- **Polishing**

They were given a mirror-like sheen using an alumina (Al2O3) slurry and a polishing cloth to get the desired result. In this study, a Metaserv brand polishing machine was used, and 230-240 V electricity and 2.85 A current are required Figure 3.14.

Figure 3.15. The machine of the polishing.

- **Etching**

Etching or engraving is the technique for describing a crystalline boundary of austenitic medium carbon steel utilizing a chemical solution of hydrogen chloride (HCl) with distilled water. The samples were initially submerged in the solution for 45-55 seconds, as indicated in Figure 3.16, before being rinsed with tap water and dried with an air dryer.

Figure 3.16. The etching process.

- **Drying**

Performs instantaneous drying by strong hot blowing for immediate prevention of specimen oxidation. Clean hot air is blown powerfully from a nozzle to instantaneously dry a specimen surface after wet polishing or etching a test piece.

- **Microstructure Examination**

The microstructure evolution of samples was investigated using a Kruss brand metallographic microscope connected to the computer to quantify the thickness of the white layer, as shown in Figure 3.17. and 3.18, samples were magnified, and photomicrographs were made.

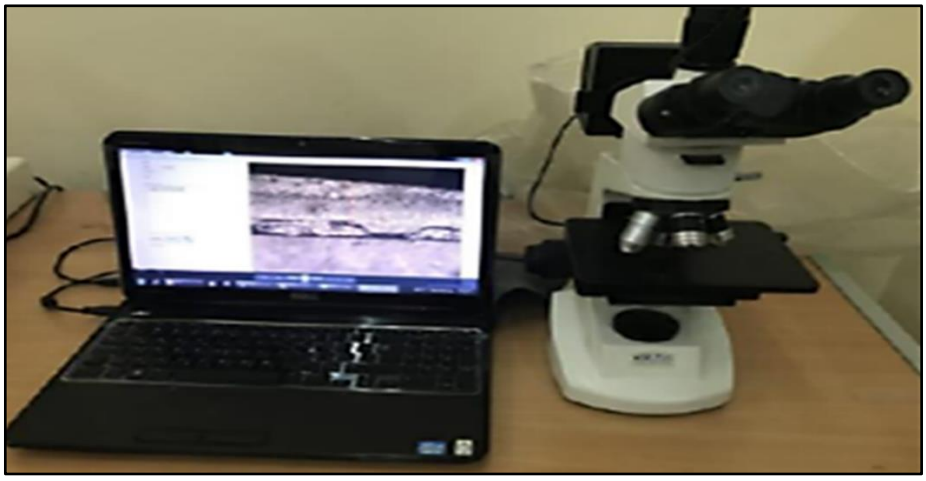

Figure 3.17. Optical microscope (400x).

3.9. THE EXPERIMENT DESIGNS

The number of experiments required is heavily influenced by the experimental design using two parameters and three layers. The effects of pulse-on-time and current parameters were studied independently for each dielectric fluid on the white layer thickness, materials removal rate, electrode wear ratio, surface roughness, and microhardness. Tables 3.10. and 3.11. show the machining parameters and levels and the fixed input parameters, respectively.

Table 3.10. Parameters and levels of machining.

Parameters	**Units**	**Level 1**	**Level 2**	**Level 3**
Peak current (I_p)	Amp	10	30	50
Pulse on time (T_{on})	µs	50	100	200
Pulse off time (T_{off})	µs	3	9	18

Table 3.11. A set of predetermined input variables.

Input Parameters	**Constant Values**
Workpiece polarity	Negative
Electrode polarity	Positive
Dielectric fluid	Transformer oil
High voltage (HV)	240V
GAP	12V
CODE of S	20
SVO of feed	100%
Time of the working	1 sec
High of the Jumping	0.8mm
Depth of cut	0.5mm

PART 4

RESULTS AND DISCUSSIONS

This part includes investigating the effect of various parameters such as current (Ip), pulse on time (Ton), and pulse off time (Toff) on white layer thickness. In this research, 27 pieces of samples made of carbon steel CK45 DIN17200 as workpieces, and a copper electrode of a consistent thickness were used. A mathematical model was built with the software Minitab 17 to predict the various responses. The model's results were then compared to the values obtained through experimentation and assessed.

4.1. EXPERIMENTAL RESULTS FOR WLT, MRR, RA AND EWR

The factorial design of the experiments under machining was created using the experimental (DOE) design for three factors and three levels. 27 experimental studies were performed individually using (DOE), as listed in Table 4.1.

Table 4.1. Experimental results for WLT, MRR, Ra, and EWR.

No.	Current (A)	Pulse on (µs)	Pulse off (µs)	M.T. (min)	W.L.T (µm)	MRR (g/min)	Ra (µm)	EWR (g/min)
1	10	50	3	5.20	8.93616	0.1879	2.987	0.00113
2	30	50	3	4.00	40.85104	0.29297	4.163	0.2428
3	50	50	3	3.01	100.851	0.64621	5.135	0.66368
4	10	50	9	5.19	6.117496	0.18815	2.889	0.00391
5	30	50	9	3.55	33.19147	0.31754	3.987	0.30397
6	50	50	9	2.59	95.74464	0.6848	5.061	0.72223
7	10	50	18	5.10	4.17946	0.1979	2.725	0.00531
8	30	50	18	3.51	30.63828	0.32319	3.876	0.32481
9	50	50	18	2.50	81.74197	0.7798	4.975	0.74964
10	10	100	3	5.00	16.07642	0.20102	3.544	0.0315
11	30	100	3	3.47	56.18469	0.35443	4.313	0.37089
12	50	100	3	2.44	131.4955	0.81	5.655	0.81041
13	10	100	9	4.50	15.75489	0.23131	3.367	0.03602
14	30	100	9	3.40	51.07976	0.41132	4.302	0.44376

15	50	100	9	2.40	119.9999	0.8319	5.522	0.83195
16	10	100	18	4.44	11.48936	0.2552	3.299	0.14313
17	30	100	18	3.35	47.23404	0.45904	4.288	0.49716
18	50	100	18	2.33	113.7778	0.8894	5.398	0.85729
19	10	200	3	4.31	25.65924	0.25594	3.796	0.17731
20	30	200	3	3.28	74.05352	0.53652	4.822	0.56024
21	50	200	3	2.00	335.7469	0.9194	6.384	0.9283
22	10	200	9	4.20	20.42552	0.26995	3.704	0.18230
23	30	200	9	3.18	65.10635	0.58867	4.639	0.61591
24	50	200	9	1.48	236.1735	1.2334	5.917	1.0529
25	10	200	18	4.05	17.68699	0.27728	3.638	0.21651
26	30	200	18	3.10	60.01355	0.60532	4.425	0.64406
27	50	200	18	1.23	169.3671	1.5650	5.874	1.1575

4.2. THE INFLUENCE OF CURRENT ON WLT

In the EDM process, the white layer is an undesirable formation and should be reduced (Fig. 4.1). WLT is affected by the main EDM parameters such as Ip (10, 30, and 50 A), Ton (50, 100, and 200 µs), and Toff (3, 9, and 18 µs). Since WLT is most affected by Ip, we started the explanation with Ip.

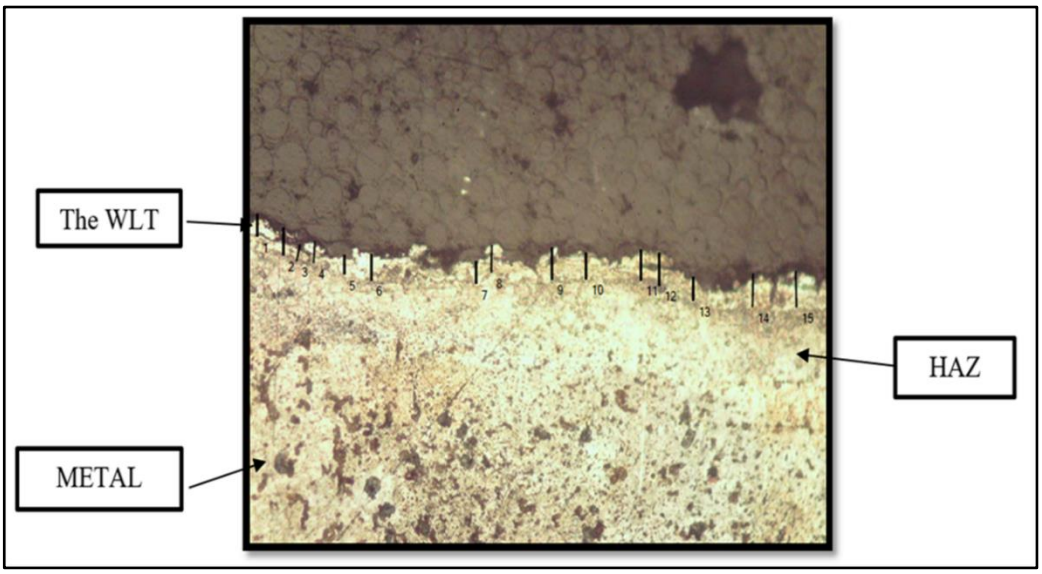

Figure 4.1. The White layer formed during EDM.

When the Ip increases, the thermal transfer increases the molten metal rate to the workpiece surface. Since the amount of liquid metal that the dielectric fluid can flush

away is constant, the dielectric fluid cannot exclude molten materials, and the material accumulates as a white or recasts layer on the machined surface. Since the increase in current from 10A to 50A leads to a rise in discharge energy producing the sparks responsible for the craters' depth and size between the cathode and anode, create white layer on the surface. Table 4.2. and Figure 4.2. illustrate the effect of changing the current from 10A to 50A at constant values of T_{ON} and T_{OFF} on WLT. As the Ip increases the WLT increases.

Table 4.2. The input parameters of charts.

	(4.2 a)				(4.2 b)				(4.2 c)			
NO.	**Ip**	**To N**	**Toff**	**WLT**	**Ip**	**Ton**	**To FF**	**WLT**	**Ip**	**Ton**	**Tof F**	**WLT**
1	10	50	3	8.936	10	100	9	15.754	10	200	18	17.686
2	30	50	3	40.851	30	100	9	51.079	30	200	18	60.013
3	50	50	3	100.851	50	100	9	119.99	50	200	18	169.36

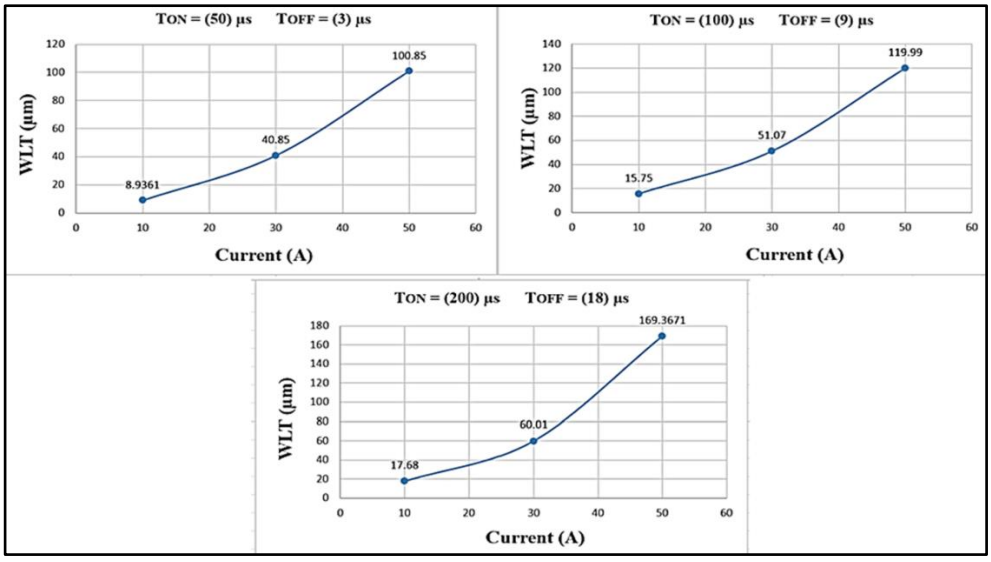

Figure 4.2. The effect of input parameters on WLT.

Table 4.3. and Figure 4.3. illustrate the effect of changing values of Ip and T_{ON} on WLT at constant T_{OFF}. WLT is directly proportional to Ip and Ton, and the maximum WLT (335.7469µm) was obtained at the Ip and Ton maximum in the experiment numbered 21. WLT is inversely proportional to Toff and the minimum WLT (4.1794µm) was obtained at the Toff maximum in the experiment numbered 7.

Table 4.3. The input parameters of charts.

	(4.3 a)				(4.3 b)				(4.3 c)			
NO.	**I_P**	**T_{ON}**	**T_{OFF}**	**WLT**	**I_P**	**T_{ON}**	**T_{OFF}**	**WLT**	**I_P**	**T_{ON}**	**T_{OFF}**	**WLT**
1	10	50	3	8.936	10	50	9	6.1174	10	50	18	4.179
2	30	100	3	56.18	30	100	9	51.079	30	100	18	47.234
3	50	200	3	335.74	50	200	9	236.17	50	200	18	169.36

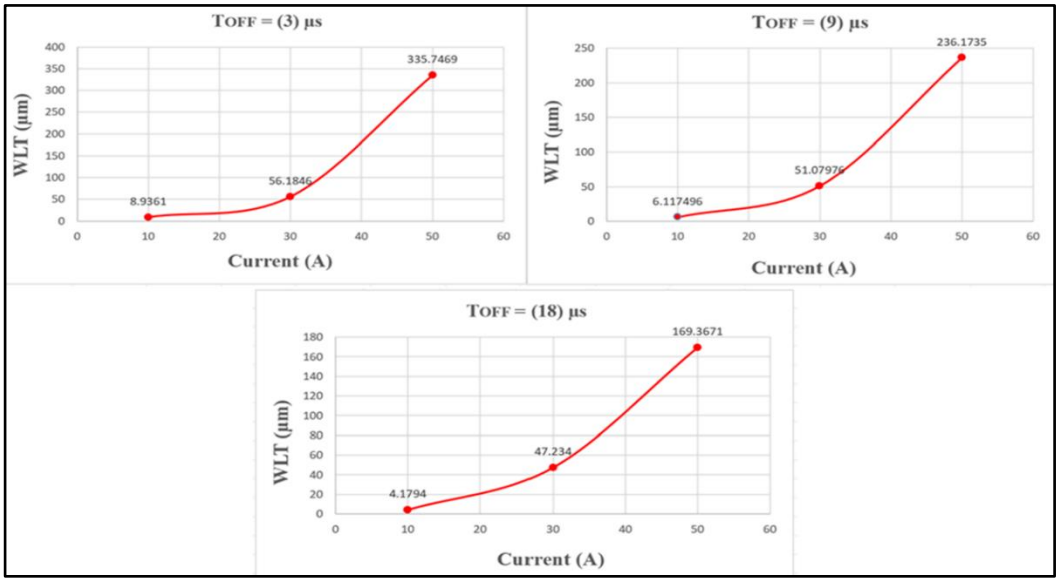

Figure 4.3. The effect of input parameters on WLT.

4.2.1. The Minimum WLT

The minimum white layer thickness (4.17946 µm) was obtained in experiment 7 with parameters Ip (10 A), Ton (50 µs) and Toff (18 µs). Because Toff is high, Ip and Ton are low, the exposure time of the machining to the workpiece is lower. The sparks are very small and haven't a high effect on the discharge energy that causes the white layer. Since the current value is lower, the intensity of the spark between the tools and workpiece is reduced due to cooling the zone rapidly, which leads to a decrease in temperature and less white layer formation as shown in Figure 4.4.

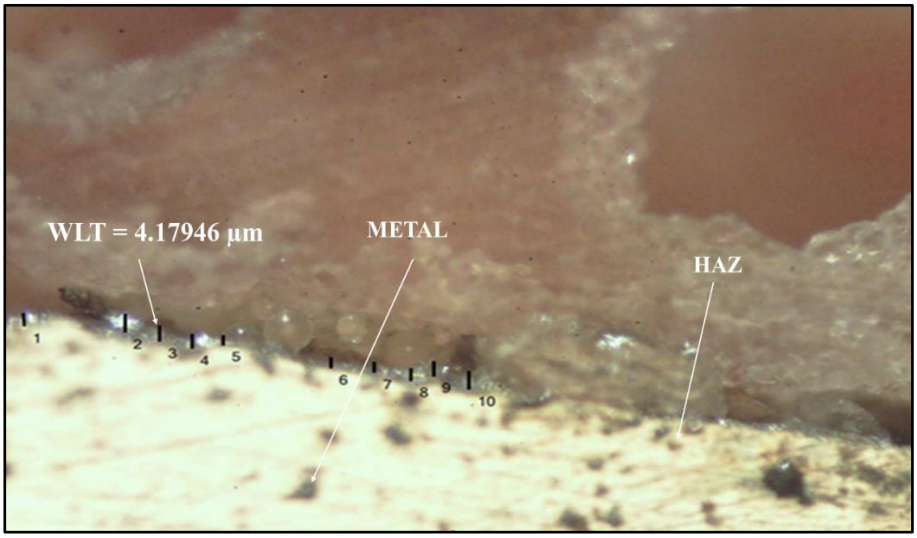

Figure 4.4. The influence of current on WLT at 400x.

4.2.2. The Maximum WLT

The maximum white layer thickness (335.7469 µm) was obtained in experiment 21 with parameters Ip (50 A), Ton (2000 µs), and Toff (3 µs). Because Toff is low, Ip and Ton are high, the exposure time of the machining to the workpiece is higher. Intense sparks and higher exposure time cause the discharge energy to form a white layer. The fact that increasing Ip increases the heat delivered to the machined surface which increases the amount of molten metal. Because the amount of molten metal that the dielectric fluid can flush away is constant, it cannot remove the molten material completely, which causes it to build up as a white or recast layer on the machined surface.

That is, a thicker white layer is formed on the heated workpiece material in these conditions. The white layer formed in experiment number 21 is shown in Figure 4.5.

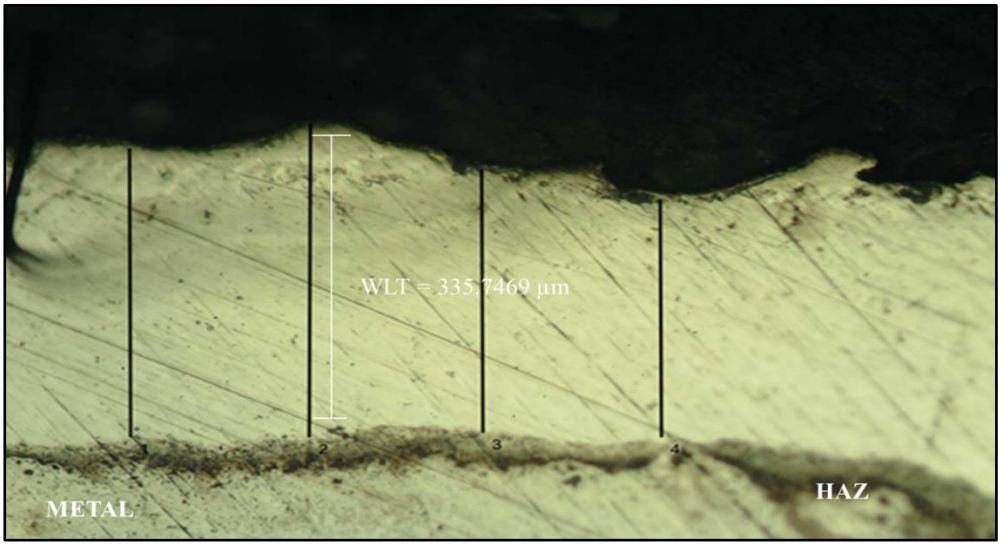

Figure 4.5. The influence of current on WLT at 400x.

4.3. EFFECT OF CURRENT ON MRR

There is a direct correlation between increasing I_P and increasing MRR, with the MRR value increasing from (0.1879) g\min to (1.5650) g\min. This is caused by increased discharge energy and a longer time to transform this energy into the tool electrode, as well as the formation of a crater on a workpiece as a result of a stronger spark that generates high temperatures and melts evaporated material. Increasing the current causes increased discharge energy and a longer time to transform this energy into the tool electrode because there is no flushing of the dielectric liquid and debris particles. This is due to the discharge gap arcing, which prevents the dielectric liquid and debris particles from being flushed out and causes arcing to occur.

Figure 4.6 shows that when the I_P reaches its maximum value (50)A, the MRR reaches its maximum value of 1.565 g/min. Table 4.4 shows how changing the I_P from 10A to 50A affects MRR when T_{ON} 50 µs and T_{OFF} 3 µs remain constant, resulting in an MRR ranging from 0.1879 to 0.642 g\min. Table 4.4. and Figure 4.6. illustrate the effect of changing the current from 10A to 50A at constant values of T_{ON} and T_{OFF} on MRR.

Table 4.4. The input parameters of charts.

	(4.4 a)				(4.4 b)				(4.4 c)			
NO.	**I_P**	**T_{ON}**	**T_{OFF}**	**MRR**	**I_P**	**T_{ON}**	**T_{OFF}**	**MRR**	**I_P**	**T_{ON}**	**T_{OFF}**	**MRR**
1	10	50	3	0.1879	10	100	9	0.2313	10	200	18	0.2772
2	30	50	3	0.2929	30	100	9	0.4113	30	200	18	0.6053
3	50	50	3	0.6462	50	100	9	0.8319	50	200	18	1.5650

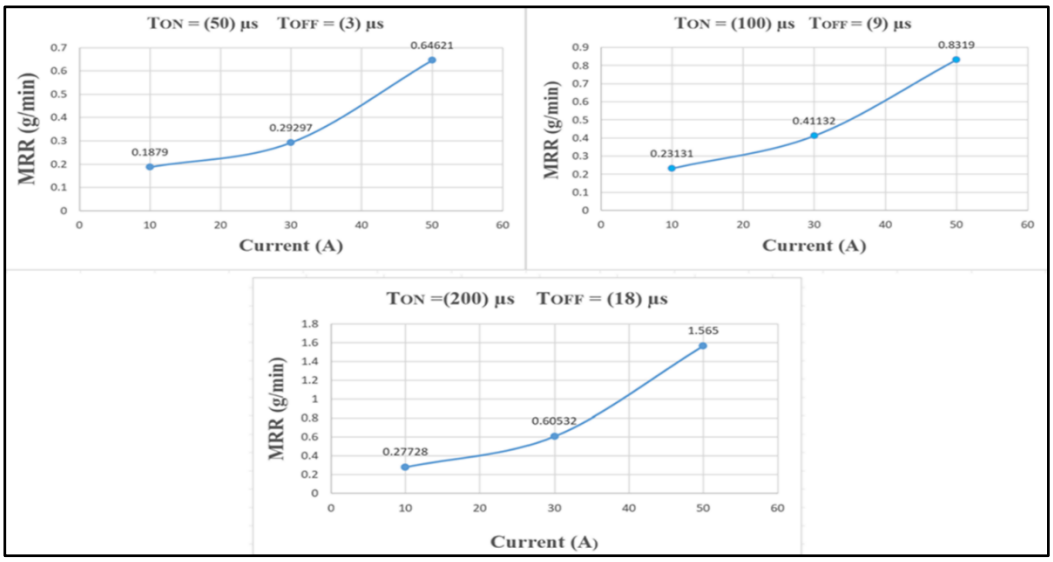

Figure 4.6. The effect of input parameters on MRR.

Table 4.5. and Figure 4.7. illustrate the effect of changing values of Ip and T_{ON} on MRR at constant T_{OFF}. MRR is directly proportional to Ip and Ton, and the maximum MRR (1.565) g/min was obtained at the Ip and Ton maximum.

Table 4.5. The input parameters of charts.

	(4.5 a)				(4.5 b)				(4.5 c)			
NO.	**I_P**	**T_{ON}**	**T_{OFF}**	**MRR**	**I_P**	**T_{ON}**	**T_{OFF}**	**MRR**	**I_P**	**T_{ON}**	**T_{OFF}**	**MRR**
1	10	50	3	0.1879	10	50	9	0.188	10	50	18	0.1979
2	30	100	3	0.3544	30	100	9	0.411	30	100	18	0.459
3	50	200	3	0.9194	50	200	9	1.233	50	200	18	1.565

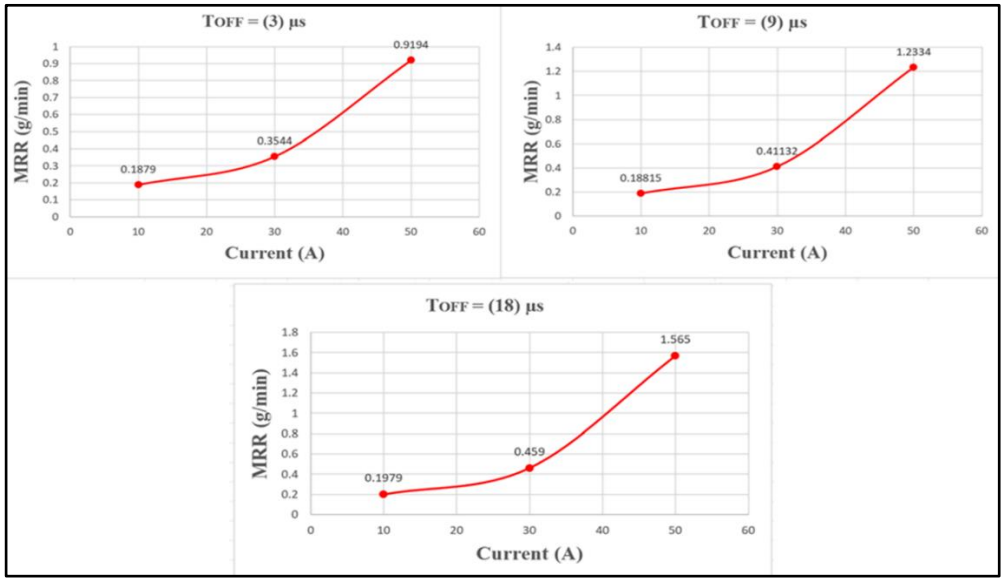

Figure 4.7. the effect of input parameters on MRR.

4.4. EFFECT OF CURRENT ON Ra

The effect of (Ip), (T_{ON}), and (T_{OFF}) on (Ra) is shown in Fig. 4.8. Ra is increased with increasing I_P from 10 to 50 A. The Ip is the most significant influencing factor on the Ra and displays the rapid rise from (2.987) µm to (5.874) µm with a rise of Ip from (10)A to (50)A, respectively.

Ra is raised with the increase of T_{ON} from 50 to 200 µs. This happened when T_{ON} was at 50 µs, resulting in a decreased surface machining temperature and more surface smoothness. Craters are insufficient; a smooth surface was achieved by selecting a low T_{ON} value. Additionally, as Ip grew, the Ra increased from 2.987µm to 6.384µm. This was due to the current's enhanced impulse force and discharge energy, which boosted surface material removal and produced deeper and larger craters for discharge. Surface roughness increased as a result of these variables. It can assess whether the current impact is larger than the impact of T_{ON}. Table 4.6. and Figure 4.8. Illustrate the effect of changing the current from 10A to 50A at constant values of T_{ON} and T_{OFF} on Ra.

Table 4.6. The input parameters of charts.

	(4.6 a)				(4.6 b)				(4.6 c)			
NO.	**I_P**	**T_{ON}**	**T_{OFF}**	**Ra**	**I_P**	**T_{ON}**	**T_{OFF}**	**Ra**	**I_P**	**T_{ON}**	**T_{OFF}**	**Ra**
1	10	50	3	2.987	10	100	9	3.367	10	200	18	3.638
2	30	50	3	4.163	30	100	9	4.302	30	200	18	4.425
3	50	50	3	5.135	50	100	9	5.522	50	200	18	5.874

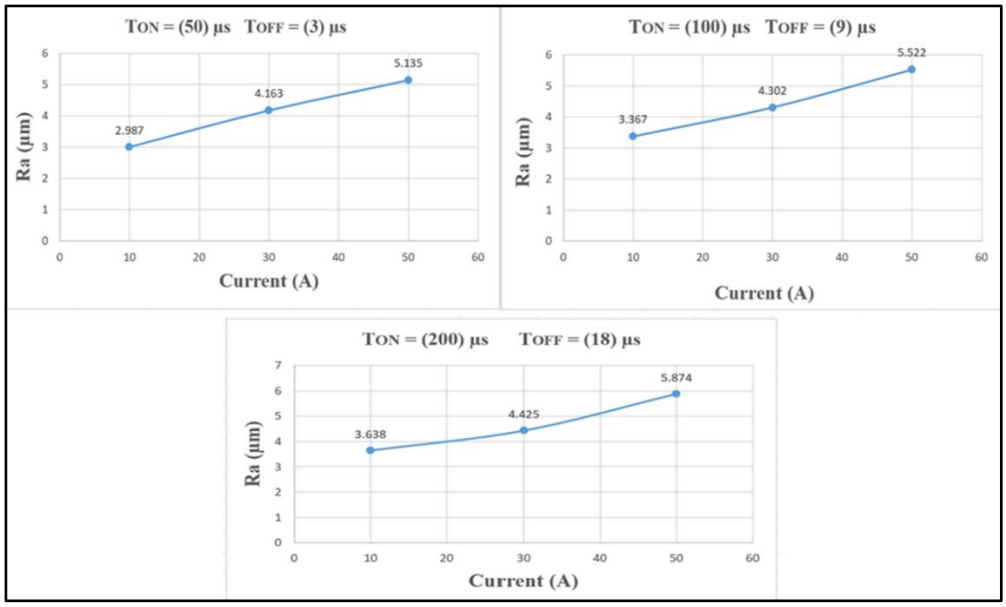

Figure 4.8. The effect of input parameters on Ra.

Table 4.7. and Figure 4.9. illustrate the effect of changing values of Ip and T_{ON} on Ra at constant T_{OFF}. Ra is directly proportional to Ip and Ton, and the maximum Ra (6.384 µm).

Table 4.7. The input parameters of charts.

	(4.7 a)				(4.7 b)				(4.7 c)			
NO.	**I_P**	**T_{ON}**	**T_{OFF}**	**Ra**	**I_P**	**T_{ON}**	**T_{OFF}**	**Ra**	**I_P**	**T_{ON}**	**T_{OFF}**	**Ra**
1	10	50	3	2.987	10	50	9	2.889	10	50	18	2.725
2	30	100	3	4.313	30	100	9	4.302	30	100	18	4.288
3	50	200	3	6.384	50	200	9	5.917	50	200	18	5.874

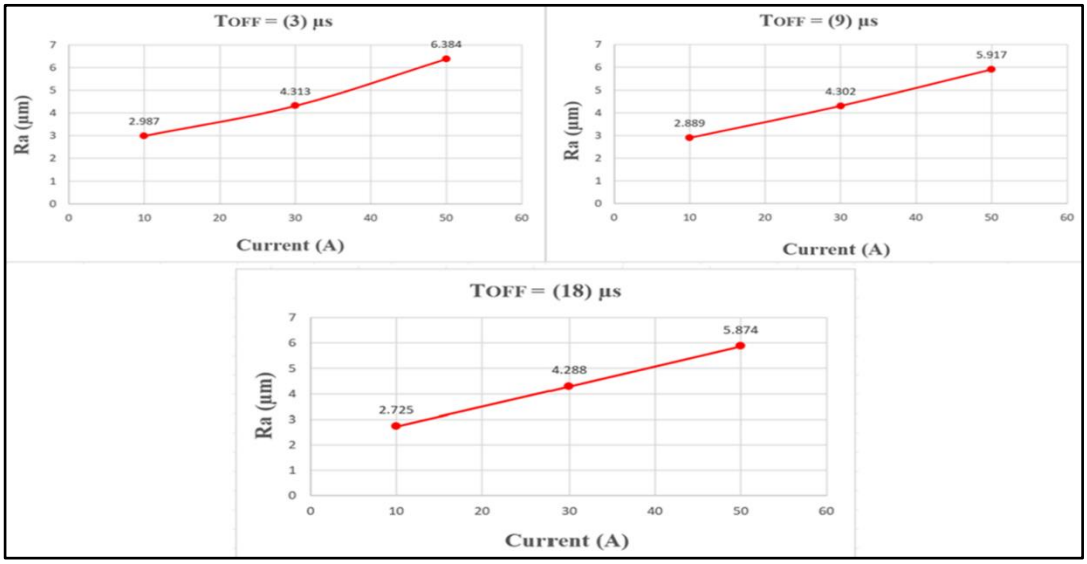

Figure 4.9. The effect of input parameters on Ra.

4.5. EFFECT OF CURRENT ON EWR

The impact of (Ip) on the electrode wear rate (EWR) at a different degree T_{ON} (50, 100, and 200 µs) and T_{OFF} values (3, 9, and 18µs) is shown in Figure 4.10.

EWR has been rising as the I_P increased from (10 A to 50 A). The material is taken from the electrode when I_p is increased because a stronger spark is produced. It was obvious that EWR has been increased as T_{ON} increased between (50 and 200 µs), which occurred as a result of the dielectric liquid's increasing pollution as Ton increased and the number of sparks decreased, which caused EWR to rise.

The relationship between I_P and T_{ON} for EWR reveals that a high I_P had a discernible impact on the enhancement of EWR. This can be observed in the interaction between the two variables. Sparks become more intense when the I_P is raised, and a greater amount of electrode material gets corroded. T_{ON} had a smaller influence than I_P, affecting boosting EWR. As the T_{ON} increases, a greater amount of time is spent degrading the electrodes. As a consequence of this aspect, the EWR gets higher. The increasing current, discharge energy, and impulsive force all contributed to a rise in the amount of material removed from the surface and the formation of larger discharge craters.

Table 4.8. and Figure 4.10. illustrate the effect of changing the current from 10A to 50A at constant values of T_{ON} and T_{OFF} on EWR.

Table 4.8. The input parameters of charts. illustrate the effect of changing the current from 10A to 50A at constant values of T_{ON} and T_{OFF} on EWR.

	(4.8 a)				(4.8 b)				(4.8 c)			
NO.	**IP**	**TON**	**TOFF**	**EWR**	**IP**	**TON**	**TOFF**	**EWR**	**IP**	**TON**	**TOFF**	**EWR**
1	10	50	3	0.0011	10	100	9	0.036	10	200	18	0.2165
2	30	50	3	0.2428	30	100	9	0.4437	30	200	18	0.6440
3	50	50	3	0.6636	50	100	9	0.832	50	200	18	1.1575

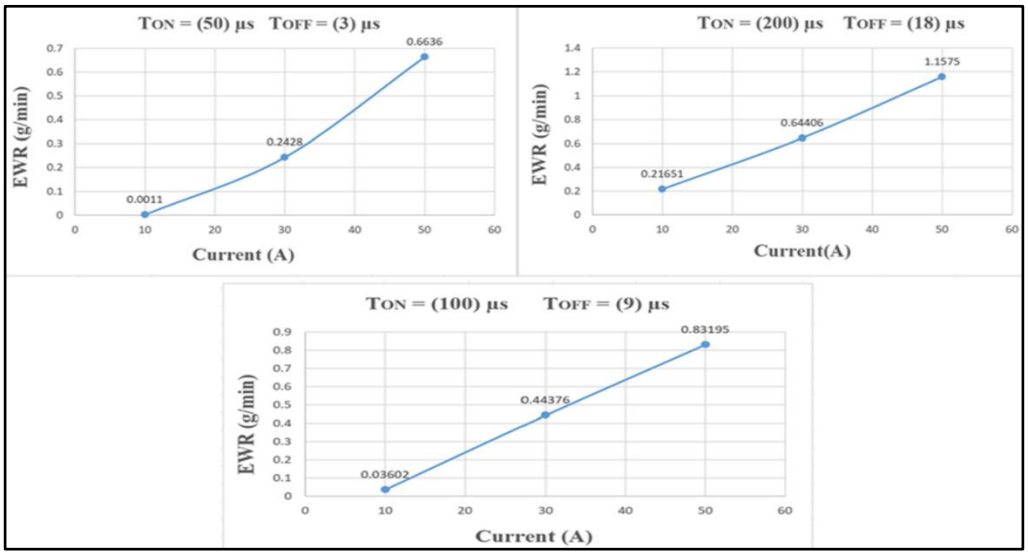

Figure 4.10. The effect of input parameters on EWR.

Table 4.9. and Figure 4.11. illustrate the effect of changing values of Ip and T_{ON} on EWR at constant T_{OFF}. EWR is directly proportional to Ip and Ton, and the maximum EWR (1.1575) g/min was obtained at the Ip and Ton maximum.

Table 4.9. The input parameters of charts.

	(4.9 a)				(4.9 b)				(4.9 c)			
NO.	**I_P**	**T_{ON}**	**T_{OFF}**	**EWR**	**I_P**	**T_{ON}**	**T_{OFF}**	**EWR**	**I_P**	**T_{ON}**	**T_{OFF}**	**EWR**
1	10	50	3	0.0011	10	50	9	0.0039	10	50	18	0.0053
2	30	100	3	0.3708	30	100	9	0.4437	30	100	18	0.4971
3	50	200	3	0.9283	50	200	9	1.052	50	200	18	1.1575

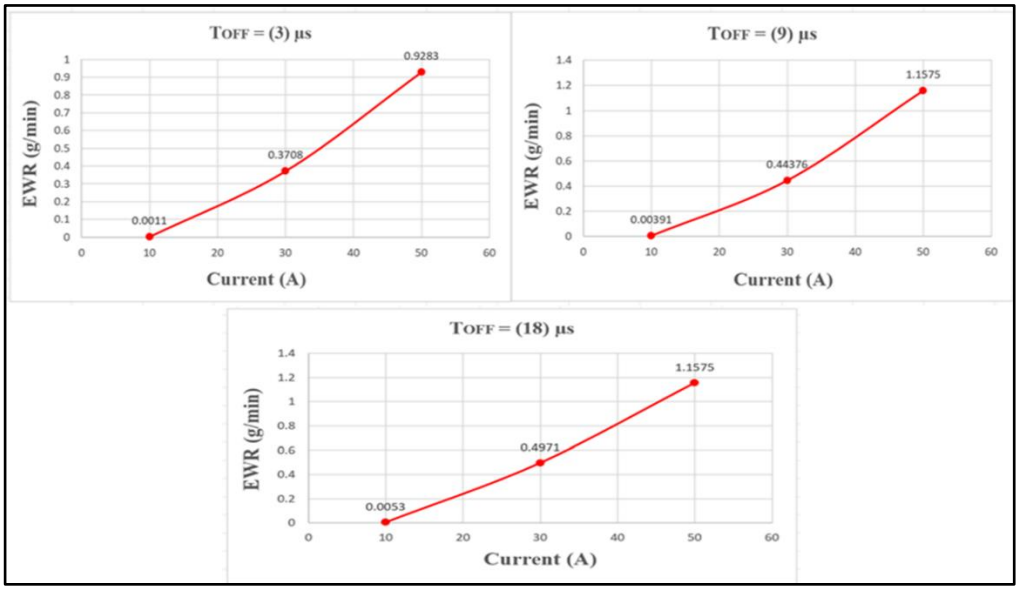

Figure 4.11. The effect of input parameters on EWR.

4.6. STATISTICAL ANALYSIS

Using full factorial statistics, three main factors are identified as controllable variables that significantly affect the disclosure process. These factors are the Ip (10, 30, and 50A), Ton (50, 100, and 200 µs), and Toff (3, 9, and 18 µs). The effects on the output response including the thickness of the white layer (WLT), material removal rate (MRR), surface roughness (Ra) and electrode wear rate (EWR) were investigated.

4.6.1. WLT Analysis

To build models for the data, regression and ANOVA analysis were used. These analyses created residual plots, which were then used to evaluate the significance of the effects. For example, normal probability plots were created between the residuals and their predicted values, assuming the distribution was normal.

The performance of (ANOVA) is shown in Table 4.10. which contains different sources, degree of freedom (DF), the total sum of squares (Adj SS), and mean sum of squares (Adj MS), the F-values and P-values to determine whether the factors are significantly related to the response. Figure 4.12. depicts the WLT normal probability residuals, and Figure 4.13. Shows the normal WLT probability plots of residuals for (I_P), (T_{ON}), and (T_{OFF}).

Table 4.10. ANOVA table for WLT.

Source	DF	Adj ss	Adj MS	F-Value	P-Value
Model	10	140334	14033.4	20.36	0.000
Linear	6	119737	19956.2	28.95	0.000
I_P	2	94546	47272.9	68.58	0.000
T_{ON}	2	21587	10793.6	15.66	0.000
T_{OFF}	2	3604	1802.2	2.61	0.104
2-Way Interactions	4	20597	5149.2	7.47	0.001
I_P * T_{ON}	4	20597	5149.2	7.47	0.001
Error	16	11028	689.3		
Total	26	151362			

The more points come closer to the red line, the more they have the correct direction as shown in Figure 4.12.

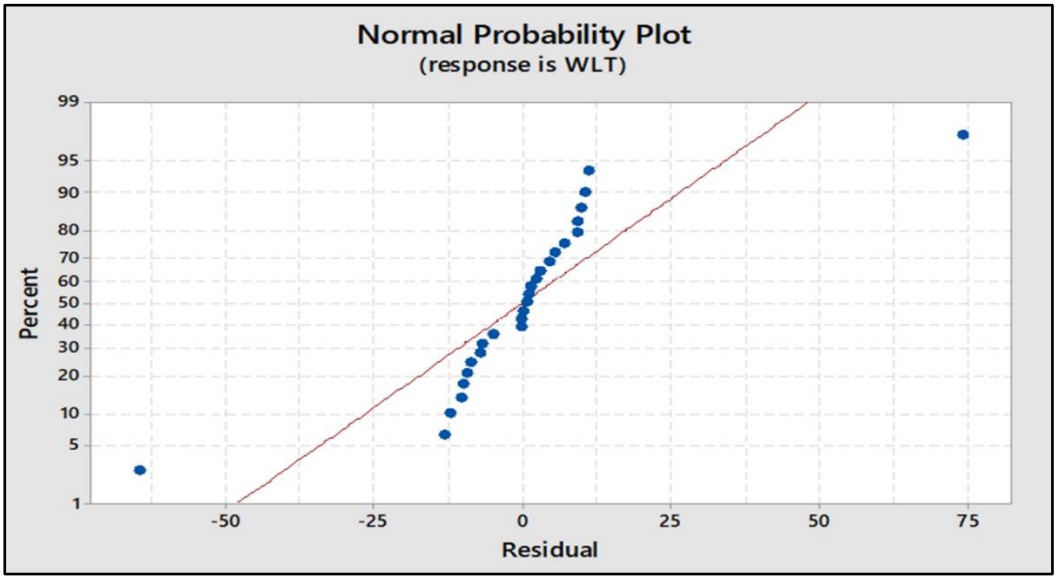

Figure 4.12. The plots of normal probability of residuals for WLT.

Since the points were set in a straight line, they exhibit a clear pattern, suggesting that each component of the regression model affects the WLT (the factorial expected value).

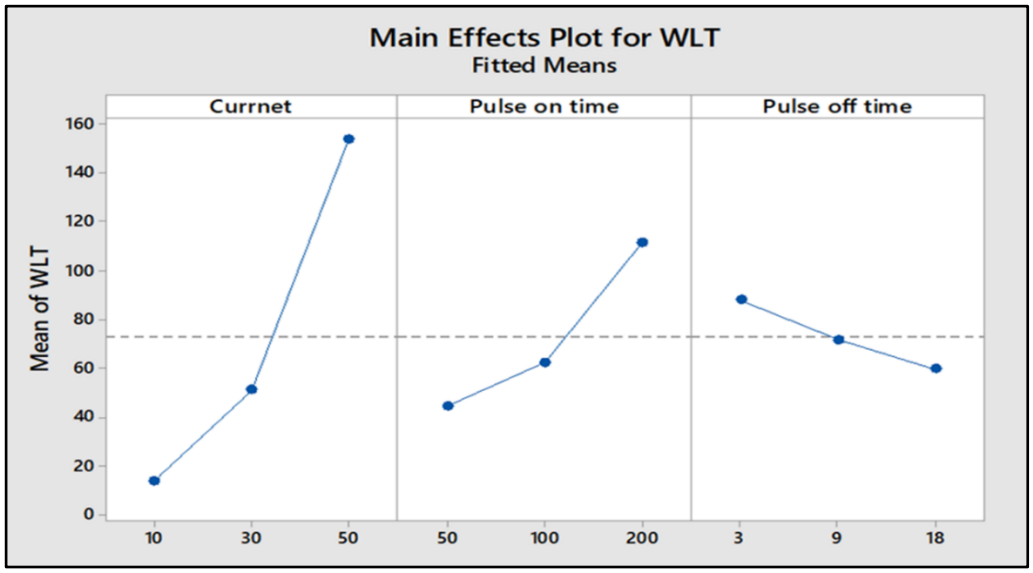

Figure 4.13. The normal WLT probability plots of residuals for input parameters

4.6.1.1. Regression Model for WLT

Mathematical models can be developed through the use of the coefficients as follows:

$$WLT = 72.95 - 58.91\ I_P(10) - 22.02\ I_P(30) + 80.93\ I_P(50) - 28.25\ T_{ON}(50) - 10.38\ T_{ON}(100) + 38.63\ T_{ON}(200) + 14.81\ T_{OFF}(3) - 1.44\ T_{OFF}(9) - 13.38\ T_{OFF}(18) + 20.6\ I_P{*}T_{ON}(10)(50) + 10.8\ I_P{*}T_{ON}(10)(100) - 31.4\ I_P{*}T_{ON}(10)(200) + 12.2\ I_P{*}T_{ON}(30)(50) + 11.0\ I_P{*}T_{ON}(30)(100) - 23.2\ I_P{*}T_{ON}(30)(200) - 32.8\ I_P{*}T_{ON}(50)(50) - 21.7\ I_P{*}T_{ON}(50)(100) + 54.6\ I_P{*}T_{ON}(50)(200) \quad (4.1)$$

4.6.1.2. Model Summary of WLT

A brief overview of the design and the statistics comparing the accuracy of several models are included in the model summary. The predicted R square (R-Sq (pred) measures how well future data will be predicted. The coefficient of determination (R-Sq) measures how much of the observed response variance can be described via a model. Regulate R-S (R. Sq- adj.) is an adjusted R which is corrected for the total of

conditions in the type's equation. A well fit is indicated by higher R-Square (R-Sq) and R-Sq (adj) values tabulated in Table 4.11.

When both the experimented and predicted bars come close to each other, this means that they are equal in outcomes as shown in Figure 4.14.

Table 4.11. The Model summary of the WLT.

S	R. sq(pred)	R. sq-adj.	R-sq
26.2539	92.71%	88.16%	79.25%

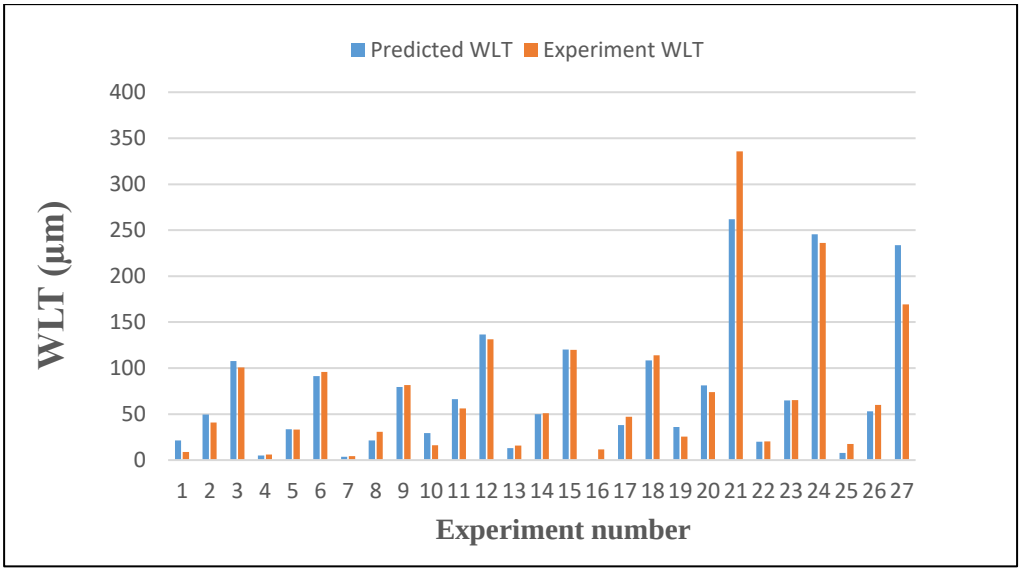

Figure 4.14. The comparison of experimented and predicted WLT values.

4.6.2. MRR Analysis

To fit models to the data, regression and ANOVA studies of factorial designs were carried out. Residual plots, such as normal probability plots between residuals and anticipated values when the distribution is normal, were constructed with these analyses to highlight how substantial the impacts were. The results of an analysis of variance (ANOVA) are presented in Table 4.12. which contains different sources, degrees of freedom (DF), a total sum of squares (Adj SS), mean sum squares (Adj MS), F-values, and P-values to determine whether the factors are significantly related to the response. Figure 4.15. Shows the MRR residual probability graphs and the

normal MRR probability plots of residuals for I_P, T_{ON}, and T_{OFF} are shown in Figure 4.16.

Table 4.12. ANOVA table for MRR.

Source	DF	Adj SS	Adj M.S	F-Value	P-Value
Model	10	2.98474	0.29847	30.15	0.000
Linear	6	2.80765	0.46794	47.27	0.000
I_P	2	2.33139	1.16570	117.74	0.000
T_{ON}	2	0.40304	0.20152	20.35	0.000
T_{OFF}	2	0.07322	0.03661	3.70	0.048
2-Way Interactions	4	0.17710	0.04427	4.47	0.013
I_P* T_{ON}	4	0.17710	0.04427	4.47	0.013
Error	16	0.15840	0.00990		
Total	26	3.14315			

The more points come closer to the red line, the more they have the correct direction as shown in Figure 4.15.

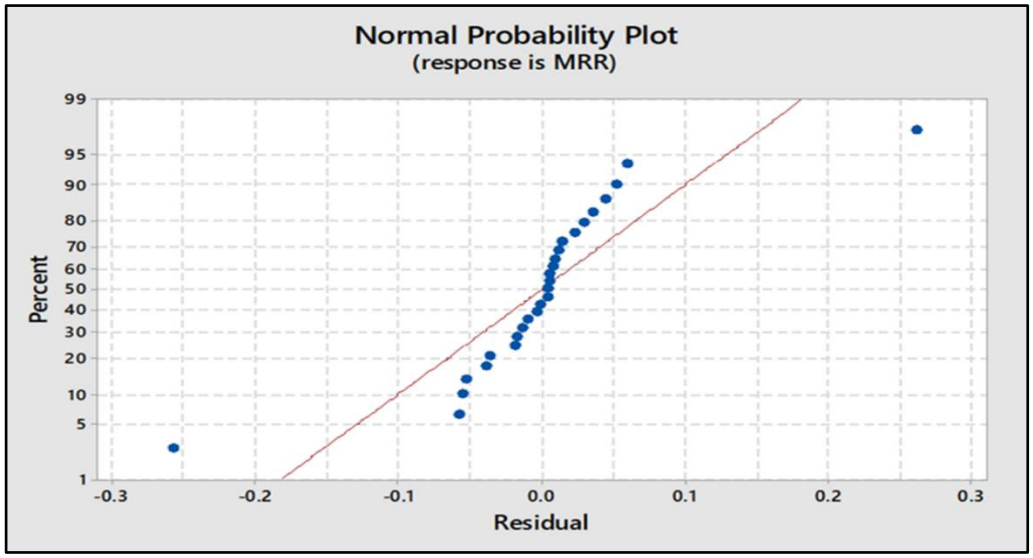

Figure 4.15. The normal MRR probability plots of residuals for input parameters.

Since the points were set in a straight line, they exhibit a clear pattern, suggesting that each component of the regression model affects the MRR (the factorial expected value).

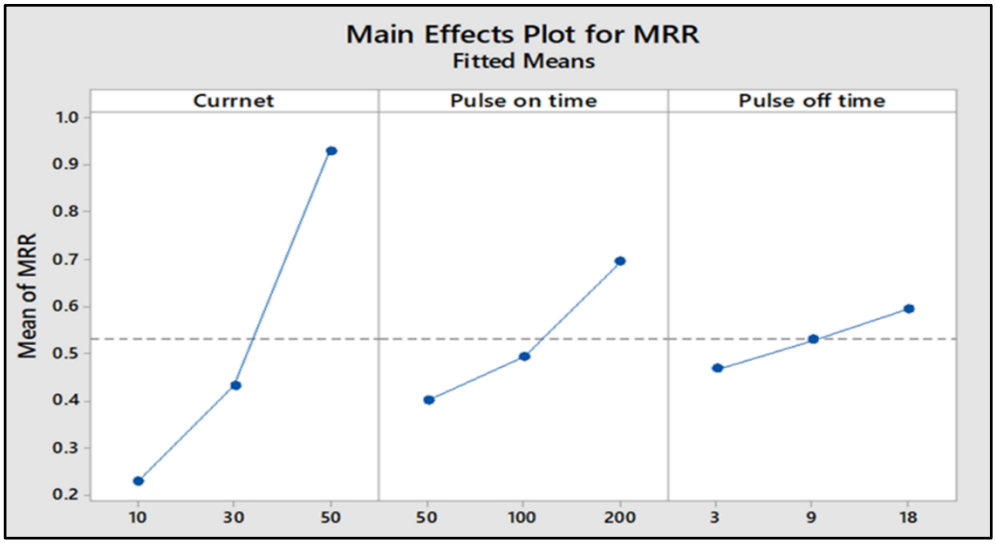

Figure 4.16. The normal MRR probability plots of residuals for input parameters.

4.6.2.1. Regression Model for MRR

Mathematical models can be developed through the use of the coefficients, as follows:

$$MRR = 0.5301 - 0.3007\ I_P\ (10) - 0.0980\ I_P\ (30) + 0.3987\ I_P\ (50) - 0.1281\ T_{ON}\ (50) - 0.0364\ T_{ON}\ (100) + 0.1645\ T_{ON}\ (200) - 0.0630\ T_{OFF}\ (3) - 0.0016\ T_{OFF}\ (9) + 0.0645\ T_{OFF}\ (18) + 0.0900\ I_P{*}T_{ON}\ (10)(50) + 0.0362\ I_P{*}T_{ON}\ (10)(100) - 0.1262\ I_P{*}T_{ON}\ (10)(200) + 0.0072\ I_P{*}T_{ON}\ (30)(50) + 0.0125\ I_P{*}T_{ON}\ (30)(100) - 0.0198\ I_P{*}T_{ON}\ (30)(200) - 0.0972\ I_P{*}T_{ON}\ (50)(50) - 0.0487\ I_P{*}T_{ON}\ (50)(100) + 0.1459\ I_P{*}T_{ON}\ (50)(200) \quad (4.2)$$

4.6.2.2. Model Summary of the MRR

A brief overview of the design and the statistics comparing the accuracy of several models are included in the model summary. The predicted R square (R-Sq (pred)) measures how well future data will be predicted. The coefficient of determination (R-Sq) measures how much of the observed response variance can be described via a model. Regulate R-S (R. Sq- adj.) is an adjusted R which is corrected for the total of conditions in the type's equation. A well fit is indicated by higher R-Square (R-Sq) and R-Sq (adj) values tabulated in table 4.13.

When both the experimented and predicted bars come close to each other, this means that they are equal in outcomes as shown in Figure 4.17.

Table 4.13. The Model summary of the MRR.

S	R-sq(pred)	R-sq(adj)	R-sq
0.0995002	94.96%	91.81%	85.65%

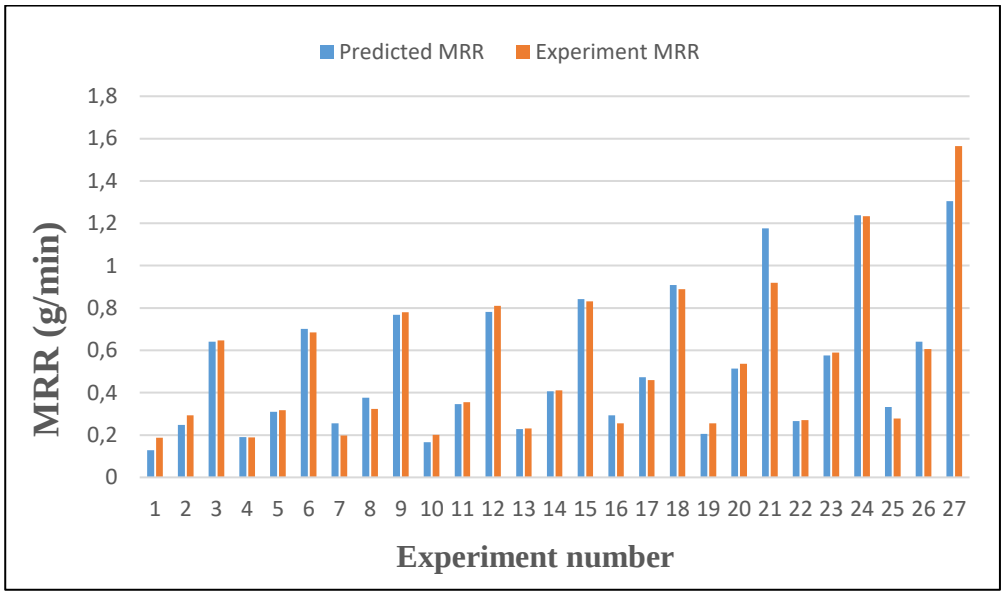

Figure 4.17. The comparison of experimented and predicted MRR values.

4.6.3. Ra Analysis

Regression and ANOVA were used to construct models for the response data (Ra) to evaluate the significance of the influences, like normal probability plots comparing residuals and their predicted values when a distribution is normal. As seen in Figure 4.18. and 4.19. The points it has been steadied in a straight line, indicating that every element influences (Ra) in a dielectric. they demonstrate the factors that have a significant impact on the response, as well as their respective degrees of freedom (DF), total sum squares (Adj SS), mean sum of squares (Adj MS), F-values, and P values to determine whether the factors are significantly related to the response. as shown in Table 4.14.

Table 4.14. ANOVA table for Ra.

Source	DF	Adj SS	Adj MS	F-value	P-value
model	10	25.7340	2.5734	383.00	0.000
Linear	6	25.5978	4.2663	634.95	0.000
I	2	22.2530	11.1265	1655.94	0.000
T_{on}	2	3.0457	1.5229	226.64	0.000
T_{off}	2	0.2992	0.1496	22.26	0.000
2-way interactions	4	0.1361	0.0340	5.07	0.008
I* T_{on}	4	0.1361	0.0340	5.07	0.008
Error	16	0.1075	0.0067		
Total	26	25.8415			

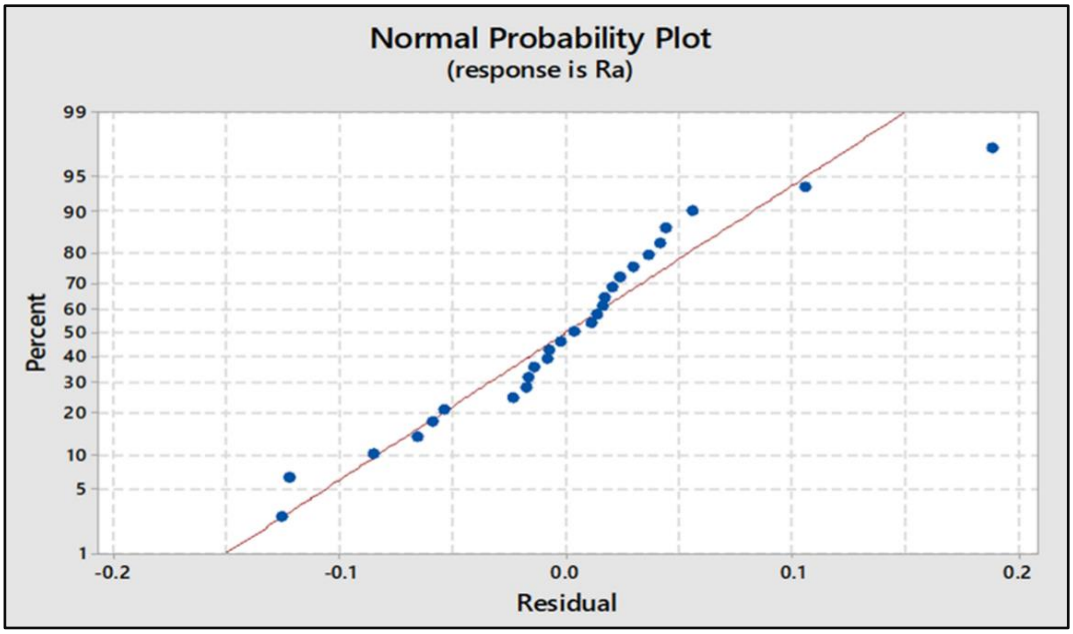

Figure 4.18. The normal probability plots of residuals for Ra.

Since the points were set in a straight line, they exhibit a clear pattern, suggesting that each component of the regression model affects the Ra (the factorial expected value).

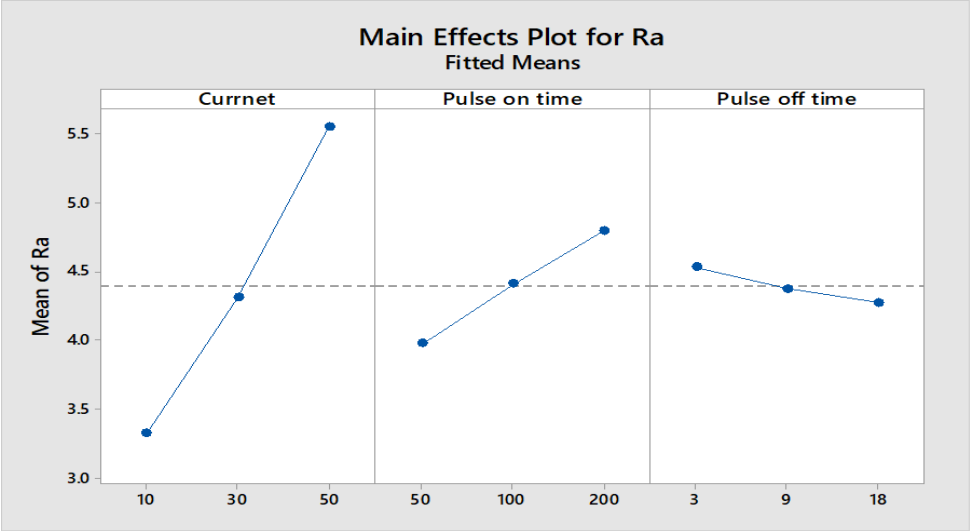

Figure 4.19. The normal Ra probability plots of residuals for input parameters.

4.6.3.1. Regression Model for Ra

Mathematical models can be developed through the use of the coefficients, as follows:

$$Ra = 4.3957 - 1.0681\ I_P(10) - 0.0830\ I_P(30) + 1.1510\ I_P(50) - 0.4182\ T_{ON}(50) + 0.0140\ T_{ON}(100) + 0.4041\ T_{ON}(200) + 0.1375\ T_{OFF}(3) - 0.0193\ T_{OFF}(9) - 0.1182\ T_{OFF}(18) - 0.0425\ I_P{*}T_{ON}(10)(50) + 0.0616\ I_P{*}T_{ON}(10)(100) - 0.0191\ I_P{*}T_{ON}(10)(200) + 0.1141\ I_P{*}T_{ON}(30)(50) - 0.0258\ I_P{*}T_{ON}(30)(100) - 0.0883\ I_P{*}T_{ON}(30)(200) - 0.0716\ I_P{*}T_{ON}(50)(50) - 0.0358\ I_P{*}T_{ON}(50)(100) + 0.1074\ I_P{*}T_{ON}(50)(200) \quad (4.3)$$

4.6.3.2. Model Summary of the Ra

A brief overview of the design and the statistics comparing the accuracy of several models are included in the model summary. The predicted R square (R-Sq (pred)) measures how well future data will be predicted. The coefficient of determination (R-Sq) measures how much of the observed response variance can be described via a model. Regulate R-S (R. Sq- adj) is an adjusted R which is a corrected total of conditions at the type's equation. A well fit is indicated by higher R-Square (R-Sq) and R-Sq (adj) values tabulated in Table 4.15.

When both the experimented and predicted bars come close to each other, this means that they are equal in outcomes as shown in Figure 4.20.

Table 4.15. The Model summary of the Ra.

S	R. sq(pred)	R. sq-adj.	R-sq
00.0819703	99.58 %	99.321 %	98.82%

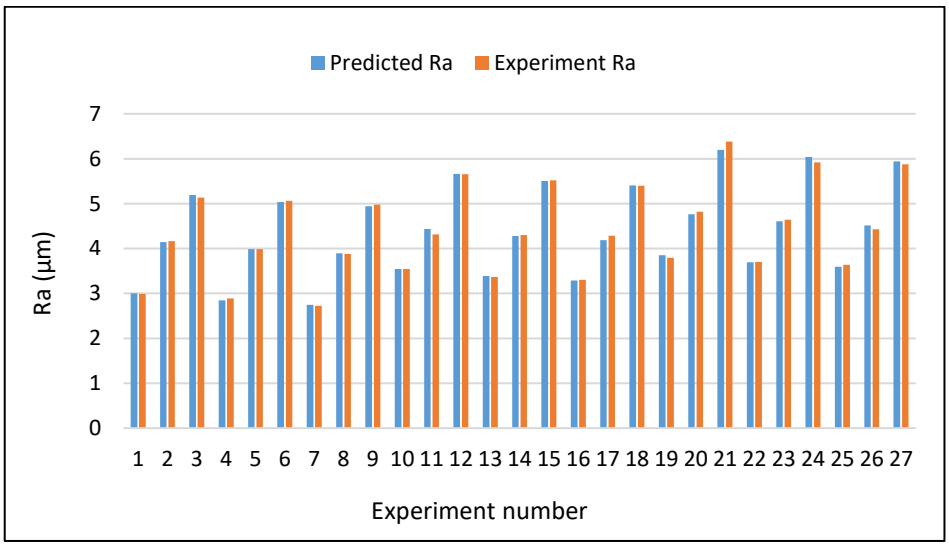

Figure 4.20. The comparison of experimented and predicted Ra values.

4.6.4. EWR Analysis

Using experimental factorial designs (EWR), regression, and analysis of variance (ANOVA) were utilized to fit models based on EWR data to obtain residuals that can be compared to normal probability plots to ascertain the degree to which the effects are significant. As a result, they exhibit a distinct pattern, indicating that the dielectric's EWR is affected by each factor, as shown in Table 4.16. which includes degrees of freedom (DF), a total sum of squares (Adj SS), the mean sum of squares (Adj MS), F-values, and P-values to decide if the variables are significantly related to the answer. Figure 4.21. and 4.22. Show a plot of the normal probability of the EWR residuals and the normal probability plots of residuals for EWR for I_P, T_{ON}, and T_{OFF}, respectively.

Table 4.16. ANOVA table for EWR.

Source	DF	Adj SS	Adj MS	F-value	P-value
Model	10	3.12348	0.31235	261.25	0.000
Linear	6	3.10335	0.51723	432.62	0.000
Ip	2	2.71008	1.35504	1133.38	0.000
T_{on}	2	0.35690	0.17845	149.26	0.000
T_{off}	2	0.03637	0.01819	15.21	0.000
2-way interactions	4	0.02013	0.00503	4.21	0.016
I* T_{on}	4	0.02013	0.00503	4.21	0.016
Error	16	0.01913	0.00120		
Total	26	3.14261			

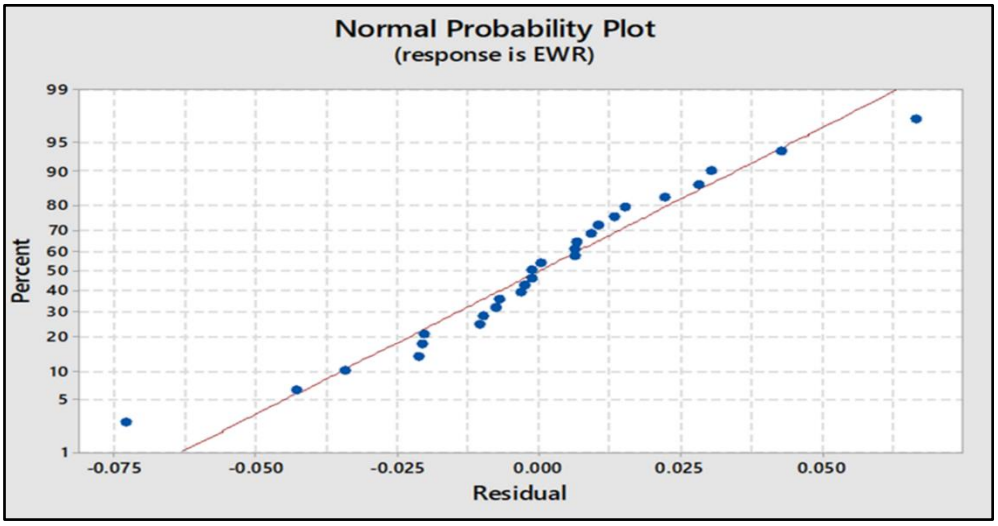

Figure 4.21. The normal probability plots of residuals for EWR.

Since the points were set in a straight line, they exhibit a clear pattern, suggesting that each component of the regression model affects the EWR (the factorial expected value).

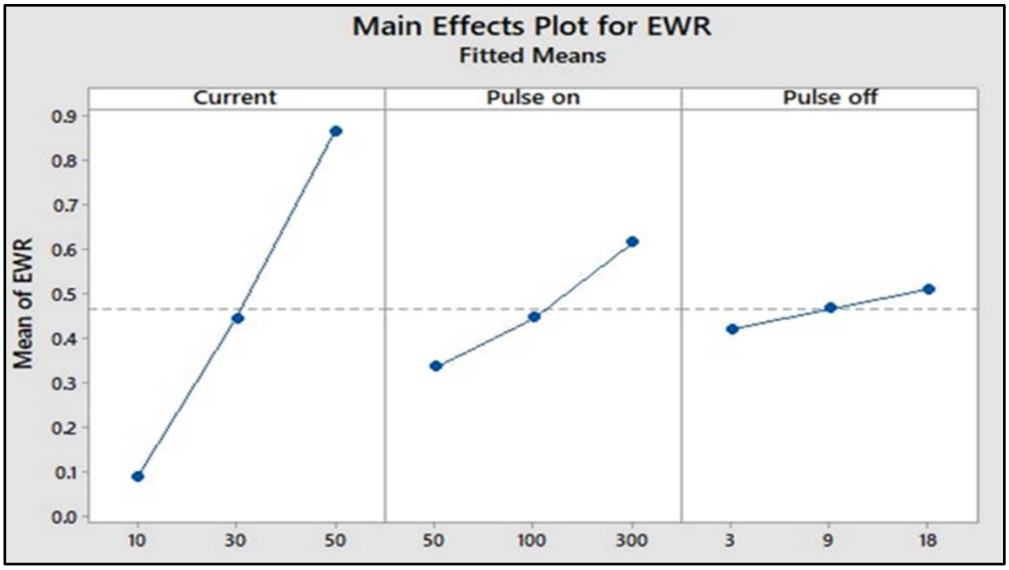

Figure 4.22. The normal EWR probability plots of residuals for input parameters.

4.6.4.1. Regression Model for EWR

Mathematical models can be developed through the use of the coefficients, as follows:

$$EWR = 0.46573 - 0.37716\ I_P(10) - 0.02088\ I_P(30) + 0.39804\ I_P(50) - 0.13045\ T_{ON}(50) - 0.01883\ Ton(100) + 0.14928\ T_{ON}(200) - 0.04503\ T_{OFF}(3) + 0.00016\ T_{OFF}(9) + 0.04487\ T_{OFF}(18) + 0.0453\ I_P{*}T_{ON}(10)(50) + 0.0005\ I_P{*}T_{ON}(10)(100) - 0.0458\ I_P{*}T_{ON}(10)(200) - 0.0239\ I_P{*}T_{ON}(30)(50) + 0.0113\ I_P{*}T_{ON}(30)(100) + 0.0126\ I_P{*}T_{ON}(30)(200) - 0.0215\ I_P{*}T_{ON}(50)(50) - 0.0117\ I_P{*}T_{ON}(50)(100) + 0.0332\ I_P{*}T_{ON}(50)(200) \quad (4.4)$$

4.6.4.2. Model Summary of EWR

A brief overview of the design and the statistics comparing the accuracy of several models are included in the model summary. The predicted R square (R-Sq (pred)) measures how well future data will be predicted. The coefficient of determination (R-Sq) measures how much of the observed response variance can be described via a model. Regulate R-S (R. Sq- adj) is an adjusted R which is a corrected total of conditions at the type's equation. The projected R-square (R-Sq (pred)) reflects how well a model predicts future data. A well fit is indicated by higher R-Square (R-Sq) and R-Sq (adj) values are tabulated in Table 4.17.

When both the experimented and predicted bars come close to each other, this means that they are equal in outcomes as shown in Figure 4.23.

Table 4.17. The Model summary of the EWR.

S	R. sq(pred)	R. sq- adj.	R-sq
0.0345771	99.39 %	99.01 %	98.27%

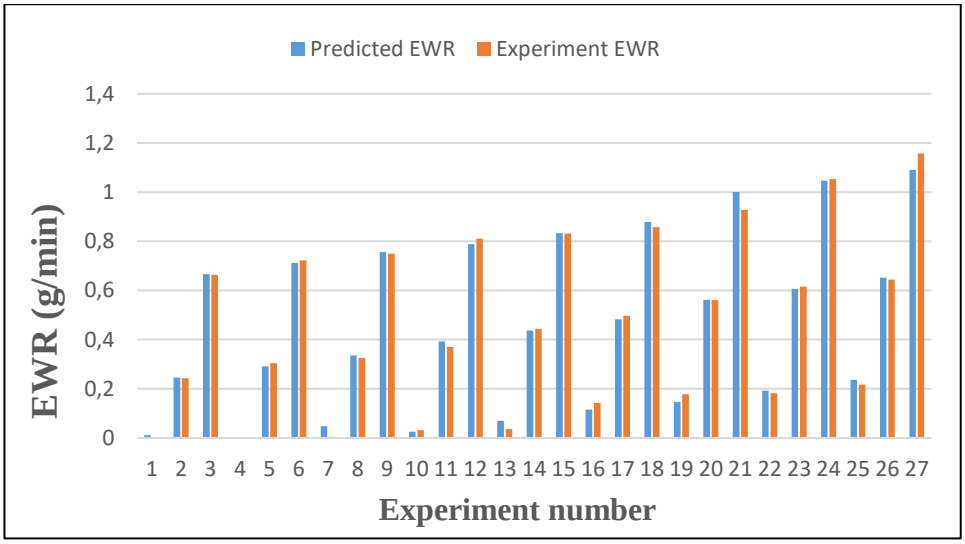

Figure 4.23. The comparison of experimented and predicted EWR values.

PART 5

CONCLUSION

5.1. INTRODUCTION

This study examined the interactions between machining parameters and EDM machining reactions to understand better how they affect one another. The machining outputs were tested with various parameters, such as current, pulse on time, and pulse off time, (WLT, MRR, Ra, and EWR). Experiment results were analyzed and evaluated by Minitab 17 was used to develop mathematical models that predicted the outcomes.

5.2. CONCLUSION

- EDM settings affect WLT, MRR, Ra, and EWR. However, the I_P has the most influence on these factors.
- The I_P needed to be decreased to achieve the desired improvements in WLT, Ra, and EWR. In addition, I_P needed to increase to improve the MRR.
- CK45 DIN 17200 has good machinability and high tensile strength because of its hardness and has wide usage areas in industry products.
- The first that all output parameters increase as I_P increase from 10A to 50A shows that I_P is the most important input parameter affecting the outputs.
- The maximum WLT (335.7469 μm) for CK45 DIN 17200 grade material occurred at the highest current and T_{ON}. The best WLT (4.17946 μm) occurred at the lowest Ip, and T_{ON}, and highest T_{OFF}.
- The highest MRR value (1.5650 g/min) occurred at the highest Ip (50A), highest T_{ON} (200 μs), and lowest T_{OFF} (18 μs). The minimum value of MRR (0.1879 g\min) occurred at minimum Ip (10A), T_{ON} (50μs), and T_{OFF}(3μs).

- The maximum Ra (6.384 μm) was obtained at the highest I_P (50 A), T_{ON} (200μs), and lowest T_{OFF} (3μs). The minimum Ra (2.725 μm) was obtained at the lowest I_P (10A) and T_{ON} (50μs) and the highest T_{OFF} value (18μs).
- The maximum value of EWR (1.1575 g\min) occurred at the highest I_P (50A), T_{ON} (200μs) and T_{OFF} (18μs). The minimum EWR (0.00113 g\min) occurred at the lowest I_P (10A) T_{ON} (50μs), and T_{OFF} (3μs).
- Current has much less effect on Ra and MRR than on WLT.
- Minitab 17's factorial model can accurately predict processing responses with high precision, and the closer to 100 percent, the more valid and reliable it is. The processing responses obtained in this study are almost 100. (R-Sq = 92.71%) for WLT, (R-Sq = 94.96%) for MRR, (R-Sq = 99.58%) for Ra, (R-Sq = 99.39%) for EWR.
- In this study, it was found that I_P has the most influence on the WLT . In fact, W.S. Khudhir et al. was found the T_{ON} is the most influencing factor that affects the WLT.

5.3. RECOMMENDATIONS FOR FUTURE WORK

- Studying the effects of employing various dielectric fluids, such as purified water, tap water, vegetable oils, etc. on WLT.
- Studying other metals including high carbon steel to see the effect on WLT.
- The effect of various EDM parameters, such as the grade of tool material used, can be explored to discover how they affect the machining process.
- A Study examining the effect of the heat-affected zone on the WLT can be conducted.
- Any alloy's EDM process can be analyzed for the effects of oxidability, electrical conductivity, and viscosity.
- Can be studied the impact of residual stress on WLT.

REFERENCES

1. Ramasawmy, H., Blunt, L., and Rajurkar, K. P., "Investigation of the relationship between the white layer thickness and 3D surface texture parameters in the die sinking EDM process", ***Precision Engineering***, 29 (4): 479–490 (2005).

2. Saxena, P. and Metkar, R. M., "Development of electrical discharge machining (EDM) electrode using fused deposition modeling (FDM)", 3D Printing and Additive Manufacturing Technologies, ***Springer***, 257–268 (2019).

3. H.L.Abdulwahhab, S. H. A., "Study the effect of different dielectric fluid on surface integrity for electrical discharge machining (EDM)", ***University of Technology***, (2019).

4. "EDM Machining Service, Sample EDM Parts, Electrical Discharge Machining, Wire EDM California", **https://wirecutcompany.com/sample_parts.html** (2022).

5. I.A. Qasim, S. H. A., "Study the Effect of Electrode Materials on Material Removal Rate and Electrode Wear Rate in EDM of AISI 304 Stainless Steel", ***University of Technology***, (2016).

6. Ubaid, A. M., Dweiri, F. T., Aghdeab, S. H., and Abdullah Al-Juboori, L., "Optimization of electro discharge machining process parameters with fuzzy logic for stainless steel 304 (ASTM A240)", ***Journal Of Manufacturing Science And Engineering***, 140 (1): (2018).

7. T.M.Salman, SH.H.Aghdeab, R. R. S., "Evaluation and analysis of residual stress in electric discharge machining process", ***University of Technology***, (2020).

8. Jameson, E. C., "Electrical Discharge Machining", ***Society Of Manufacturing Engineers***, 1–3 (2001).

9. Jameson, E. C., "Electrical Discharge Machining (EDM)", Electrical Discharge Machining (EDM), 7–8 (2001).

10. W.S.KHudhir, S.K.Shather, S. H. A., "Improvement the Surface Inegrity of AISI-A2 Steel by Post (EDM/ECM) Processes", ***University of Technology***, (2019).

11. Aghdeab, S. and Ahmed, A., "Effect of Pulse on Time and Pulse off Time on Material Removal Rate and Electrode Wear Ratio of Stainless Steel AISI 316L in EDM", ***Eng. &Tech.Journal***, 34: 2940–2949 (2016).

12. R.A.Al-Jarah, S. K. A., "Improving working surface in electro discharge machining by additaves powder", ***University of Technology***, (2010).

13. A.B.Abdulwahhap, M.A.Tawfiq, S. H. A., "Affecting The Material Removal Rate (Mrr) And Electrode Wear (Ew) In Electro Discharge Machining (Edm)", ***University of Technology***, (2012).

14. V.N.Najim, S. H. A., "Effect Of Machining Parameters On Material Removal Rate And Electrode Wear In Edm", ***University of Technology***, (2014).

15. Ranganath, B. J., "Thermal metal cutting Processes", “Thermal Metal Cutting Processes Hardcover", May 5. Ed., ***IK International***, (2008).

16. Abu Qudeiri, J. E., Saleh, A., Ziout, A., Mourad, A.-H. I., Abidi, M. H., and Elkaseer, A., "Advanced electric discharge machining of stainless steels: Assessment of the state of the art, gaps and future prospect", ***Materials***, 12 (6): 907 (2019).

17. O.S.Sabbar, A. A. K., "Evaluation of Electrode Wear in Electrical Discharge machining", ***University of Technology***, (2016).

18. Nguyen, M. D., Rahman, M., and San Wong, Y., "Simultaneous micro-EDM and micro-ECM in low-resistivity deionized water", ***International Journal Of Machine Tools And Manufacture***, 54: 55–65 (2012).

19. Abdudeen, A., Abu Qudeiri, J. E., Kareem, A., Ahammed, T., and Ziout, A., "Recent advances and perceptive insights into powder-mixed dielectric fluid of EDM", ***Micromachines***, 11 (8): 754 (2020).

20. Shirguppikar, S. S. and Dabade, U. A., "Experimental investigation of dry electric discharge machining (Dry EDM) process on bright mild steel", ***Materials Today: Proceedings***, 5 (2): 7595–7603 (2018).

21. McGeough, J. A. and Rasmussen, H., "A model for the surface texturing of steel rolls by electrodischarge machining", ***Proceedings Of The Royal Society Of London. Series A: Mathematical And Physical Sciences***, 436 (1896): 155–164 (1992).

22. Kainz, A., Paesold, D., Riha, G., Krimpelstätter, K., and Zeman, K., "Finite Element Modeling of Temper Rolling with Particular Emphasis on Roughness Transfer", (2005).

23. Elkoca, O., "A study on the characteristics of electrical discharge textured skin pass mill work roll", ***Surface And Coatings Technology***, 202 (12): 2765–2774 (2008).

24. N.H.M. Alsfalchi, S.K.Shather, A. F. I., "Study and Analysis of the Surface Integrity on the Electro-Discharge Machining", ***University of Technology***, (2016).

25. Prakash, V., Shubham, Kumar, P., Singh, P. K., Das, A. K., Chattopadhyaya, S., Mandal, A., and Dixit, A. R., "Surface alloying of miniature components by micro-electrical discharge process", ***Materials And Manufacturing Processes***, 33 (10): 1051–1061 (2018).

26. Kumar, D., Mer, K. K. S., Payal, H. S., and Kumar, K., "WHITE-LAYER THICKNESS ON EDM-PROCESSED AISI A2 STEEL–MATHEMATICAL MODELING AND ANALYSIS", ***Materials And Technology***, 56 (2): 97–106 (2022).

27. Li, L., Lai, D., Ji, Q., Huang, J., Lin, Y., Pan, M., Wei, J., and He, S., "Influence of tool characteristics on white layer produced by cutting hardened steel and prediction of white layer thickness", ***The International Journal Of Advanced Manufacturing Technology***, 113 (3): 1215–1228 (2021).

28. Neslušan, M., Uríček, J., Mičietová, A., Minárik, P., Píška, M., and Čilliková, M., "Decomposition of cutting forces with respect to chip segmentation and white layer thickness when hard turning 100Cr6", ***Journal Of Manufacturing Processes***, 50: 475–484 (2020).

29. Muthuramalingam, T., Saravanakumar, D., Babu, L. G., Huu Phan, N., and Pi, V. N., "Experimental investigation of white layer thickness on EDM processed silicon steel using ANFIS approach", ***Silicon***, 12 (8): 1905–1911 (2020).

30. Ali, S. M., Al-Khazraji, A., and Amin, S. A., "The Effect of Electrical Discharge Machining Total Heat Generated on White Layer Thickness (WLT) and Fatigue Life for Die Steel", (2021).

31. Aghdeab, S. H. and Aldulaimy, H. L., "The effect of different dielectrics on material removal rate, sur-face roughness and white layer thickness in EDM process", ***International Journal Of Engineering & Technology***, 7 (4): 4455–4461 (2018).

32. Arfaoui, S., Zemzemi, F., and Tourki, Z., "Relationship between cutting process parameters and white layer thickness in orthogonal cutting", ***Materials And Manufacturing Processes***, 33 (6): 661–669 (2018).

33. Maher, I., Sarhan, A. A. D., and Marashi, H., "1.9 Effect of Electrical Discharge Energy on White Layer Thickness of WEDM Process", ***Comprehensive Materials Finishing***, 1: 231–266 (2017).

34. Klocke, F., Hensgen, L., Klink, A., Ehle, L., and Schwedt, A., "Structure and composition of the white layer in the wire-EDM process", ***Procedia CIRP***, 42: 673–678 (2016).

35. Al-Khazraji, A., Amin, S. A., and Ali, S. M., "The effect of SiC powder mixing electrical discharge machining on white layer thickness, heat flux and fatigue life of AISI D2 die steel", ***Engineering Science And Technology, An International Journal***, 19 (3): 1400–1415 (2016).

36. Maher, I., Sarhan, A. A. D., Marashi, H., Barzani, M. M., and Hamdi, M., "White layer thickness prediction in wire-EDM using CuZn-coated wire electrode–ANFIS modelling", ***Transactions Of The IMF***, 94 (4): 204–210 (2016).

37. Balraj, U. S., Anitha, P., and Gopalakrishna, A., "A study on white layer thickness and surface crack density in rotary EDM of RENE80 nickel superalloy", (2014).

38. Azad, Y., Shabgard, M., and Matin, R., "An Experimental Study on the Effect of Primary Depth of Hole on the Surface Integrity of Tool Steel (DIN 1.2379) in Electrical Discharge Machining (EDM)", (2013).

39. Hasçalık, A. and Çaydaş, U., "A comparative study of surface integrity of Ti–6Al–4V alloy machined by EDM and AECG", ***Journal Of Materials Processing Technology***, 190 (1–3): 173–180 (2007).

40. Tomlinson, W. J., Blunt, L. A., and Spraggett, S., "The effect of workpiece speed and grinding-wheel condition on the thickness of white layers formed on EN. 24 ground surfaces", ***Journal Of Materials Processing Technology***, 25 (1): 105–110 (1991).

41. Aghdeab, S. H., Shwaishb, R. R., and Salmanc, T. M., "Effect of Input Parameters on SR and MRR for Tool Steel AISI L2 By Electric Discharge Machine (EDM)", ***Engineering And Technology Journal***, 39 (06): 928–935 (2021).

42. Jafari, E., Afsari, A., and Abedpour, S., "Predicting the Influence of Electrical Discharge Machining (EDM) Parameters on the Finished Work Surface in CK45 Steel", ***Journal Of Modern Processes In Manufacturing And Production***, 9 (1): 63–78 (2020).

43. Aghdeab, S. H., Khudhier, W. S., and Elias, R. R., "Experimental Study on Electrodes Types in Electrical Discharge Machining (EDM) of High-Speedd Steel", (2020).

44. Aghdeab, S. H. and Abdulnabi, A. Q., "Effect of Voltage on Electrode Wear Rate (EWR) in the Electrical Discharge Machining (EDM) for Stainless Steel AISI 444", ***Engineering And Technology Journal***, 40 (6): 0 (2022).

45. Aghdeaba, S., Hasan, M. M., and Makhribc, G. A., "Effect of gap space on surface roughness (Ra) in the electrical discharge machining (EDM) for tool steel AISI M6", ***Design Engineering***, 11358–11366 (2021).

46. Santos, R. F., Silva, E. R., Sales, W. F., and Raslan, A. A., "Analysis of the surface integrity when nitriding AISI 4140 steel by the sink electrical discharge machining (EDM) process", ***Procedia CIRP***, 45: 303–306 (2016).

47. Singh, H. and Singh, A., "Effect of pulse on/pulse off time on machining of AISI D3 die steel using copper and brass electrode in EDM", ***International Journal Of Engineering And Science***, 1 (9): 19–22 (2012).

48. Rodriguez, G. P., Simao, J., and Herranz, G., "Surface alloying of AISI H13 steel during electrical discharge machining (EDM)", (2009).

49. Abedpour, S., Jafar, E. I., Afsari, A., and Hadidi Mood, S., "Influence of EDM characteristic parameters on the surface microstructure in CK45 alloy steel", ***Journal Of Simulation And Analysis Of Novel Technologies In Mechanical Engineering***, 1 (4): 31–40 (2008).

50. Tsai, Y. Y. and Lu, C. T., "Influence of current impulse on machining

characteristics in EDM", ***Journal Of Mechanical Science And Technology***, 21 (10): 1617–1621 (2007).

51. KUNIEDA, M., TOHI, M., and OHSAKO, Y., "Reaction forces observed in pulse discharges of EDM", ***International Journal Of Electrical Machining***, 8: 51–56 (2003).

52. Zhao, Y., Zhang, X., Liu, X., and Yamazaki, K., "Geometric modeling of the linear motor driven electrical discharge machining (EDM) die-sinking process", ***International Journal Of Machine Tools And Manufacture***, 44 (1): 1–9 (2004).

53. Kunieda, M. and KIYOHARA, M., "Simulation of die-sinking EDM by discharge location searching algorithm", ***International Journal Of Electrical Machining***, 3: 79–85 (1998).

APPENDIX

PARAMETER

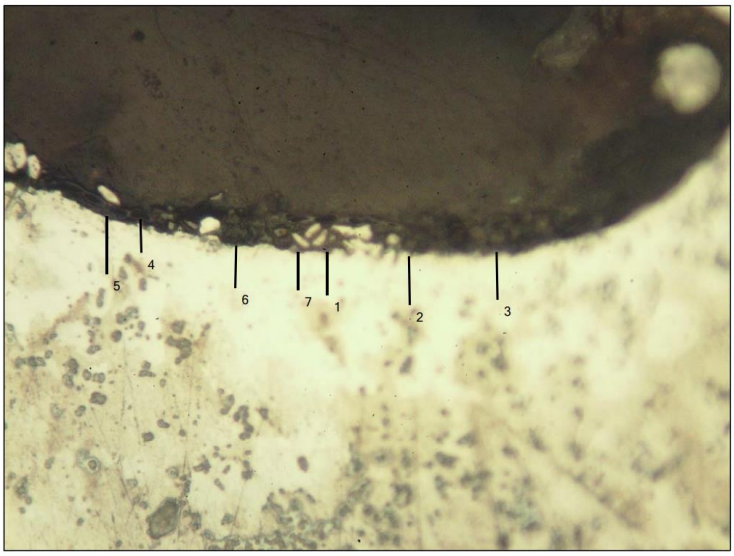

Fig. (A-1) The parameter impact on WLT (400x).

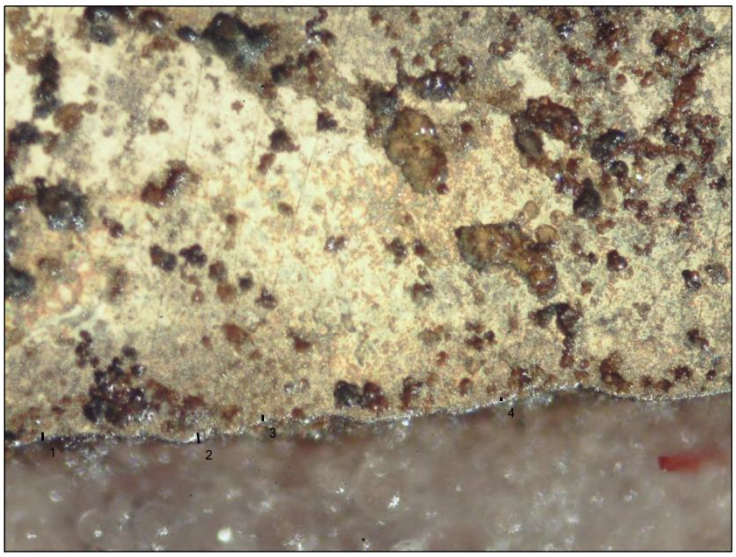

Fig. (A-2) The parameter impact on WLT (400x).

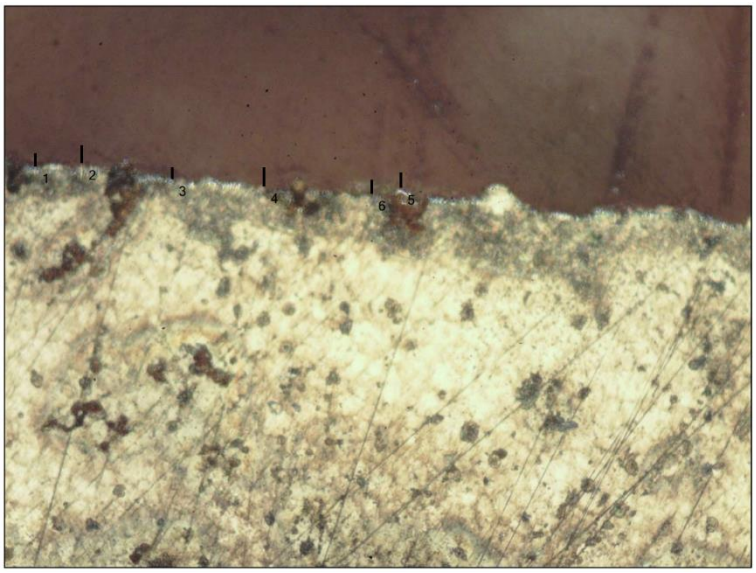

Fig. (A-3) The parameter impact on WLT (400x).

Fig. (A-4) The parameter impact on WLT (400x).

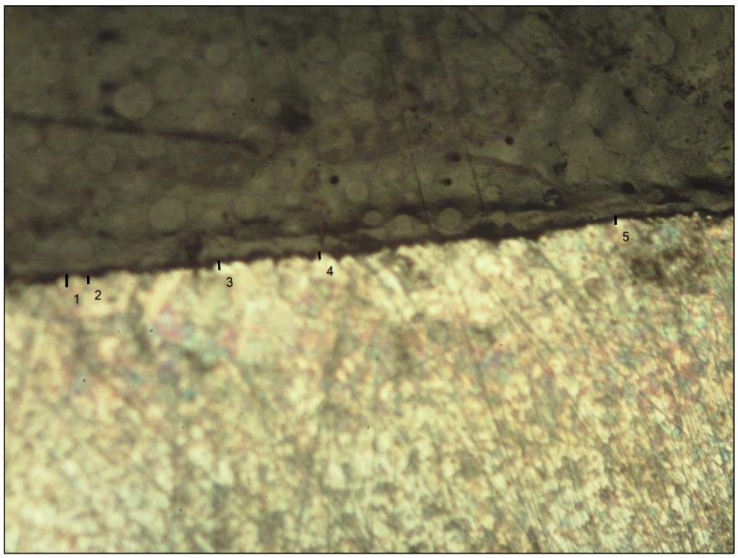

Fig. (A-5) The parameter impact on WLT (400x).

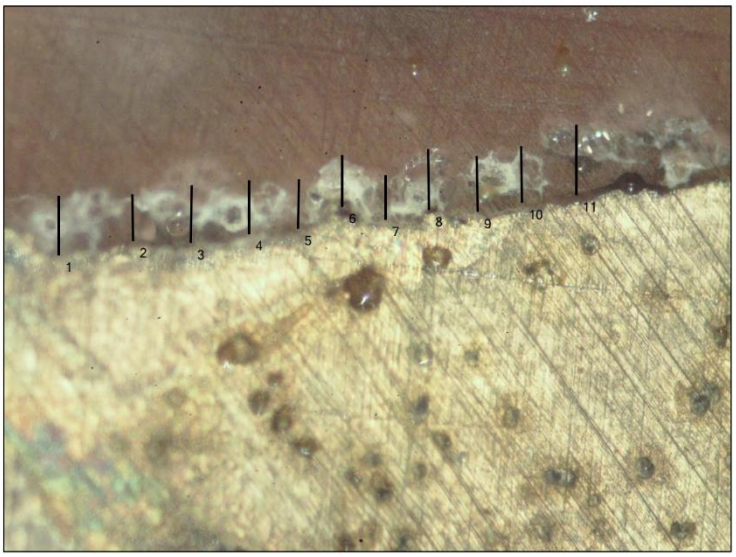

Fig. (A-6) The parameter impact on WLT (400x).

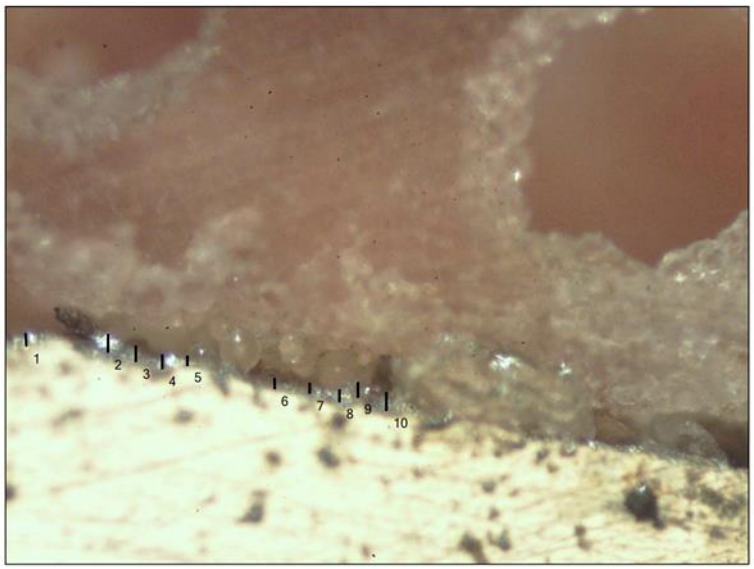

Fig. (A-7) The parameter impact on WLT (400x).

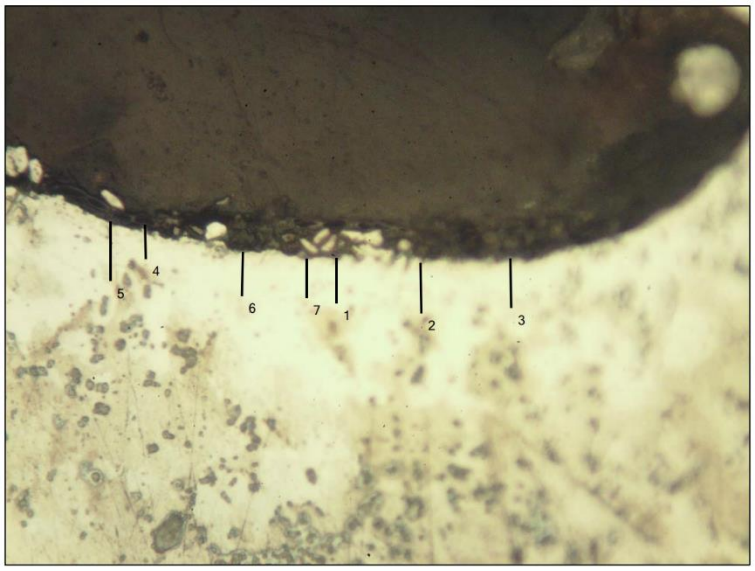

Fig. (A-8) The parameter impact on WLT (400x).

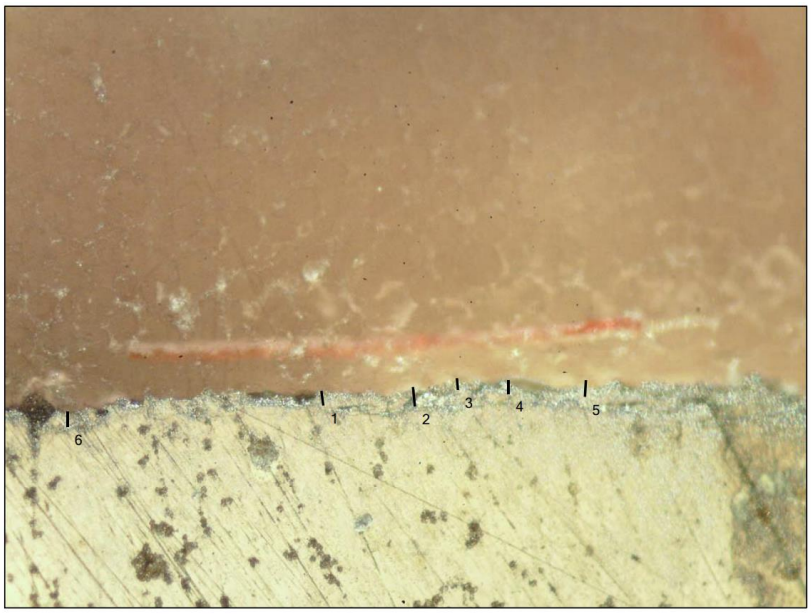

Fig. (A-9) The parameter impact on WLT (400x).

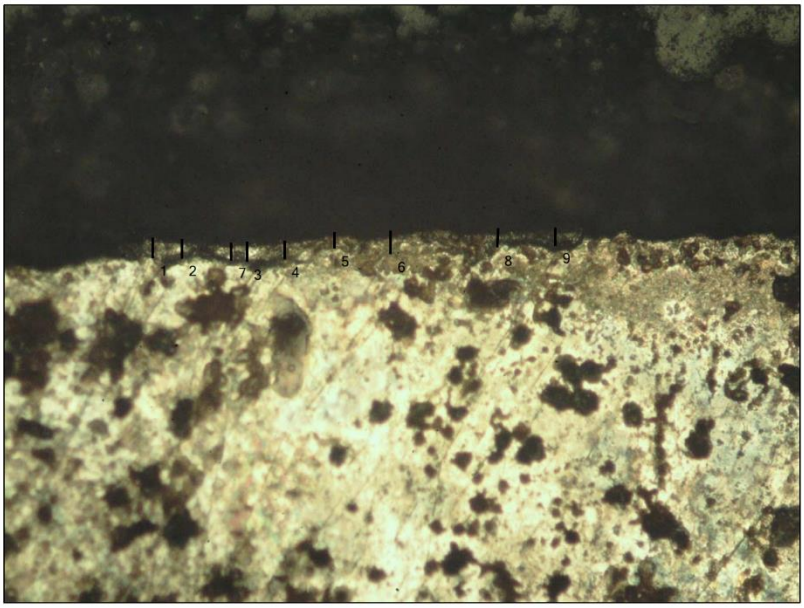

Fig. (A-10) The parameter impact on WLT (400x).

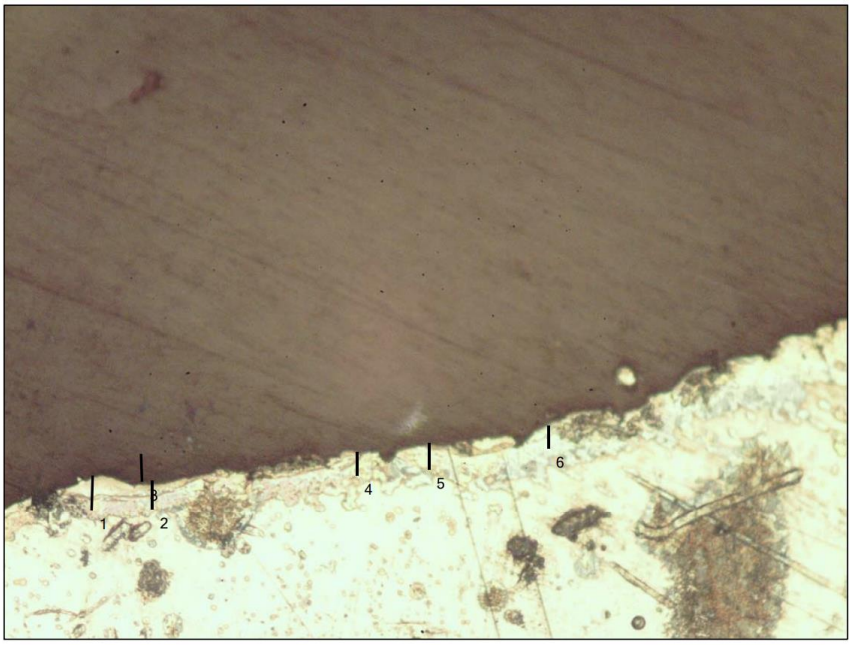

Fig. (A-11) The parameter impact on WLT (400x).

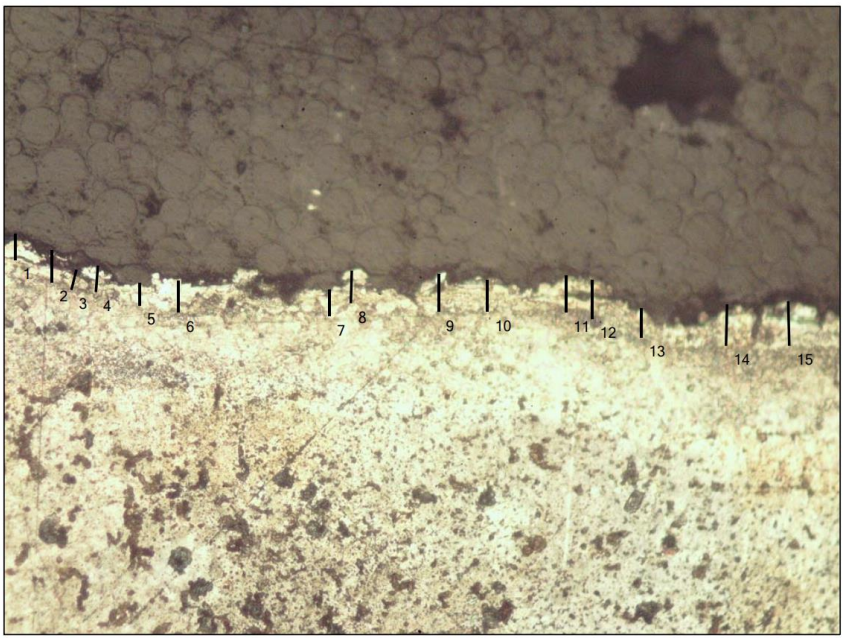

Fig. (A-12) The parameter impact on WLT (400x).

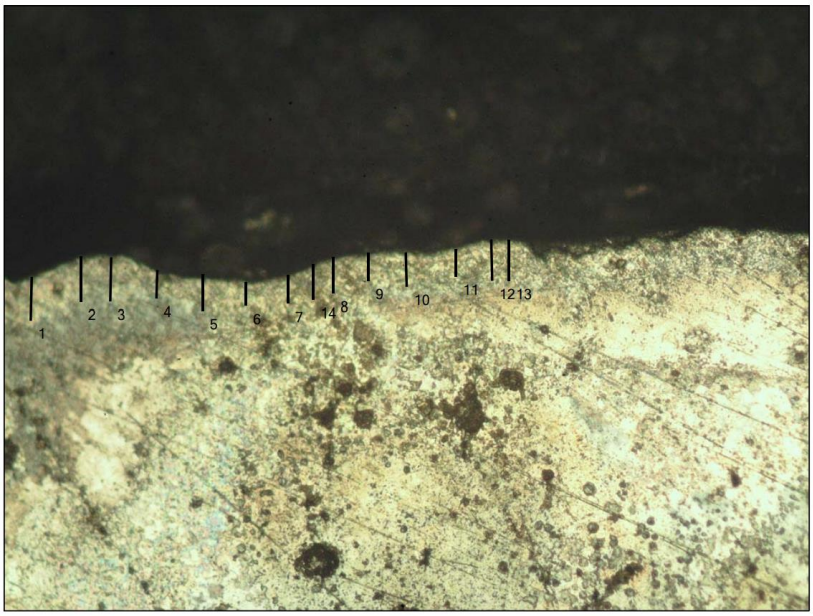

Fig. (A-13) The parameter impact on WLT (400x).

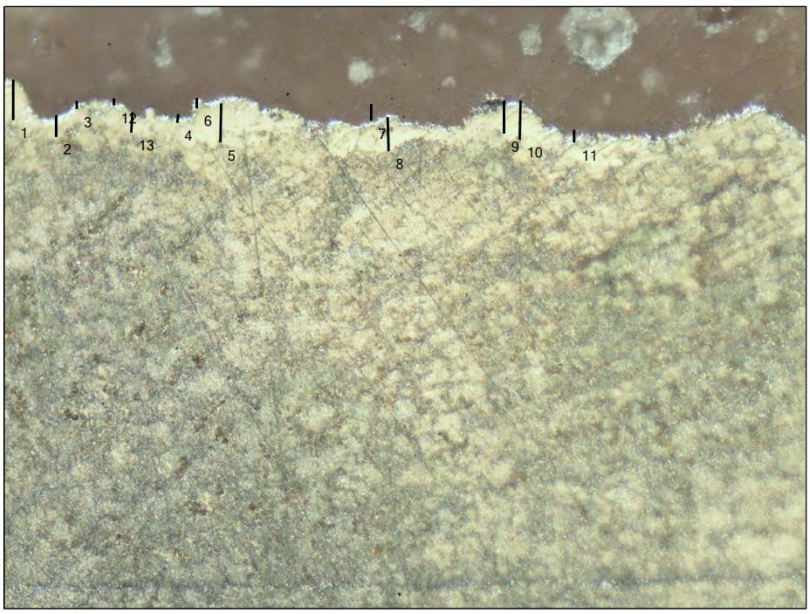

Fig. (A-14) The parameter impact on WLT (400x).

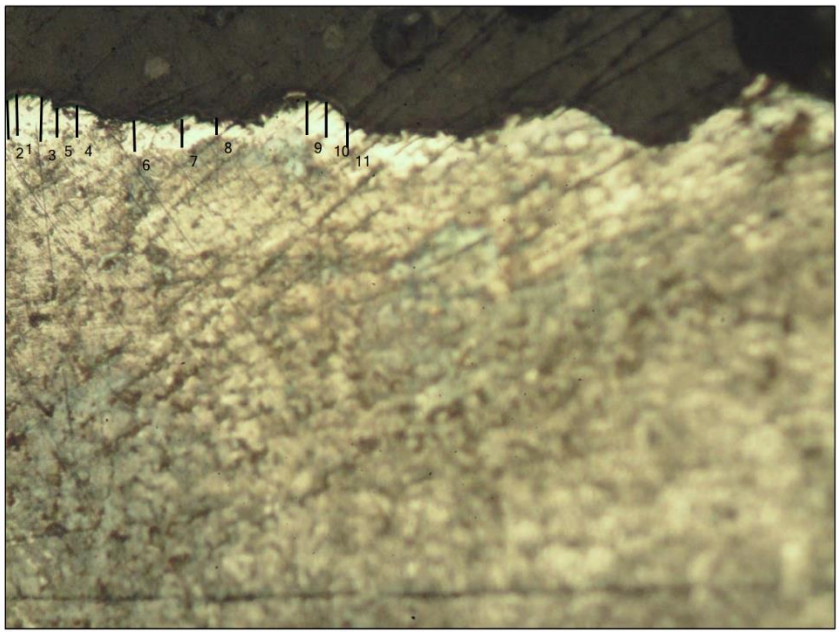

Fig. (A-15) The parameter impact on WLT (400x).

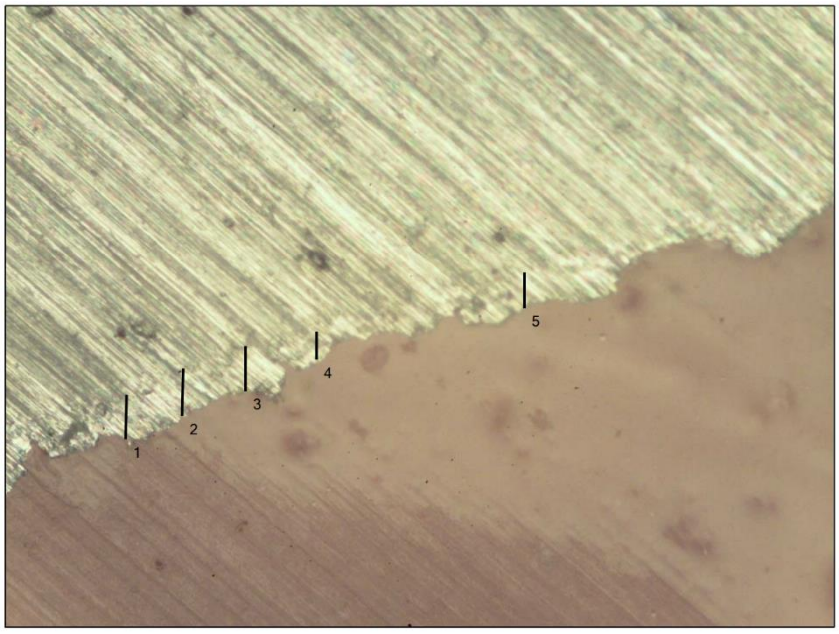

Fig. (A-16) The parameter impact on WLT (400x).

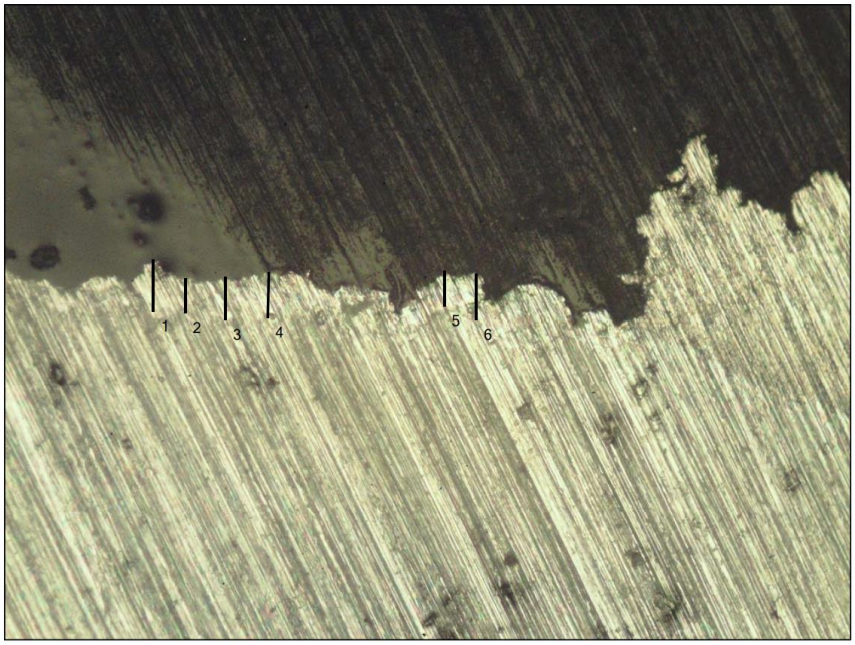

Fig. (A-17) The parameter impact on WLT (400x).

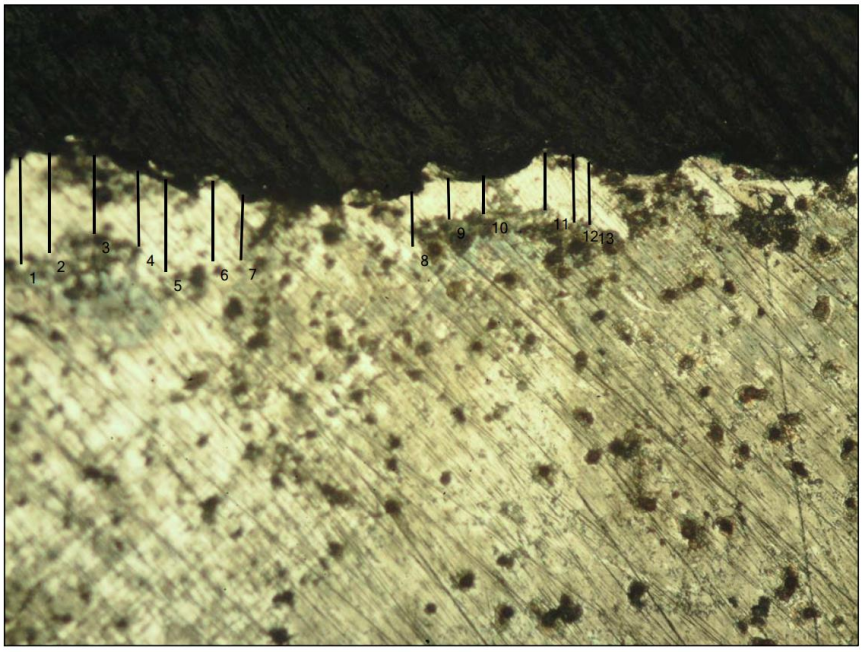

Fig. (A-18) The parameter impact on WLT (400x).

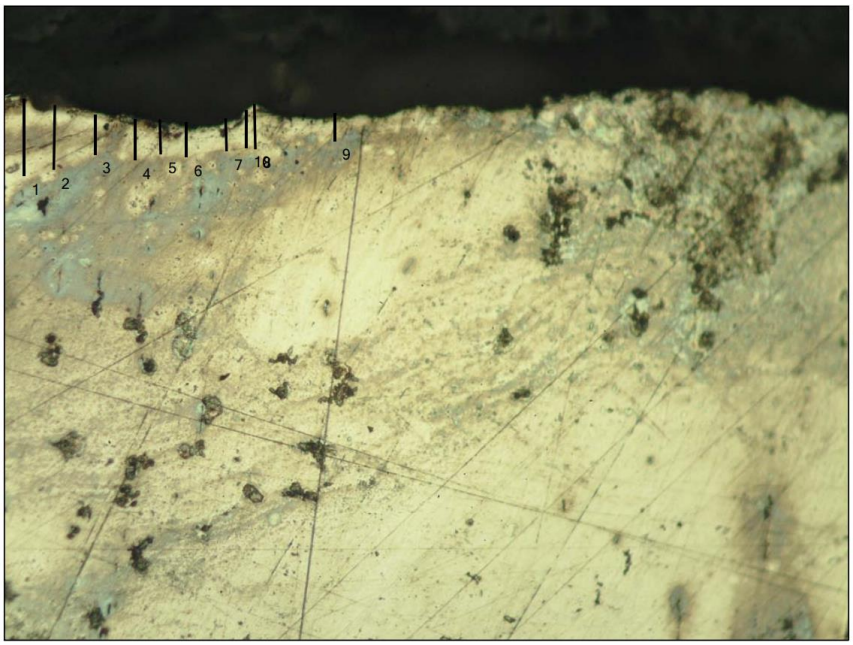

Fig. (A-19) The parameter impact on WLT (400x).

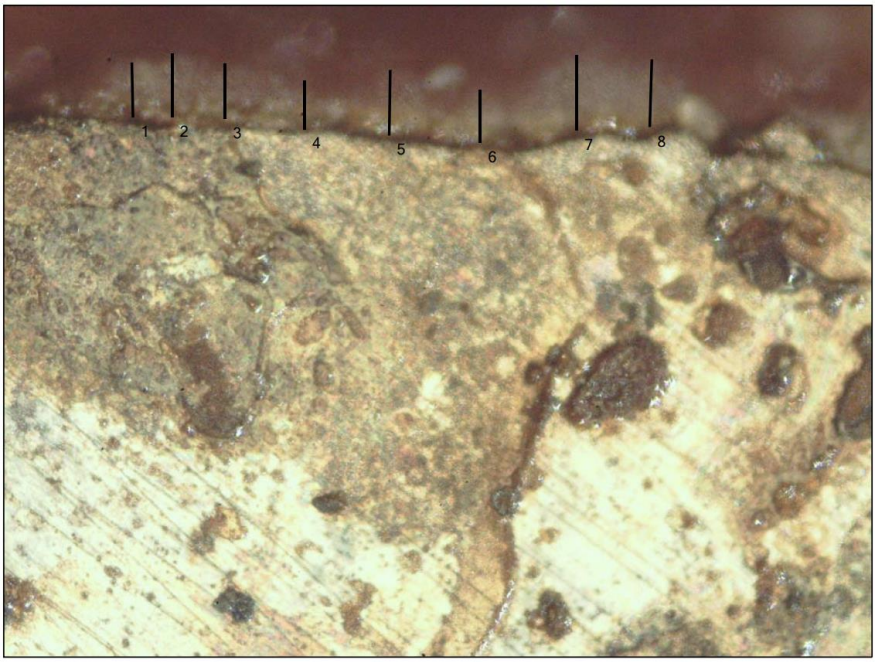

Fig. (A-20) The parameter impact on WLT (400x).

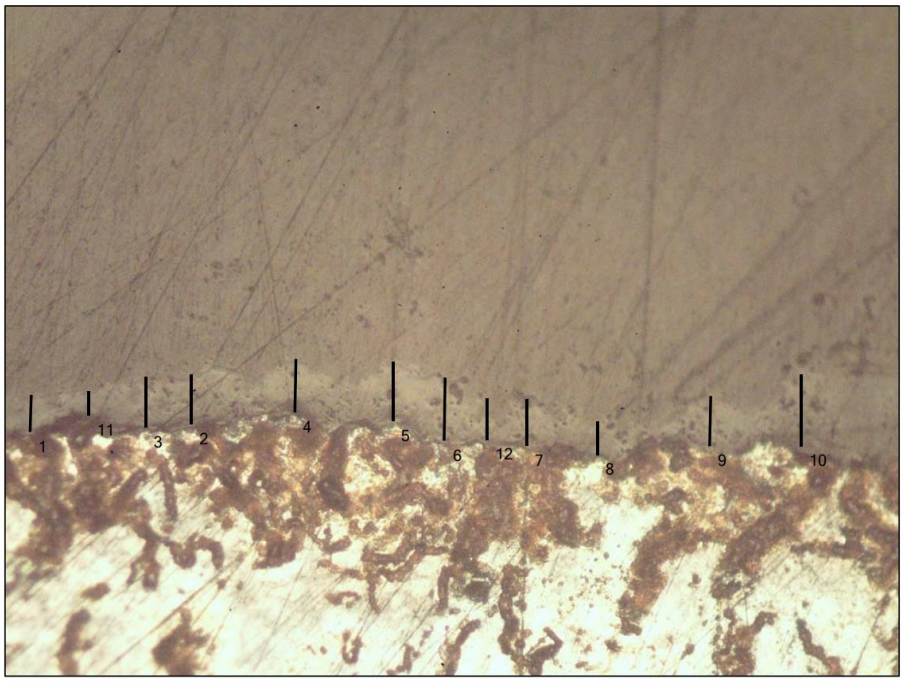

Fig. (A-21) The parameter impact on WLT (400x).

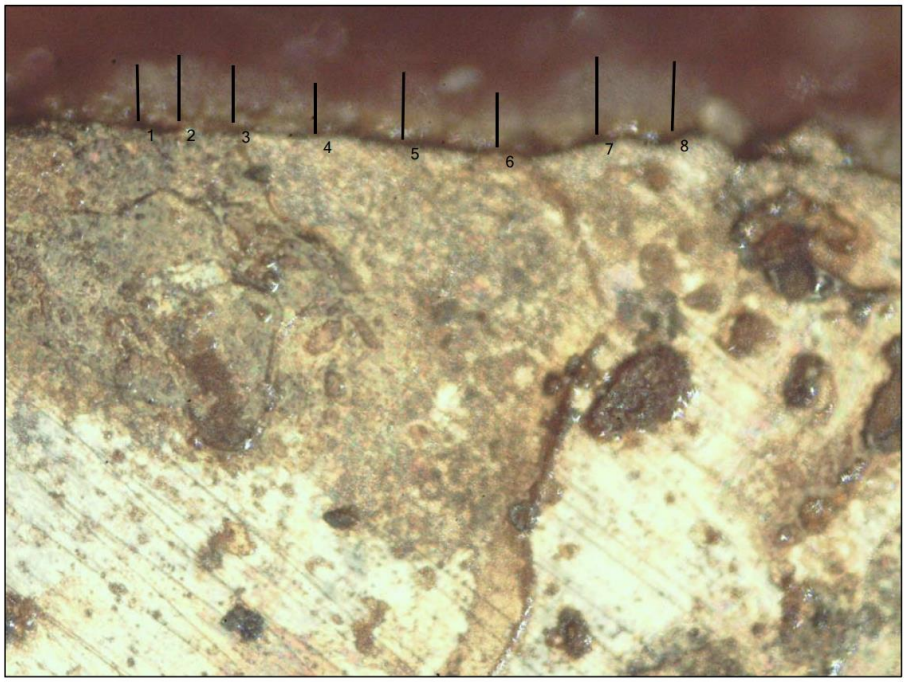

Fig. (A-22) The parameter impact on WLT (400x).

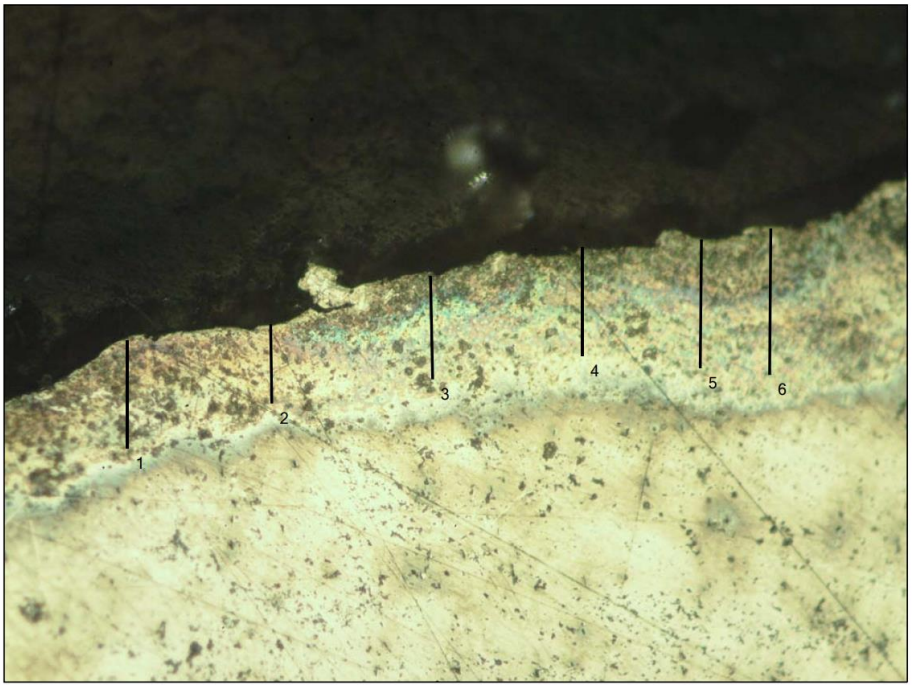

Fig. (A-23) The parameter impact on WLT (400x).

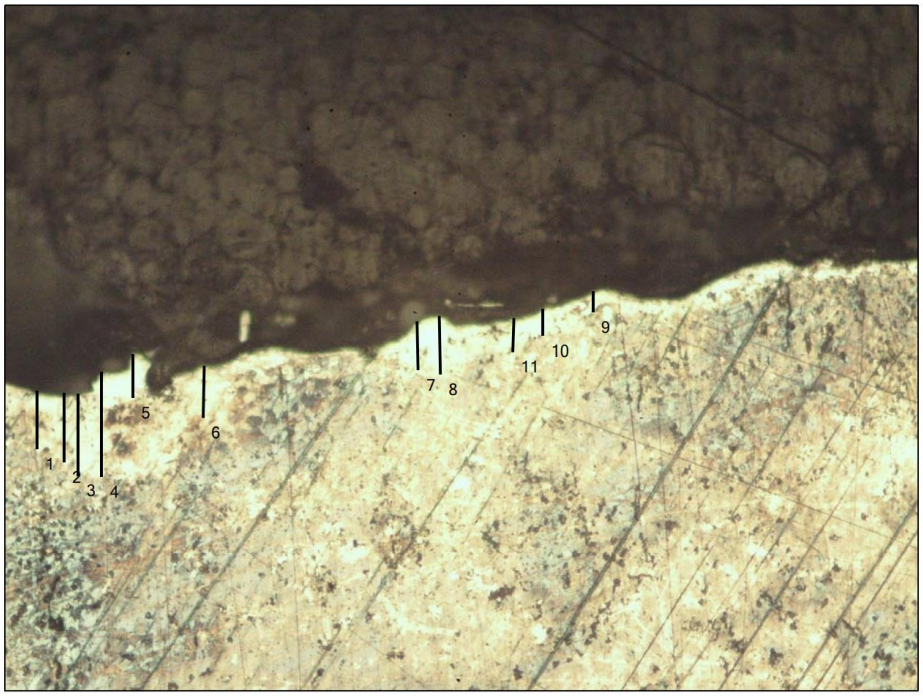

Fig. (A-24) The parameter impact on WLT (400x).

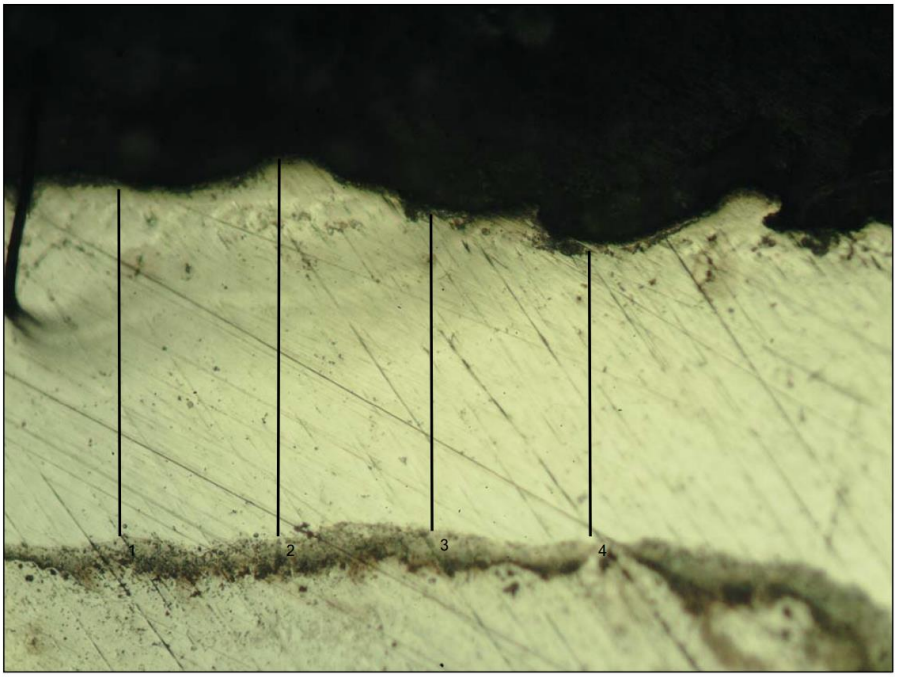

Fig. (A-25) The parameter impact on WLT (400x).

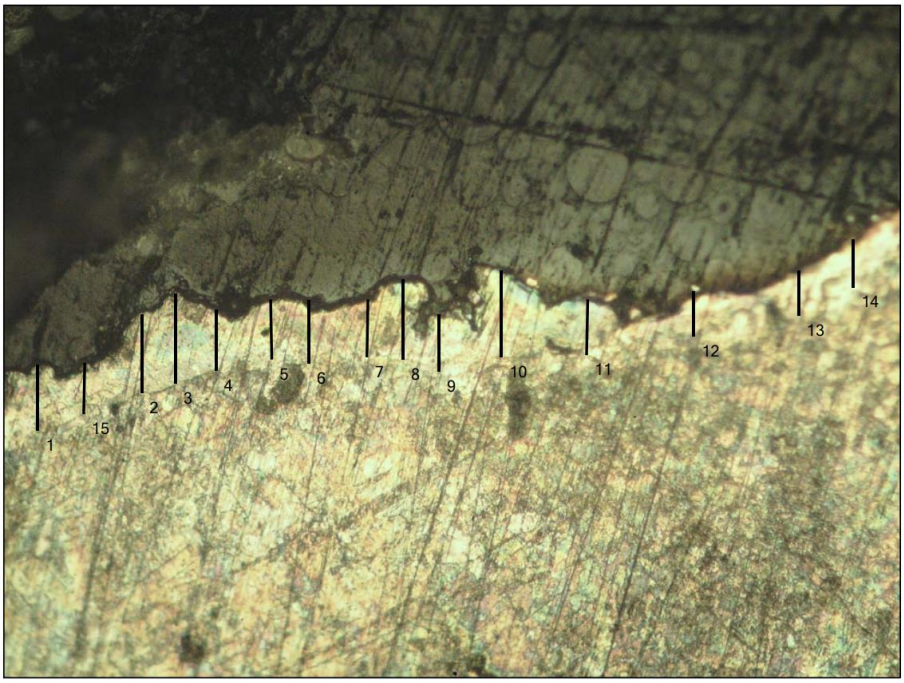

Fig. (A-26) The parameter impact on WLT (400x).

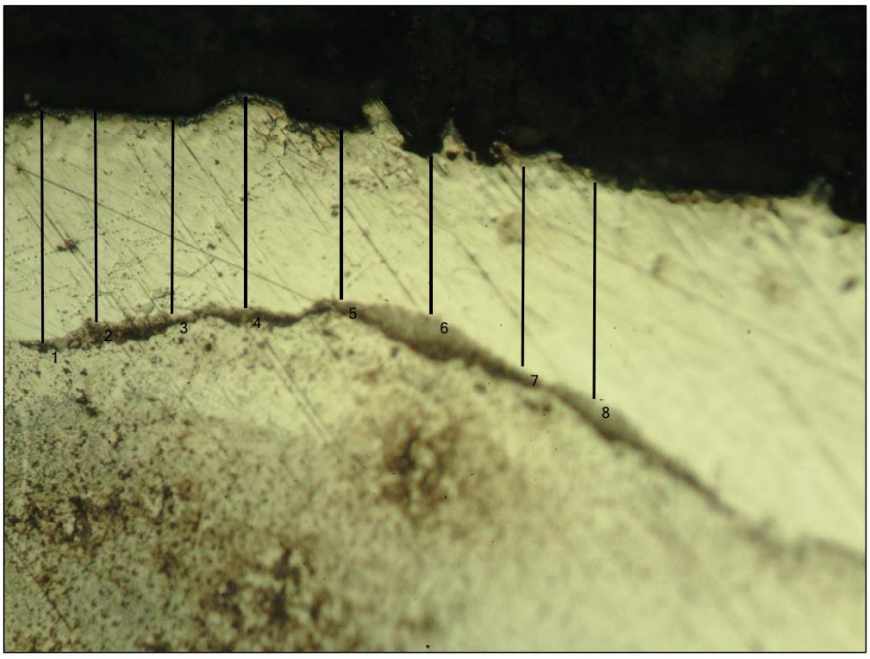

Fig. (A-27) The parameter impact on WLT (400x).

RESUME

Shahad Hatem Hasan HASAN finished her elementary education in Iraq. She graduated from university of technology, department of production and metallurgy year 2014 - 2015. Then she started her Master’s degree in mechanical engineering at Karabuk University.